AD-A158 850 COMPARATIVE ANALYSIS OF FLOOD ROUTING METHODS(U) 1/2
HYDROLOGIC ENGINEERING CENTER DAVIS CA T STRELKOFF
SEP 80 HEC-RD-24

UNCLASSIFIED F/G 13/2 NL

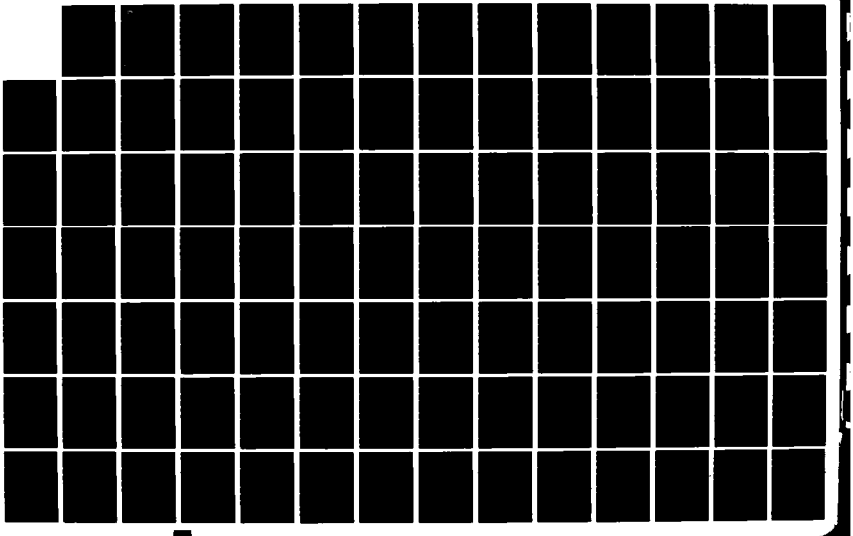

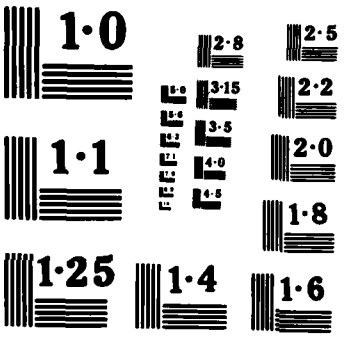

US Army Corps
of Engineers

The Hydrologic
Engineering Center

Comparative Analysis of Flood Routing Methods

Research Document No. 24

September 1980

COMPARATIVE ANALYSIS OF FLOOD ROUTING METHODS

by

Theodor Strelkoff

Hydraulic Engineer

Prepared for the Hydrologic Engineering Center, U.S. Army Corps of Engineers

under Contract No. DACW05-80-P-0323

ABSTRACT

Given inflow hydrographs were routed downstream using several different techniques. The resulting outflow and stage hydrographs were then compared. The standard for comparison was chosen to be the solution of the one-dimensional Saint-Venant equations. The approximate techniques considered were the zero-inertia equations, kinematic-wave model, and Modified-Puls with optional subdivision of the reach lengths. The effect of floodplains was considered in contrast to channels of simple cross section. Downstream boundary conditions consisted of one of the following: normal-depth stage-discharge relation, broad-crested overflow weir, or free overfall.

Dimensionless graphs of hydrograph-peak attenuation and arrival time as computed by the various techniques are presented. The accuracy of the approximate techniques is found to depend on the values of certain dimensionless parameters. This suggests numerical limits on those parameters for application of a particular method.

San Francisco, California

September 1980

PREFACE

The work reported herein is a product of the Hydrologic Engineering Center's continuing effort to improve both the accuracy and efficiency of techniques used by the Corps of Engineers to route floods through natural and modified river channels. This research defines the relative performance of various flood routing methods in channels of relatively simple geometry. Results were obtained by numerical experiments. Application of the results to prototype conditions is demonstrated in a companion report titled "Modified Puls Routing in Chuquatonchee Creek."

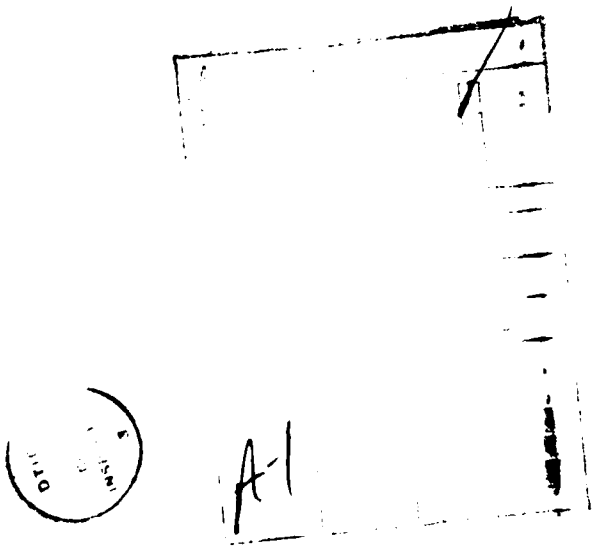

TABLE OF CONTENTS

Page

LIST OF FIGURES

Page

LIST OF TABLES

Comparative Analysis of Flood Routing Methods

1. Introductory summary.

Hydrographs of outflow from a reach of channel with given inflow hydrographs were computed by several different techniques and compared, to discern their relative accuracy under various conditions. The channel reaches were prismatic, except for the downstream end. The terminal conditions studied were (a) indefinite continuation of the given channel, with prescription of a normal-depth stage-discharge downstream boundary condition for the reach; (b) a channel obstruction causing backwater, schematicized by a broad-crested overflow weir; (c) a free overfall, with its critical-depth stage-discharge relation, schematizing sudden expansion of the given channel into a much larger waterway. The channel cross sections considered were either simple rectangles, or composites, composed of a rectangular in-bank portion and a single, slightly (laterally) sloping, broad flood plain terminating in vertical bluffs. Flood-plain resistance, characterized by the Manning n, was generally assumed much larger than that for in-bank flow.

The standard, for comparison with other routing methods, was obtained by numerical solution of the complete one-dimensional, nonlinear momentum and mass-conservation equations applied simultaneously to a large number (20) of subreaches comprising, together, the total reach length. Each subreach was sufficiently short that curvature of stage and discharge profiles over its length was negligible. All inflow hydrographs were sufficiently slow rising to preclude bore formation within the length of channel studied.

Modified-Puls routing comprised the principal alternate routing technique studied. Storage-outflow curves were prepared for each channel by integrating, over the length of the reach, steady-state profiles of cross-sectional area

computed for a sequence of flow rates. The Modified-Puls method was applied to the entire reach length, in a single computation for each time step, and also, for further comparison, to various numbers (2, 4, 10, etc.) of subreaches, successively, in a search for an optimum size of subreach for a given time step. This proved to be unrelated to the travel time through the subreach. Closest agreement of outflow hydrographs (primarily, peaks) with those of the standard were achieved when the subreach length was around half the normal depth under base-flow conditions, divided by the bottom slope.

In apportioning amongst the subreaches the total storage volume computed for each discharge, the profile of cross-sectional areas was assumed linear, i.e., changes in subreach storage over a time step were assumed proportional to subreach length. This is exactly true when the downstream boundary condition for the reach is a normal-depth stage-discharge relation. In this last case, as the number of subreaches is increased indefinitely, the results of the Modified-Puls method approach those of a kinematic-wave analysis.

A kinematic-wave analysis results when a stage-discharge relationship is specified for every station in a channel reach and is introduced into the continuity equation. The most nearly exact numerical implementation of this approach utilizes a network of characteristic curves, or simply, characteristics. A study of these curves showed that kinematic waves can attenuate under certain conditions. Such attenuation is enhanced by overflow into flood plains, but can occur even in channels of simple cross section. Attenuation of hydrograph peaks occurs when kinematic shocks (as distinguished from bores) are formed in the channel at intersections of the characteristics. The hydrograph peak is found sometimes to comprise the high side of the kinematic shock. Shock speed is less than the speed of lower-stage elements in the

trailing limb of the wave. These ultimately overtake the higher stages on the upstream side of the shock and result in the disappearance of these stages from the flood wave (see section 5.4.2).

Intermediate between solution of the complete dynamic equations governing the flow and the kinematic-wave or Modified-Puls approaches, is the zero-inertia or equilibrium solution, sometimes called a diffusion technique. Here, pressure, weight, and resistance forces are assumed essentially in equilibrium, so that local and convective accelerations are negligible. In this formulation, instabilities associated with near-critical flow especially in irregular channels, play no role, because Froude-number considerations have no relevance to the flow equations in this case. Consequently, routine computation of unsteady flows in rivers and streams by this method may prove more trouble free than solution of the complete dynamic equations.

This comparative study was undertaken to find the conditions under which the simpler routing techniques yield results close to those of the standard solution, the latter accurate in principle, but complex to program, expensive to execute, and subject to aborts in the course of routine computation. In order to establish through a minimum of computational experiments the influence of channel slope, roughness, cross-sectional configuration, base flow, and inflow-hydrograph peak and rise time, the pertinent equations and boundary conditions were expressed in dimensionless form. By this means, the number of parameters affecting the outflow hydrograph was kept to the minimum possible without excessively sacrificing the scope of the study.

For a given cross-sectional configuration and downstream control, the reduction in hydrograph peaks with distance down the channel is governed primarily by (1) F^*, a characteristic Froude number embodying channel slope, roughness, and base flow, (2) $t_{Q_p}{}^*$, dimensionless inflow-hydrograph rise time,

and (3) Q_p^*, the ratio of peak inflow discharge to base flow. Of lesser import is the influence of channel length, characterized by its dimensionless value L*. The attenuation of hydrograph peaks (relative to base flow) with dimensionless distance as computed by the various techniques is shown in Figs. 10 to 21, and forms the basis for technique comparisons.

Discharge maximums are plotted in Figs. 10-15, stage maximums in Figs. 16-21, and arrival time of discharge peaks in Figs. 22-27; stage peaks generally arrive just a little later. The first three figure numbers of each set refer to the rectangular channel, the last three to the channel with flood plains. In each set of three the first numbered figure refers to a normal-depth rating curve downstream, the second to a weir downstream boundary, and the third to the overfall condition downstream. Each numbered figure (e.g., 10) has lettered parts (e.g., 10a, 10b, ...), each referring to a different rise time for the inflow hydrograph, or in special cases, a different inflow peak.

2. Dimensionless governing equations.

In dimensionless form (see section 5.1) the partial differential equations of mass and momentum are, respectively,

$$\frac{\partial Q^*}{\partial x^*} + \frac{\partial A^*}{\partial t^*} = 0 \qquad (1)$$

and

$$F^{*2}\left(\frac{\partial Q^*}{\partial t^*} + \frac{\partial \frac{Q^{*2}}{A^*}}{\partial x^*}\right) + A^* \frac{\partial h^*}{\partial x^*} + S_F^* \frac{Q^{*2}}{K_D^{*2}} = 0 \qquad (2)$$

In this formulation, the reference discharge Q_0 is the base flow, so that Q*, above, represents the multiple of base flow extant at any particular station and time. I.e., $Q^* = Q/Q_0$, in which Q is the actual discharge. The quantity A* is flow area A referred to the product B_0Y_0, $A^* = A/B_0Y_0$. The reference depth Y_0 is chosen normal depth under base-flow conditions; the reference

breadth B_0 is the top width under normal base-flow conditions. Distance along the channel x is referred to a longitudinal scale X_0 characteristic of the channel under base-flow conditions. Thus $x^* = x/X_0$, in which

$$X_0 = \frac{Y_0}{S_0} \tag{3}$$

with S_0 the channel-bottom slope. Similarly, flow time t is referred to a characteristic time T_0 to yield dimensionless time $t^* = t/T_0$, in which

$$T_0 = \frac{X_0 Y_0 B_0}{Q_0} \tag{4}$$

The Froude number F^* is also characteristic of base-flow conditions and is defined

$$F^{*2} = \frac{Q_0^2}{g B_0^2 Y_0^3} \tag{5}$$

The quantity h^* represents dimensionless water-surface elevation, $h^* = h/Y_0$, with h the actual, dimensioned, surface elevation.

The last term on the left-hand side of Eq. 2 is the dimensionless resistance force per unit length. The coefficient K_D^* is given by the formula

$$K_D^{*2} = A^* R^{*4/3} \tag{6}$$

and is seen to be related to the dimensionless conveyance $K^* = A^* R^{*2/3}$. This follows from the definition of friction slope $S_f = Q^2/K^2$ as the ratio of drag force per unit length of channel, to stream weight, also per unit length of channel. In this last expression, K is the (dimensioned) conveyance. In Eq. 6, R^* is the dimensionless hydraulic radius

$$R^* = \frac{A^*}{W^*} \tag{7}$$

in which W^* is the dimensionless wetted perimeter, $W^* = W/B_0$, with W the actual, dimensioned, wetted perimeter. The quantity S_F^* is given by the equation

$$S_F^* = \frac{1}{S_0} \frac{Q_0^2 n^2}{C_u^2 B_0^2 Y_0^{10/3}} = A^{*2}(1)\ R^{*4/3}(1) = K^{*2}(1) \qquad (8)$$

in which n is the Manning n for the in-bank flow and C_u is a units coefficient in the Manning formula (C_u = 1.0 $m^{1/2}/s$ in the SI system; $C_u \simeq 1.486$ $ft^{1/2}/sec$ in the English system). In a channel of rectangular cross section,

$$S_F^* = \left(\frac{B_0}{W_0}\right)^{4/3} = \left(\frac{1}{1 + 2R_{YB}}\right)^{4/3} \qquad (9)$$

in which R_{YB} is the aspect ratio Y_0/B_0 of the rectangle under normal flow conditions; with a very broad rectangular channel $S_F^* = 1$, while narrower channels lead to smaller values of S_F^*. In any event S_F^* is seen to characterize the cross-sectional geometry from the point of view of bed resistance.

For a given configuration of channel cross section, Eqs. 1 and 2 are seen to contain just one free parameter, F*, embodying the combined influence of channel slope, roughness, and base flow.

The shape of the channel cross section is specified by a series of length ratios. A rectangular main-channel cross section is defined by R_{YB}, the aspect ratio of the rectangle, and by the bank-full depth, relative to normal depth in the channel at base-flow conditions, R_{DY}. The flood plain, if any, is characterized by R_{FPS}, its transverse bottom slope, relative to the aspect ratio of the main channel, and by R_{FPB} its width, relative to the width of the main channel. Further, the ratio of flood-plain Manning n to main-channel Manning n is given by the value R_{FPN}. The effect of the differing n values in flood plain and channel was accounted for by evaluating the conveyance of the entire cross section as the sum of the conveyances of main channel and flood plain computed separately.

In the given study, the channel cross-sectional geometry was characterized by the aspect ratio of main-channel depth to width,

$$R_{YB} = 0.1 \qquad (10)$$

When the effect of floodplains was studied, the values

$$R_{DY} = 1.0 \quad (11)$$

(bank-full depth in ratio to normal depth at the base flow);

$$R_{FPS} = 0.01 \quad (12)$$

(transverse flood-plain slope relative to aspect ratio of main channel);

$$R_{FPB} = 100 \quad (13)$$

(width of flood plain relative to width of main channel);

$$R_{FPN} = 5 \quad (14)$$

(flood-plain Manning n relative to main-channel n)
were assumed, in order to exaggerate these effects.

When the Froude number F* characteristic of a given base flow is very low, it can be set to zero in the governing equations. This results in the so-called zero-inertia model, because all terms involving fluid acceleration are deleted.

If the depth gradient $\partial y/\partial x$ is a very small fraction of the water-surface slope $\partial h/\partial x$, or in dimensionless terms, if $\partial y^*/\partial x^* << 1$, then each cross section has essentially uniform flow. Then a normal-depth stage-discharge relation holds for all cross sections, in dimensionless form, $Q^* = K^*/\sqrt{S_F^*}$. This, combined with the continuity equation yields a kinematic-wave model.

If flow-area profiles are obtained for a series of steady flows and integrated over reach lengths to yield storage volume as a function of discharge, and this is combined with the continuity equation, also integrated over reach length (see section 5.5), the result is a Modified-Puls technique. Evidently, if the flow-area profiles are obtained under uniform-flow conditions (long prismatic channel, arbitrary cross-sectional shape), and a sufficiently large number of subreaches are used, the results of this Modified-Puls technique and the normal-depth kinematic-wave model must agree.

In order to reduce the number of additional solution-governing variables to a minimum, inflow hydrographs were taken of fixed shape, and allowed to vary only in the ratio Q_p^* of peak discharge to base flow, and in dimensionless rise time $t_{Qp}^* = t_{Qp}/T_0$, in which t_{Qp} is the actual, dimensioned, time to peak. The form of the hydrograph is the so-called Pearson Type III, which is characterized by the equation

$$Q^* = 1 + (Q_p^* - 1)\left(\frac{t^*}{t_{Qp}^*}\right)^a e^{a\left(1 - \frac{t^*}{t_{Qp}^*}\right)} \tag{15}$$

in which the coefficient a is related to the skew s of the hydrograph by the equation

$$a = \frac{1}{s - 1} \tag{16}$$

In the studies reported, s was given the constant value

$$s = 1.2 \tag{17}$$

The downstream end of the channel, of dimensionless length $L^* = L/X_0$, was characterized by one of three boundary conditions: (a) a normal-depth stage-discharge relation, in dimensionless terms,

$$Q^* = K_D^* \sqrt{A^*} / \sqrt{S_F^*} \tag{18}$$

(b) a broad-crested weir of dimensionless height $p^* = p/Y_0$, leading to the following dimensionless relation between stage and discharge

$$y^* + \frac{Q^{*2}\,\mathbb{F}^{*2}}{2A^{*2}} = p^* + \frac{3}{2}\sqrt[3]{\frac{Q^{*2}\,\mathbb{F}^{*2}}{B_w^{*2}}} \tag{19}$$

In the derivation of this relationship (section 5.1.2), the breadth of the channel end section at elevations greater than the weir crest was assumed equal to that at the crest. In the studies reported herein, the dimensionless weir height, whenever a downstream weir was postulated, was held constant at

$$p^* = 2.0 \tag{20}$$

(c) a free overfall with a critical-depth stage-discharge relation, viz.,

$$Q^* = \frac{\sqrt{A^{*3}/B^*}}{\mathbb{F}^*} \tag{21}$$

formed the third downstream boundary condition tested.

3. Dimensionless parameters governing the outflow hydrograph.

Thus, taking into account both the governing equations and their boundary conditions, the dimensionless outflow hydrographs are determined once values are assigned to $\mathbb{F}^*$, Q_p^*, t_{Qp}^*, and L^*.

The graphs, Figs. 10 to 27, were prepared by selecting a series of characteristic Froude numbers F^*

$$0.1 < F^* < 0.8 \tag{22}$$

and letting the relative time to peak t_{Qp}^* vary in the range

$$0.5 < t_{Qp}^* < 20 \tag{23}$$

The ratio of peak inflow to base flow Q_p^* was held fixed at

$$Q_p^* = 5 \tag{24}$$

while the dimensionless reach length varied mostly in the range

$$1 < L^* < 4 \tag{25}$$

L^* was held to 1 or 2 with weir or overfall downstream, in order to exaggerate their effect.

The significance of these ranges can be seen by noting what they would mean in dimensional terms if applied to a channel of given cross section. For a given ratio R_{YB} of channel depth to width under normal conditions, Eqs. 3-5 can (using Eq. 9) be rewritten in the following form

$$Q_0 = \frac{\sqrt{g}\, F^*\, Y_0^{5/2}}{R_{YB}} \tag{26}$$

$$S_0 = \frac{g\, F^{*2}\, n^2 (1 + 2R_{YB})^{4/3}}{C_u^{\,2}\, Y_0^{1/3}} \tag{27}$$

$$X_0 = \frac{Y_0^{4/3}\, C_u^{\,2}}{(1 + 2R_{YB})^{4/3}\, g\, F^{*2}\, n^2} \tag{28}$$

$$T_0 = \frac{Y_0^{5/6}\, C_u^{\,2}}{(1 + 2R_{YB})^{4/3}\, g^{3/2}\, F^{*3}\, n^2} = \frac{Y_0^{1/2}}{g^{1/2}\, S_0\, F^*} \tag{29}$$

For example, in a channel of rectangular cross section with normal depth Y_0 = 10 feet, breadth B_0 = 100 feet, and Manning n = 0.03, a given choice of F^* corresponds to the following values of characteristic time T_0, characteristic distance X_0, base flow Q_0, and bottom slope S_0.

Table 1. Example Dimensional Values.

F*	T_0	X_0(miles)	Q_0(cfs)	S_0
0.1	20 hrs	24	1,790	0.00008
0.2	2.5 hrs	6.1	3,590	0.0003
0.3	0.74 hrs	2.7	5,380	0.0007
0.4	19 min	1.5	7,180	0.0012
0.5	9.6 min	0.98	8,970	0.0019
0.6	5.5 min	0.68	10,800	0.0028
0.7	3.5 min	0.50	12,600	0.0038
0.8	2.3 min	0.38	14,400	0.0050

Thus, with this channel cross section, a chosen parameter F* = 0.2, t_{Qp}^* = 10 would correspond to a base flow of about 3600 cfs, a peak inflow of 18,000 cfs and a time to peak of about 25 hours. At L* = 4, the outflow hydrograph would pertain to a station 24.4 miles downstream of the inflow.

4. Analysis of results.

The dimensionless plots of hydrograph peaks shown in Figs. 10 - 27 can be analyzed from several different points of view. (a) The results of the complete hydrodynamic model can be viewed as indicating the general behavior of floodwave speed and attenuation as functions of base-flow and flood-event characteristics. (b) Results of the simpler models show what stream and event parameters appear to affect flood-wave attenuation when certain hydraulic phenomena are ignored. (c) Intermodel comparisons shed light on the nature of some of the simpler models, and (d) delineate useful ranges for application of such models. The emphasis of the present work is directed to the last two areas.

4.1 Floodwave speed and attenuation--an overview.

The accuracy of the complete hydrodynamic model is limited only by its assumption of one dimensionality, i.e., a level water surface transverse to the flow and an essentially uniform velocity distribution. These assumptions, while questionable in the event of overbank flow, are well met in channels of simple cross section. Other errors, stemming from finite computational time and distance increments or nonhydrostatic pressure distribution are negligible. Thus the curves do represent the true behavior of flood peaks, especially in channels of simple section.

It may be possible to derive empirical formulas describing this behavior, or to generalize it still further by use of appropriate scaling factors for abscissa and ordinate, but this is not the primary concern here, and was not attempted.

It is evident, from the curves presented, that attenuation decreases with increasing base-flow Froude number, regardless of how that is achieved (steeper slope, smaller roughness, or greater discharge). As expected, attenuation increases with increasing relative sharpness of the flood wave, i.e., as inflow-hydrograph rise time decreases or characteristic time increases (see section 4.4). The rate of attenuation with distance is relatively unaffected by reach length once it is in excess of some minimum. Of course, attenuation is greatly enhanced in the event of extensive overbank flooding.

With dimensionless rise times in excess of about 10, attenuation is very small in the rectangular channel with normal-depth rating curve at the downstream end (Fig. 10). With the weir downstream, similar small attenuation occurs with rise times perhaps half that size (Fig. 11). The overfall downstream causes similar behavior (Fig. 12). With the floodplain, significant attenuation was achieved at the largest rise time tested, $t_{Q_p}^* = 20$ (Fig. 13).

Stage peaks exhibit less attenuation than discharge peaks, especially with the floodplain. They are less sensitive to Froude number (Figs. 16-21).

The effect of the downstream boundary is to pull up the discharge peaks at channel end slightly (Figs. 10-15). With normal-depth, and weir rating curves downstream, peak stages are brought up somewhat, and sharply, respectively, near the channel end; the overfall of course produces the opposite effect (Figs. 16-21).

Speed of propagation of hydrograph peaks remains consistently nearly equal to the wave speed (Figs. 22-27)

$$w \tilde{=} \frac{\partial Q}{\partial A} \tilde{=} L \frac{dQ_0}{dV} \qquad (30)$$

i.e., travel time,

$$t_T \tilde{=} \frac{dV}{dQ_0} \qquad (30a)$$

Note the ten-fold larger time scale used in the graphs for the floodplain, to accommodate the very great dispersal of the wave in this case.

4.2 Flood-wave characteristics as computed with simple models.

The influence of channel bottom slope, roughness, and base flow is manifested in the dimensionless governing differential equations only through the base-flow Froude number F^*. In the zero-inertia, kinematic-wave, and Modified-Puls techniques, with a normal-depth stage-discharge downstream boundary condition, this parameter is totally absent. Thus, hydrograph-peak attenuation is independent of base-flow Froude number. It is affected only by the dimensionless inflow hydrograph, as characterized by peak and rise time. Speed of propagation in the kinematic-wave or Modified-Puls method is independent of both the Froude number and the inflow hydrograph rise time.

In the Modified-Puls technique, base-flow Froude number plays a small role with weir and free-overfall downstream boundary conditions, because it affects, somewhat, the shapes of the succession of steady-flow profiles from which storage-outflow curves are drawn.

With a normal-depth downstream boundary condition, the kinematic-wave and Modified-Puls approaches yield attenuation with distance from the upstream end, independent of total reach length. In other words, the wave behavior at any point is governed solely by conditions upstream from that point.

With the weir or free-overfall downstream boundary conditions, as the channel becomes very long, it begins to behave like one with a normal-depth downstream boundary condition.

4.3 The Modified-Puls method in the light of kinematic-wave theory.

All of the flood-routing techniques studied involve numerical integration or differentiation over finite increments of distance or time, or both. Generally speaking, the smaller are these increments, the more accurate are the results. Furthermore, as step sizes are reduced, the results approach limiting values; further reductions in step size lead to no further significant changes in results. At such time, it can be said that the results reflect the basic assumptions of the technique, rather than the numerical accuracy with which that technique is carried out. In the studies described, step sizes were indeed reduced to the point that the results became, for practical purposes, independent of step size.

The one exception to this general rule was seen with the Modified-Puls method. At its foundation, the Modified-Puls technique differs from the others, in that in concept it is based on a presupposed relation between storage in a finite, perhaps very long, reach and the outflow from the downstream end of that reach. All of the other techniques have as a basis, some given relationship between depth and discharge variations locally. This can be expressed algebraically, if depth and discharge profile shapes, say straight lines, are assumed over a short span (as in sections 5.1-5.3). The total reach length of interest and total time of interest are covered by simultaneous or sequential solution of the algebraic equations written for each sub-span.

As stated, the smaller are the sub-spans, the more nearly are the actual profiles linear over a sub-span, and the more accurate are the solutions of the governing algebraic equations.

The Modified-Puls method is like this in time only. And as the time step is reduced, the calculated hydrographs rapidly approach a limit; this is essentially what appears in the plots presented. In a variation of the Modified-Puls method tested in this study, however, storage-outflow relations were prepared for sub-reaches of the main reach by apportioning the total volume in the channel, computed for each steady-state discharge, equally amongst the subreaches. Thus each subreach is provided with a storage-outflow relation.

In one sense, the computed storage is prism storage only, because it is assumed to depend on outflow only, rather than upon inflow also, as in the case of wedge and prism storage. On the other hand, because the steady-state profiles which are integrated to yield the storage values are not necessarily profiles of uniform flow--note the varied-flow profiles behind the weir (M1) (Figs. 1a,b) and overfall (M2) (Fig. 1c)--the water volumes computed are not really prismatic in shape. Still, a rapidly rising floodwave, in a channel of finite cross-sectional proportions, would yield an additional wedge component not computed in the given variant of Modified-Puls. In reservoir routing, for which the technique originated, the pool, of course, remains essentially level during passage of floods and prism storage of the type computed is all that, in fact, exists. This is the situation approached in the flood flow behind weir and overfall, especially for the slowly rising inflow hydrographs.

In any event, as the number of sub-reaches is increased, it is evident that the channel is ever more nearly being provided with cross-sectional area vs. discharge, Q(A), relationships for a series of stations along the channel,

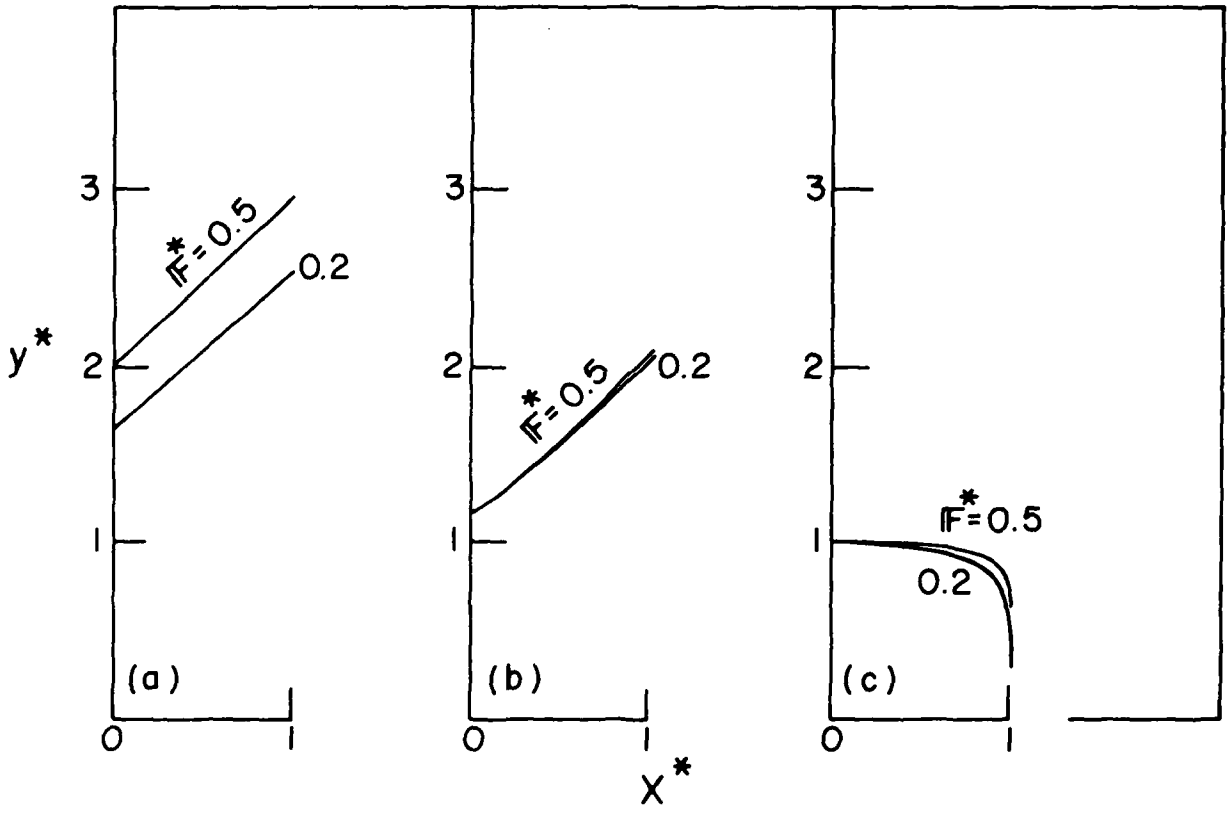

Fig. 1. Initial conditions. Base-flow depth profiles.

(a) Rectangular Channel, Weir Downstream Boundary Condition.

(b) Channel with Floodplain, Weir Downstream Boundary Condition.

(c) Rectangular Channel and Channel with Floodplain, Overfall Downstream Boundary Condition.

leading thereby to a kinematic-wave analysis (section 5.4). Indeed the resulting behavior of hydrograph peaks more and more nearly approaches the results of a pure kinematic-wave analysis. In fact computed attenuation of the wave can be reduced to any amount desired (presumably up to that dictated by the formation of kinematic shocks--see section 5.4.2) by a suitable choice of sub-reach length.

An examination of the peak-attenuation curves shows that, empirically, there appears to be a dimensionless sub-reach length δx^*, that yields an attenuation closest to that of the standard, as given by the complete hydrodynamic model. This "optimum" value is generally in the range

$$0.3 < \delta x_o^* < 1.0 \tag{31}$$

The reader is cautioned that this information is strictly empirical; no theoretical basis has been found for the existence of such an "optimal" value. Nothing can be said about δx_o^* for conditions outside of those tested.

Apart from these purely empirical considerations, theoretical questions arise: (a) does decreasing sub-reach length in the Modified-Puls method yield more accurate results, and (b) does decreasing sub-reach length yield results more nearly in accord with the basic assumptions of the Modified-Puls method. The answer to both questions, in general, is: no. For if one were to apply this sub-reach volume apportionment to the case of a real, large reservoir, which maintained a truly level surface during passage of a flood, the computed attenuation would be smaller than the true one, the difference being greater as the number of subreaches increased (and as the rise time decreased). The true attenuation would be computed in this case by the Modified-Puls method with δx_o equal to the entire reservoir length.

Furthermore, decreasing sub-reach length doesn't necessarily reflect the basic assumptions of the Modified-Puls method more closely. The key assumption in this method is the existence of a known relationship between storage in

a reach (or subreach) and discharge at the end of that reach (or subreach). The given method of apportioning storage amongst subreaches gives a relationship between storage in a subreach and discharge, not at the end of that subreach, but at the end of the entire reach. Except for floods that rise so slowly (say, $tQ_p^* > 20$) that the flow in the entire reach can be viewed as a succession of steady states, discharge is not the same at all stations, and so the storage-discharge relation postulated for the subreaches will be in error. Only if the flow is locally controlled, say essentially at normal depth for the local discharge, will the storage-discharge relation be correct for the subreaches, i.e., within the context of the Modified-Puls assumptions. In that case, the flow conditions satisfy the key assumption of the kinematic-wave procedure, namely, there is a (known) stage-discharge relationship at each cross section. Consequently, there is no attenuation other than that engendered by formation of kinematic shocks, and the Modified-Puls method would yield the most accurate results with the largest number of subreaches (because only prism storage is accounted for, even 99 subreaches, the largest number that could be handled by the present computer programming, were insufficient to mimic exactly the results of true kinematic-wave analysis [see e.g., Fig. 13d]). Thus, subdivision of the reach reduces the inevitable attenuation that occurs with the Modified-Puls method.

In conclusion, the following may be stated about the Modified-Puls method and apportioning of steady-state varied-flow-profile storage to subreaches. For flow that is heavily controlled from downstream, in the limit a large reservoir with outflow, Modified-Puls should work well with the full length of the reach used, without subdivision. For flow that is controlled locally (e.g., depth gradient negligible), if Modified-Puls is to be used, the larger the number of subdivisions the better. For the flow in this case

would be truly modeled by kinematic-wave analysis, and this is approached by Modified-Puls with a very large number of subdivisions.

In most cases, even without a controlling hydraulic structure downstream, simply with so-called friction control, a normal-depth downstream boundary condition, the relation between depth and discharge at a given section depends upon conditions in neighboring portions of the channel. Neither kinematic-wave nor Modified-Puls basic assumptions are satisfied. As mentioned earlier, empirical evidence shows that the Modified-Puls method with the reach subdivided can yield attenuation of flood-wave peaks close to that observed.

4.4 Intermodel comparisons.

In interpreting the peak-attenuation curves, the significance of the dimensionless parameters should not be overlooked. The characteristic distance and time to which real distance and time are referred to yield their dimensionless counterparts are defined by Eqs. 3 and 4 in section 3; the characteristic Froude number is defined by Eq. 5. These variables are viewed again in Eqs. 26 - 29. It is seen, for example, through combination of Eqs. 27 and 29, that

$$T_0 = \frac{Y_0^{1/2}}{g^{1/2} S_0 \, IF^*} \tag{32}$$

Thus, the steepness of a channel is manifested in these curves not only in the Froude number of flow, but in the characteristic time and distance as well. A given real time of rise has, typically, a larger $t_{Q_p}{}^*$ in a steep channel, than a flat one.

An overview of the figures suggests that for a given channel geometry, the most significant parameter affecting the behavior of a flood wave, or the accuracy of its computation by one or another method, is the dimensionless

rise time t_{Q_p}*, and when this is small, $\mathbb{F}$* as well. The ratio Q_p* of peak discharge to base flow is distinctly of secondary importance. In addition to the evidence offered by comparison, for example, of Figs. 13d and 13g, the following approximate analysis is helpful in explanation. In a channel of broad rectangular cross section, the characteristic depth is given by

$$Y_0 = \left(\frac{q_0 \, n}{C_u \sqrt{S_0}} \right)^{3/5}$$

in which q_0 is the base flow per unit width of channel. In accord with Eqs. 3 - 5, the remaining characteristic parameters are

$$X_o = \frac{q_0^{3/5} \left(\frac{n}{C_u} \right)^{3/5}}{S_0^{13/10}}$$

$$T_0 = \frac{q_0^{1/5} \left(\frac{n}{C_u} \right)^{6/5}}{S_0^{8/5}}$$

$$\mathbb{F}^* = \frac{q_0^{1/10}}{g^{1/2}} \left(\frac{\sqrt{S_0}}{n/C_u} \right)^{9/10}$$

For a given peak flood discharge, doubling the base flow would change t_{Q_p}* by only 15% and the Froude number by but 7%. Even a 10-fold increase in base flow decreases t_{Q_p}* by just over one third (37%), and increases $\mathbb{F}$* by only 20%. While L* is inversely proportional to the 3/5 power of base flow, dimensionless reach length, as discussed previously, is not a very important factor.

In the channel with floodplains, the effect of characteristic Froude number $\mathbb{F}$* was seen to be negligible; in the rectangular channel $\mathbb{F}$* played a significant role only for t_{Q_p}* < 2. The range of base-flow Froude numbers for

which the zero-inertia model yields useful results increases as the time to peak of the inflow hydrograph increases. As evident in Fig. 10, with $t_{Q_p}^* = 0.5$, the zero-inertia model yields good accuracy for $F^* < 0.2$; at $t_{Q_p}^* = 1.0$, the same accuracy is achieved at $F^* < 0.3$; at $t_{Q_p}^* = 2.0$, all $F^* < 0.4$ yield good results with the zero-inertia model. Figure 13 shows that in the channel with a flood plain, zero-inertia analysis was suitable for all flows with F^* less than 0.5 at least.

The "optimum" δx^* for application of the Modified-Puls method varied somewhat with the nature of the channel cross section, the downstream boundary condition, and the inflow hydrograph rise time. The discharge-attenuation curves with Modified Puls do not always follow, exactly, the trend of the hydrodynamic solutions. Thus, selection of an optimum δx^* emphasizes the value of hydrograph peak at the end of the channel reach.

Figures 10 and 13 show that with a normal-depth downstream boundary condition, $\delta x_o^* \approx 0.35$ with a floodplain, and perhaps twice that value in the rectangular channel. With the weir downstream boundary (Figs. 11, 14), $\delta x_o^* \approx 0.4 - 0.5$ with the floodplain, and $0.7 < \delta x_o^* < 1.0$ in the rectangular channel, the larger values appropriate to rise times greater than about unity. With a floodplain and the overfall downstream, δx_o^* lay between about 0.22 - 0.30, the larger values pertinent by and large to the larger rise times (Fig. 15). In the rectangular channel δx_o^* is around 0.33 - 0.5 for $t_{Q_p}^* = 0.5$ and increases to 0.7 for $t_{Q_p}^* = 1.0$. At $t_{Q_p}^* = 2.0$, $\delta x_o^* \simeq 0.5$ to model $F^* = 0.2$, and $\delta x_o^* = 1.0$ to represent $F^* = 0.5$ well. At $t_{Q_p}^* = 5.0$, there is very little attenuation, and $\delta x_o^* = 1.0$ worked well for both Froude numbers.

An examination of the attenuation of stage peaks (Figs. 16-21) shows, first, that stage attenuation is far smaller than discharge attenuation. Second, it is much less sensitive to Froude number, and finally, it is less sensitive to choice of δx^* in the Modified-Puls method.

Time of arrival (Figs. 22-27) is relatively uninfluenced by δx^*, provided only that the latter is less than about 2. A value of $\delta x^* = 0.5$ leads to close approximation of the travel time in most cases.

An overview of Figs. 10-15 explains the mixed success with which the Modified-Puls method is used in practice. In floods without overbank flow a small dimensionless rise time ($t_{Q_p}{}^* < 2$) leads to true attenuation dependent upon normal Froude number F^*. The band of correct solutions $Q_m{}^* (x^*, t_{Q_p}{}^*, F^*, \ldots)$ gets narrower and narrower with increasing $t_{Q_p}{}^*$, so that with $t_{Q_p}{}^* > 5$, attenuation is virtually independent of F^* (as well as very small). The band of solutions $Q_{m_{M_i}}{}^* (x^*, t_{Q_p}{}^*, \delta x^*, \ldots)$, showing attenuation computed by the Modified Puls method, is more spread out with various δx^* at $t_{Q_p}{}^* = 1.0$ than at $t_{Q_p}{}^* = 0.5$. But then, with further increases in $t_{Q_p}{}^*$, the dependence upon δx^* diminishes, and the band of solutions gets narrower and narrower, squeezed mostly into the ever smaller region between the correct attenuation curve and zero attenuation. At small $t_{Q_p}{}^*$, then, a choice of δx^* can be made with the Modified Puls method that will reflect correct attenuation for the given Froude number. At large $t_{Q_p}{}^*$, the (very small) attenuation can be computed with little regard for δx^*.

With overbank flooding, these circumstances with regard to δx^* are somewhat exaggerated. The influence of F^* upon the true solution is negligible, especially with a normal-depth rating curve downstream. However, at small $t_{Q_p}{}^*$, the influence of δx^* in the Modified Puls method is also minimal. The width of the solution band $Q_{m_{MP}}{}^* (x^*, t_{Q_p}{}^*, \delta x^*, \ldots)$ is still very narrow at $t_{Q_p}{}^* < 1$. In this range Modified Puls can work very well without careful

choice of δx^*. As $t_{Q_p}{}^*$ increases, band width increases--without limit at least to $t_{Q_p}{}^* = 20$ with the normal-depth downstream rating curve. In this range, successful use of Modified Puls requires a good choice for δx^*. Under the conditions tested, this appears to be about $\delta x_0{}^* \approx 0.35$ (0.25 for the overfall downstream). However, because the observed close correlation between the true physical attenuation and the computed mathematical attenuation of the Modified Puls method is entirely empirical, it may well fail to persist under different conditions. Optimal values of $\delta x_0{}^*$ may well be different. The influence of $Q_p{}^*$ and L^* appears to be minimal, but other, geometric, factors may play a role.

With very large dimensionless rise times ($t_{Q_p}{}^* > 20$), at least with weir or overfall downstream rating curves, the very small attenuation again compresses the Modified-Puls-solution band width, so that successful computation can be performed without much regard for the size of δx^*.

4.5 Sample application.

The user contemplates routing a hydrograph peak of 24,000 cfs, over a reach of 60 miles down a river in which the base-flow prior to the flood is $Q_0 = 1400$ cfs. The inflow hydrograph rises to its peak value in about 2 1/2 days. The average slope of the channel is 0.5 feet per mile. The river channel, approximated by a rectangle, is 300 feet across and 6 feet deep when bank full. Overflow spills into the floodplains, sloping laterally at approximately 1 foot per mile. Manning n in the floodplains is estimated at 0.05.

At the flow of 1400 cfs, the average depth is 5 feet. The Manning n for the main channel is evidently $n = 0.044$. Froude number of the base flow, assuming normal depth, is $F_0 = 0.07$.

The characteristic distance is (Eq. 3) X_0 = 52,800 = 10 miles; characteristic time is (Eq. 4) T_0 = 56,571 sec = 15.71 hours; dimensionless time to peak is t_{Q_p}* = 2.5 * 24/15.71 = 3.82.

Examination of Figs. 10c and 10d, for channels of aspect ratio 0.1 (as oposed to the given channel of about 0.02, or less when the flood plains are inundated), and t_{Q_p}* = 2 and 5 respectively (as opposed to 3.82 in the given case) suggests that the zero-inertia model would be entirely accurate, and that the kinematic-wave model would be grossly inaccurate. Modified-Puls with distance steps of about 10 miles may yield adequate outflow discharge peaks. Figures 13c and d, depicting similar rise times in a channel with floodplains, also show that the zero-inertia model should give excellent results. With the Modified-Puls method, dimensionless distance steps of about 0.3, i.e., steps of about 3 miles, would appear to give adequate results. It is difficult to estimate a suitable distance step for this method.

Figure 2 shows computed peaks obtained for the given case by way of the Saint-Venant equations, the zero-inertia model, and Modified Puls with distance steps of 3, 5, and 10 miles, supporting the predictions made. The zero-inertia model is seen to give results virtually identical to those of the complete hydrodynamic model, as expected. The Modified-Puls method gives reasonably good results with an appropriate choice of distance step, but it is difficult to predict that optimum size.

4.6 Conclusions.

The actual passage of a natural flood down a river is governed by the complete hydrodynamic equations of flow, i.e., the one-dimensional Saint-Venant equations of continuity and motion. Additionally, two-dimensional terms and equations may be needed to describe greatly different flow parameters in main channel and floodplains or gradual lateral inundation of the floodplains,

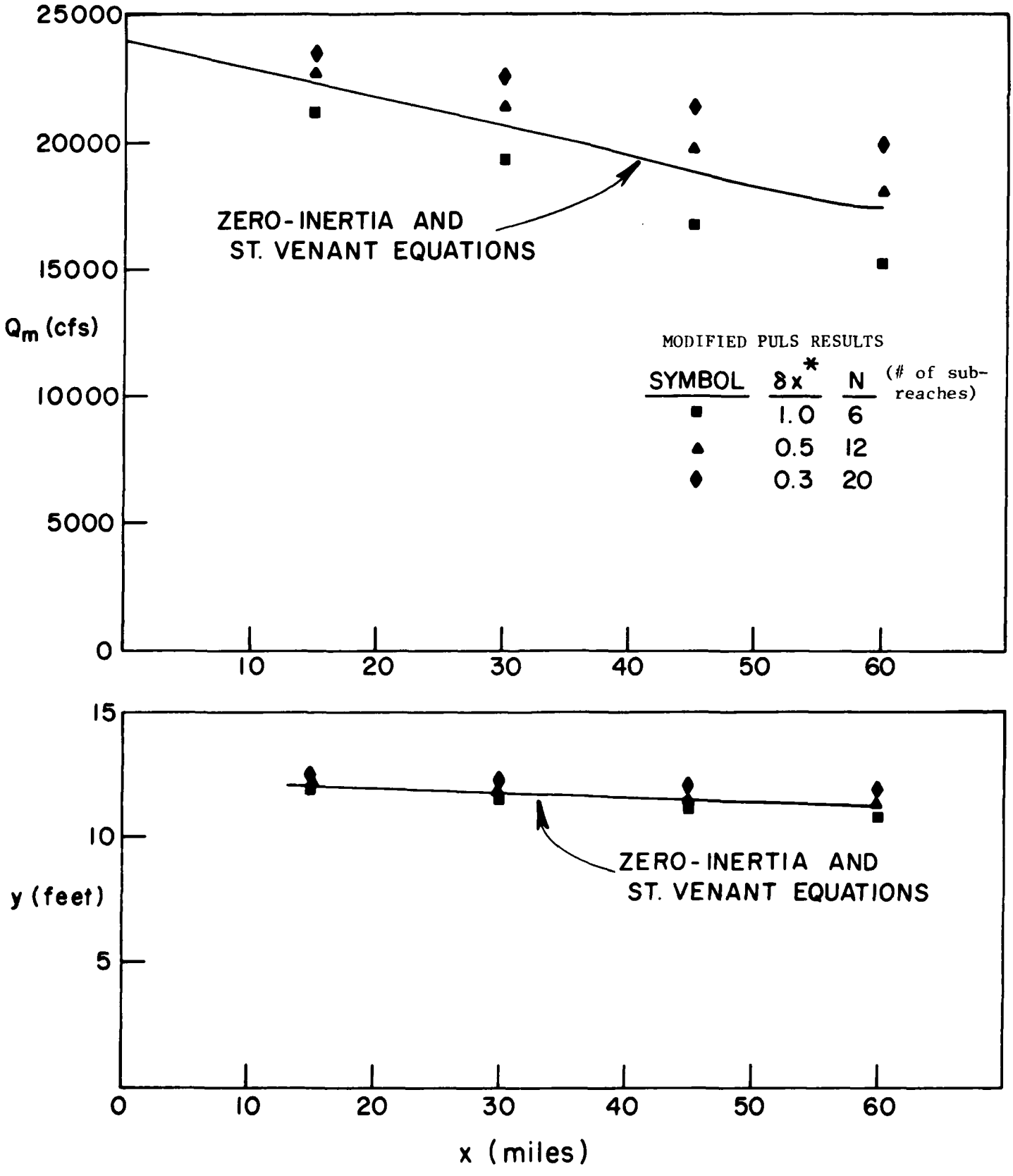

Fig. 2. Test case solution.

rather than the instantaneous flooding implied by the laterally horizontal free surface assumed in the one-dimensional model.

Any physically based routing model takes cognizance of these equations, either directly or indirectly. In the present study, two-dimensional effects have been ignored, and the one-dimensional equations of Saint-Venant have been assumed adequately to represent the physical circumstances. Solutions of these equations are hence taken as standards, against which other models can be measured.

The zero-inertia model is seen in many cases to yield results very close to those of the standard. The graphs of Figs. 10-15 show that only at relatively small values of dimensionless rise time, say $t_{Q_p}^* \leq 2$, is the steady-state base-flow normal-depth Froude number a significant variable. And even then, if it is low, the zero-inertia model will yield satisfactory results.

The kinematic-wave model with a normal-depth stage-discharge relationship postulated at all stations has deleted from the motion equation not only the acceleration terms, but also the effect of the depth gradient. Despite the incidence of kinematic shocks, which can cause a predicted flood-peak subsidence, in the natural floods studied, only those floods with dimensionless rise times in excess of about 10, which exhibit practically no subsidence, are well modelled by kinematic-wave theory. This limit applies only to the channel without floodplains; in the opposite case, even with a rise time of 20, the largest tested with a normal-depth rating curve downstream, subsidence was substantially greater than that predicted by kinematic-wave analysis. The reader is reminded that large dimensionless rise times are typically associated with smooth, steep channels with large base-flow Froude numbers (see the second of Eqs. 29).

The Modified-Puls method is often characterized as one utilizing the continuity equation alone, but it too is dependent in one way or another upon the equation(s) of motion as well. The storage-outflow relation used in conjunction with the inflow-outflow-storage-rate equation (continuity), whether obtained empirically from past flood events, or hypothetically from steady-flow backwater curves, contains inherently one or another dynamic relationship. The empirical relation contains all the terms of the complete Saint-Venant equations in the proportions in which they existed for that particular event. The hypothetical ones reflect only those terms which were retained for the analysis.

The Modified-Puls method based upon an empirically derived storage-outflow relationship, stemming from actual past flood events in the given reach, can yield results superior to the variant, based on steady-state profiles for various discharge rates, tested here. In this latter case, the storage-outflow curve for a real flood event will agree with the hypothetical one only if the contribution of the unsteadiness of the flow to $\partial V/\partial t$, $V\partial V/\partial x$, and $\partial y/\partial x$ is very small, compared to the contribution to the last two terms by the nonuniformity of the flow. Such is evidently the case with short channels and a weir or free-overfall downstream boundary condition, especially for a flood event with a large rise time. Empirically gathered data, on the other hand, yield a storage-outflow relationship that is absolutely correct, for *that particular event*. Provided the various terms in the motion equation retain about the same values each time a given outflow from the reach is attained, the storage-outflow relation will remain unchanged. Once measured, it can be used confidently for all future floods of that magnitude, the Modified-Puls method applied, furthermore, to the full length of the reach, without subdivision into subreaches.

With the storage-outflow relationship obtained theoretically through a succession of steady-state profiles, the Modified-Puls method can yield reasonably good results with an appropriate choice of distance step, but it is difficult to predict that optimum size. The difficulty arises because there is no rational correlation between the mathematical attenuation of the Modified-Puls method, and the physical attenuation predicted by the hydrodynamic or zero-inertia models. The former is a continuous function of distance-step (sub-reach) size, while the latter is independent of step size, once this is small enough to make truncation errors insignificant.

As regards arrival time of the flood peak, the correct value, given by solution of the Saint-Venant equations, is considerably greater than that based on the celerity of an infinitessimal gravity wave, as computed by the same equations, $c = \sqrt{gA/B}$. Solution of the zero-inertia equations leads in most cases, as indicated, also to the correct value of arrival time, in contrast to the instantaneous arrival of an infinitessimal wave predicted by this model. Kinematic-wave theory leads, on the other hand, to about the correct arrival time independent of wave height. The Modified-Puls method as described, predicts relatively small arrival times. In the case of the channel with floodplains, with no subdivision of the reach (N = 1), even when Q_{max} was predicted with fair accuracy, the time of arrival of the peak was very, very early, with up to 90% error. The predicted time of arrival gradually approaches the correct value as the number of subreaches is increased, with good results generally obtained at $\delta x^* = 0.5$.

5. Derivation of the governing equations.

5.1 Complete one-dimensional hydrodynamic equations.

5.1.1 Equations governing flow in a subreach.

Although the present study excluded nonprismatic channels and tributary inflows, the governing equations are derived, for completeness, with these features included.

The physical principles of mass and momentum conservation are expressed for a subreach of small (not necessarily infinitessimal) length δx. With reference to Fig. 3, conditions pertinent to the left-hand cross section at some time t are subscripted L, those for the right-hand cross section at the same time are subscripted R. At a time slightly earlier than t ($t - \delta t$ with δt small, not necessarily infinitessimal) the left and right stations are subscripted J and M, respectively. If δx is sufficiently small, then over that span, the water-surface profile can be assumed straight, as can the variation of the cross-sectional area, with distance.

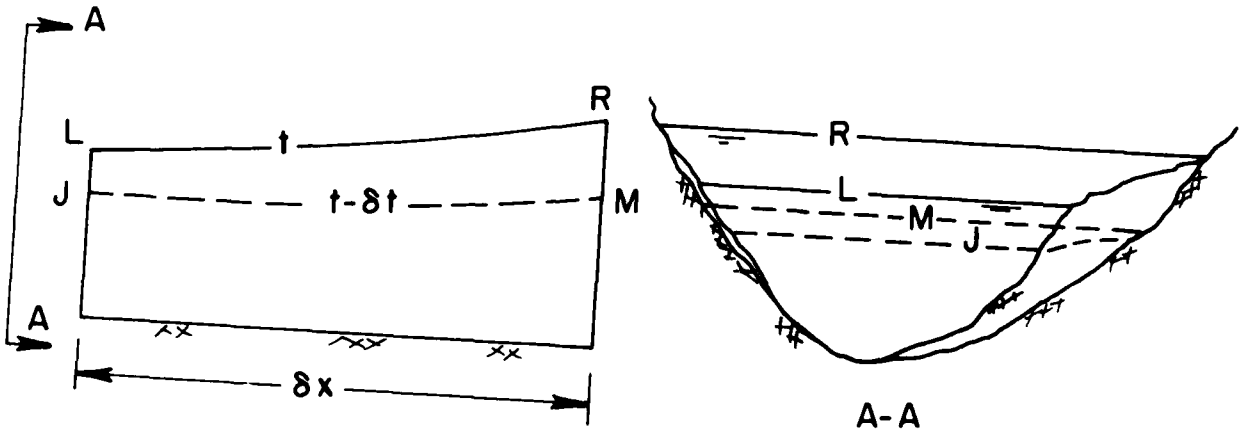

Fig. 3. Elementary water volume.

Expression of mass conservation for a fluid of negligible compressibility contained between the given left and right cross sections is

$$[\theta(Q_L - Q_R + q_{LR}\,\delta x) + (1 - \theta)(Q_J - Q_M + q_{JM}\,\delta x)]\delta t$$

$$= \left[\left(\frac{A_L + A_R}{2}\right) - \left(\frac{A_J + A_M}{2}\right)\right]\delta x \qquad (33)$$

Q is channel discharge, q is lateral (tributary) inflow per unit length, and A is cross-sectional area. Provided that discharge is assumed to vary linearly with time over the interval δt, the weighting factor θ should, for precision, equal one half. The stability of the numerical scheme which expresses mass and momentum conservation over large times and distances, however, requires $\theta > 1/2$. In computations it is set as close to 1/2 as will yield relatively

smooth hydrographs and profiles, but never exceeds unity. In the present study, except as noted, this weighting factor was held constant at

$$\theta = 0.6 \tag{34}$$

The double subscript LR refers to the average value taken over the length of the increment δx, at time t, while JM corresponds to the average value at $t - \delta t$.

Momentum conservation, or more properly an impulse-momentum relationship, can be written for the same changing volume of water over the same period of time, as follows.

$$\left\{\theta\left(\gamma\left[P_L + R_{x_{LR}}\,\delta x - P_R\right] + \rho\left[\frac{Q_L^2}{A_L} + u_{LR}\,q_{LR}\,\delta x - \frac{Q_R^2}{A_R}\right] + \gamma\frac{(A_L + A_R)}{2}(z_{0_L} - z_{0_R})\right.\right.$$

$$\left. - \gamma\, D_{LR}\,\delta x\right) + (1 - \theta)\left(\gamma\left[P_J + R_{x_{JM}}\,\delta x - P_M\right] + \rho\left[\frac{Q_J^2}{A_J} + u_{JM}\,q_{JM}\,\delta x - \frac{Q_M^2}{A_M}\right]\right.$$

$$\left.\left. + \frac{A_J + A_M}{2}(z_{0_L} - z_{0_R}) - D_{JM}\,\delta x\right)\right\}\delta t = \rho\left\{\frac{Q_L + Q_R}{2} - \frac{Q_J + Q_M}{2}\right\}\delta x \tag{35}$$

The hydrostatic pressure force on a cross section is given by γP, in which

$$P = \int_0^y (y - \eta)\, B(\eta, x)\, d\eta \tag{36}$$

with B the breadth of the channel at any elevation η above bottom. In a prismatic channel, the dependence of B on x vanishes. In a nonprismatic channel, the pressures on the sidewalls have a component in the direction of flow $\gamma R_x\,\delta x$, in which

$$R_x = \int_0^{\bar{y}} (\bar{y} - \eta)\frac{\partial B(\eta, x)}{\partial x}\, d\eta \tag{37}$$

Accordingly,

$$P(x) + R_x \delta x - P(x + \delta x) = (R_x - \frac{\partial P}{\partial x}) \delta x = \bar{A} \frac{\partial y}{\partial x} \delta x \qquad (38)$$

The bar over a variable implies an average value over the length δx.

The net pressure and weight forces can evidently be combined into a single term involving the longitudinal change in water-surface elevation, e.g.,

$$\gamma\left[P_L + R_{x_{LR}} \delta x - P_R + \frac{A_L + A_R}{2} (z_{0_L} - z_{0_R})\right] = \gamma \frac{A_L + A_R}{2} (h_L - h_R) \qquad (39)$$

The momentum flux $\rho Q^2/A$ is computed on the assumption that the flow is distributed uniformly over the entire cross section, flood plains included. The momentum flux entering the volume element with tributary inflow is assumed distributed over the length of the element δx; the volumetric inflow rate is q per unit length of channel, and the momentum brought in thereby per unit volume is ρu, with u the longitudinal component of velocity possessed by the tributary inflow. The momentum content, per unit length, of the volume element lying between the given cross sections, is the mass of the element per unit length, ρA, multiplied by the momentum per unit mass V, i.e., ρQ; consequently the momentum content of the element at any time is $\rho \bar{Q} \delta x$.

The average drag of the channel walls over the length δx is given by

$$\gamma \bar{D} = \gamma \frac{\bar{Q}|\bar{Q}|}{\bar{K}_D^2} \qquad (40)$$

in which $1/K_D^2$ is a drag coefficient dependent upon the cross-sectional flow geometry and roughness of the bed. It is related to the conveyance K of the channel, as follows

$$K_D^2 = K^2/A = A C_h^2 R \qquad (41)$$

in which R is the hydraulic radius, and the Chezy C_h is given by the Manning formula

$$C_h = \frac{C_u}{n} R^{1/6} \tag{42}$$

with C_u a units coefficient: $C_u = 1.0\ m^{1/2}/s$ in the metric system; $C_u \simeq 1.486\ ft^{1/2}/sec$ in the English system. In a composite cross section, K is assumed the sum of the individual conveyances of the main channel and flood plains.

With Eqs. 39 and 40 in force and following division by $\gamma\,\delta t$ (δt in the case of Eq. 33), Eqs. 33 and 35 can be written

$$\theta(Q_L - Q_R + q_{LR}\,\delta x) + (1 - \theta)(Q_J - Q_M + q_{JM}\,\delta x) = \left(\frac{A_L + A_R}{2} - \frac{A_J + A_M}{2}\right)\frac{\delta x}{\delta t} \tag{43}$$

$$\theta\left[\frac{A_L + A_R}{2}(h_L - h_R) + \frac{1}{g}\left(\frac{Q_L^2}{A_L} - \frac{Q_R^2}{A_R} + u_{LR}\,q_{LR}\,\delta x\right) - D_{LR}\,\delta x\right]$$

$$+ (1 - \theta)\left[\frac{A_J + A_M}{2}(h_J - h_M) + \frac{1}{g}\left(\frac{Q_J^2}{A_J} - \frac{Q_M^2}{A_M} + u_{MJ}\,q_{MJ}\,\delta x\right) - D_{JM}\,\delta x\right]$$

$$= \frac{1}{g}\left[\frac{Q_L + Q_R}{2} - \frac{Q_J + Q_M}{2}\right]\frac{\delta x}{\delta t} \tag{44}$$

5.1.2 Downstream boundary conditions.

With the equations of mass and momentum conservation given for all subreaches, and with initial conditions specified as steady state with the base flow, and with the upstream boundary condition given by the inflow hydrograph, the remaining factor governing the outflow hydrograph is the downstream boundary condition at x = L.

A normal-depth stage-discharge relation there is given by

$$D = A\,S_0 \tag{45}$$

in which S_0 is the bottom slope.

A broad-crested weir at the downstream boundary of a reach implies critical depth on its crest. The depth y and discharge Q at the downstream end of the subreach just upstream from the weir, of height p above channel bottom, is given by the relation,

$$y + \frac{Q^2}{2gA^2} = p + \frac{3}{2}\left(\frac{Q^2}{B_W^2 g}\right)^{1/3} \tag{46}$$

in which B_W is the breadth of the channel at the crest.

A critical-depth stage-discharge relation at the downstream boundary implies the Froude number is unity there, i.e.,

$$F^2 = \frac{Q^2}{g A^3/B} = 1 \tag{47}$$

in which B is the top width.

5.1.3 Reduction of governing equations to nondimensional form.

Non-zero reference variables Q_0, Y_0, B_0, X_0, T_0 with dimensions L^3/T, L, L, L, T respectively (L: length; T: time), but otherwise (momentarily) undefined, are introduced. The following nondimensional variables are then defined,

$$Q^* = \frac{Q}{Q_0}, \quad q^* = \frac{q}{Q_0/X_0}, \quad A^* = \frac{A}{B_0 Y_0}, \quad h^* = \frac{h}{Y_0}, \quad y^* = \frac{y}{Y_0},$$

$$u^* = \frac{u}{Q_0/(Y_0 B_0)}, \quad x^* = \frac{x}{X_0}, \quad t^* = \frac{t}{T_0}, \quad W^* = \frac{W}{B_0}, \quad p^* = \frac{p}{Y_0} \tag{48}$$

in which W is wetted perimeter.

This allows Eqs. 43 and 44 to be written

$$\frac{Q_0 T_0}{B_0 Y_0 X_0}\left\{\theta(Q_L^* - Q_R^* + q_{LR}^* \delta x^*) + (1-\theta)(Q_J^* - Q_M^* + q_{JM}^* \delta x^*)\right\}$$

$$= \left(\frac{A_L^* + A_R^*}{2} - \frac{A_J^* + A_M^*}{2}\right)\frac{\delta x^*}{\delta t^*} \tag{49}$$

$$B_0 Y_0^2 \left\{ \theta \left[\frac{A_L^* + A_R^*}{2} (h_L^* - h_R^*) + \frac{Q_0^2}{g B_0^2 Y_0^3} \left(\frac{Q_L^{*2}}{A_L^*} - \frac{Q_R^{*2}}{A_R^*} + u_{LR}^* q_{LR}^* \delta x^* \right) \right. \right.$$

$$\left. - \frac{Q_0^2 n^2 B_0^{4/3} X_0}{C_u^2 (B_0 Y_0)^{7/3} B_0 Y_0^2} D_{LR}^* \delta x^* \right] + (1 - \theta) \left[\frac{A_J^* + A_M^*}{2} (h_J^* - h_M^*) \right.$$

$$\left. \left. + \frac{Q_0^2}{g B_0^2 Y_0^3} \left(\frac{Q_J^{*2}}{A_J^*} - \frac{Q_M^{*2}}{A_M^*} + u_{JM}^* q_{JM}^* \delta x^* \right) - \frac{Q_0^2 n^2 B_0^{4/3} X_0}{C_u^2 (B_0 Y_0)^{7/3} B_0 Y_0^2} D_{JM}^* \delta x^* \right] \right\}$$

$$= \frac{Q_0 X_0}{g T_0} \left(\frac{Q_L^* + Q_R^*}{2} - \frac{Q_J^* + Q_M^*}{2} \right) \frac{\delta x^*}{\delta t^*} \tag{50}$$

It is now specified that Q_0, Y_0, and B_0 represent, respectively, base flow, normal depth at base flow, and top width under base-flow normal-depth conditions, and also, that

$$X_0 = \frac{Y_0}{S_0} \tag{51}$$

in which S_0 is a representative bottom slope of the channel. This makes dimensionless slope unity,

$$- \frac{dz_0^*}{dx^*} = S_0^* = \frac{S_0}{Y_0/X_0} = 1 \tag{52}$$

Further, the characteristic time is set to the value

$$T_0 = \frac{X_0 B_0 Y_0}{Q_0} \tag{53}$$

Then the continuity and momentum equations can be written, respectively,

$$R_C = \theta (Q_L^* - Q_R^* + q_{LR}^* \delta x^*) + (1 - \theta)(Q_J^* - Q_M^* + q_{JM}^* \delta x^*)$$

$$- \left(\frac{A_L^* + A_R^*}{2} - \frac{A_J^* + A_M^*}{2} \right) \frac{\delta x^*}{\delta t^*} = 0 \tag{54}$$

$$R_M = \theta\left[\frac{A_L^* + A_R^*}{2}(h_L^* - h_R^*) + \mathbb{F}^{*2}\left(\frac{Q_L^{*2}}{A_L^*} - \frac{Q_R^{*2}}{A_R^*} + u_{LR}^* q_{LR}^* \delta x^*\right)\right.$$

$$\left. - S_F^* D_{LR}^* \delta x^*\right] + (1 - \theta)\left[\frac{A_J^* + A_M^*}{2}(h_J^* - h_M^*) + \mathbb{F}^{*2}\left(\frac{Q_J^{*2}}{A_J^*} - \frac{Q_M^{*2}}{A_M^*}\right.\right.$$

$$\left.\left. + u_{JM}^* q_{JM}^* \delta x^*\right) - S_F^* D_{JM}^* \delta x^*\right] - \mathbb{F}^{*2}\left(\frac{Q_L^* + Q_R^*}{2} - \frac{Q_J^* + Q_M^*}{2}\right)\frac{\delta x^*}{\delta t^*}$$

$$= 0 \tag{55}$$

in which two dimensionless parameters, a Froude number and a drag number, characteristic of the channel under base-flow conditions appear,

$$\mathbb{F}^{*2} = \frac{Q_0^2}{g B_0^2 Y_0^3} \tag{56}$$

and

$$S_F^* = \frac{Q_0^2 n^2 X_0}{C_u^2 B_0^2 Y_0^{13/3}} = A^{*2}(1)\ R^{*4/3}(1) = K^{*2}(1) \tag{57}$$

The dimensionless drag is computed in accordance with

$$D^* = \frac{Q^{*2}}{K_D^{*2}} \tag{58}$$

in which

$$K_D^{*2} = A^*\ R^{*4/3} \tag{59}$$

The dimensionless hydraulic radius is given in terms of the dimensionless area and wetted perimeter,

$$R^* = \frac{A^*}{W^*} \tag{60}$$

Numerical solution of Eqs. 54 and 55 was achieved by bringing the residuals R_C and R_M close to zero for all channel elements in a reach at

each time step while maintaining the specified relation between downstream depth and discharge, Eqs. 63-65. In the present study,

$$R_C \leq 10^{-4} \tag{61}$$

$$R_M \leq 10^{-4} \tag{62}$$

5.1.4 Nondimensional downstream boundary conditions.

In terms of the previously defined dimensionless variables, the normal-depth downstream boundary condition (Eq. 45) is given by the equation

$$Q^* = A^* R^{*2/3} / \sqrt{S_F^*} \tag{63}$$

The critical-depth stage-discharge relation Eq. 47, expressed in dimensionless terms is

$$Q^* = \frac{1}{\mathbb{F}_0^*} \sqrt{\frac{A^{*3}}{B^*}} \tag{64}$$

whereas, the weir equation, Eq. 46, reduces to the following implied relationship between dimensionless downstream depth and discharge,

$$y^* + \mathbb{F}_0^{*2} \frac{Q^{*2}}{2A^{*2}} = p^* + \frac{3}{2} \mathbb{F}^{*2/3} \left(\frac{Q^*}{B_W^*} \right)^{2/3} \tag{65}$$

5.1.5 Reduction of governing equations to differential form.

If none of the pertinent functions are discontinuous with distance or time (no bores), Eqs. 54 and 55 can be reduced to partial differential equations simply by division by δx^* and going to the limit as $\delta x^* \to 0$, $\delta t^* \to 0$. The result is

$$\frac{\partial Q^*}{\partial x^*} + \frac{\partial A^*}{\partial t^*} - q^* = 0 \tag{66}$$

$$\mathbb{F}_0^{*2} \left(\frac{\partial Q^*}{\partial t^*} + \frac{\partial}{\partial x^*} \frac{Q^{*2}}{A^{*2}} - u^* q^* \right) + A^* \frac{\partial h^*}{\partial x^*} + S_F^* D^* = 0 \tag{67}$$

the form of Eqs. 1 and 2, when tributary inflow q^* is negligible.

5.2 The zero-inertia equations.

As the Froude number characteristic of the channel under base flow conditions is reduced, the importance of the inertial terms (in parentheses, on the left side of Eq. 67) declines. As an approximation, if F^* is set to zero in Eqs. 67 or 55, the so-called zero-inertia or equilibrium model (because pressure, weight, and drag forces are in equilibrium) results. This is a combination of the continuity equation, Eq. 66 or its elementary-volume-integrated counterpart, Eq. 55, and the partial differential equation,

$$A^* \frac{\partial h^*}{\partial x^*} + S_F^* D^* = 0 \tag{68}$$

or its elementary-volume-integrated counterpart.

5.3 The normal-depth kinematic-wave model.

If, in addition, the depth gradient is much smaller than the bottom slope, it too may be neglected. Then Eq. 68 becomes

$$\frac{Q^{*2}}{K_D^{*2} A^*} = \frac{1}{S_F^*} \tag{69}$$

or

$$Q^* = K^* \sqrt{S_F^*} \tag{70}$$

a normal-depth stage-discharge relationship. This, inserted into the continuity equation Eq. 66 or 55 yields one kind of kinematic-wave model.

5.4 Kinematic-wave models.

5.4.1 General theory.

In the material following, the symbols can be understood to represent either real physical variables or their dimensionless counterparts.

A kinematic-wave model results when any stage-discharge relationship is introduced into the continuity equation. For example, if a relationship between discharge and cross-sectional flow area is known

$$Q = Q(A,x) \tag{71}$$

for each point along a river (not necessarily prismatic) and this is inserted into the continuity equation,

$$\frac{\partial Q(x,t)}{\partial x} + \frac{\partial A}{\partial t} = q \tag{72}$$

the result is

$$\frac{\partial Q(x,t)}{\partial x} + \frac{1}{w}\frac{\partial Q(x,t)}{\partial t} = q \tag{73}$$

in which,

$$w = \frac{\partial Q(A,x)}{\partial A} \tag{74}$$

Introduction of an orthogonal s-n coordinate system inclined at some angle $\alpha(x,t)$ (see Fig. 4) to the x-axis allows Eq. 73 to be written

$$\frac{\partial Q}{\partial s}\frac{\partial s}{\partial x} + \frac{\partial Q}{\partial n}\frac{\partial n}{\partial x} + \frac{1}{w}\left(\frac{\partial Q}{\partial s}\frac{\partial s}{\partial t} + \frac{\partial Q}{\partial n}\frac{\partial n}{\partial t}\right) = q \tag{75}$$

in which

$$\frac{\partial s}{\partial x} = \cos\alpha; \quad \frac{\partial n}{\partial x} = -\sin\alpha; \quad \frac{\partial s}{\partial t} = \sin\alpha; \quad \frac{\partial n}{\partial t} = \cos\alpha \tag{76}$$

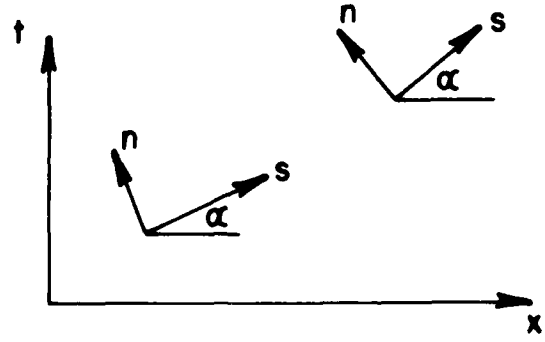

Fig. 4. Characteristic coordinates.

Then

$$\left(\cos\alpha + \frac{1}{w}\sin\alpha\right)\frac{\partial Q}{\partial s} - \left(\sin\alpha - \frac{1}{w}\cos\alpha\right)\frac{\partial Q}{\partial n} = q \tag{77}$$

If for each pair of coordinates x,t α is chosen such that

$$\tan \alpha = \frac{1}{w} \tag{78}$$

with w dependent upon the relationship between Q and A at that x and t, then the coefficient of $\partial Q/\partial n$ in Eq. 77 vanishes and the latter becomes the ordinary differential equation

$$\left[1 + \tan^2\alpha\right] \frac{dQ}{ds} = \sec^2\alpha \frac{dQ}{ds} = \frac{q}{\cos \alpha} \tag{79}$$

with the differentiation performed with respect to arc length s along a curve inclined everywhere at the local value of slope 1/w. Now along such a curve (see Fig. 5),

$$\frac{dQ}{dt} = \frac{dQ}{ds}\frac{ds}{dt} = \frac{1}{\sin \alpha}\frac{dQ}{ds} \tag{80}$$

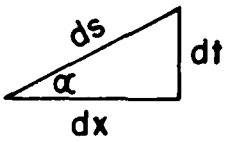

Fig. 5. Relation between increments of x, t, and s.

Consequently Eq. 79 can be written

$$\frac{dQ}{dt} = q \frac{\partial Q(A,x)}{\partial A} \tag{81}$$

the differentiation valid along a so-called characteristic curve on which

$$\frac{dx}{dt} = \frac{\partial Q(A,x)}{\partial A} \tag{82}$$

Physically, these equations can be interpreted as stating that the discharge at a cross section moving with velocity w increases at the rate wq. In a flow with no tributary inflow, the discharge across such a moving section remains constant:

$$\frac{dQ}{dt} = 0 \tag{83}$$

If in addition the channel cross section and roughness distribution therein is the same at all stations, as in the present study, the characteristic

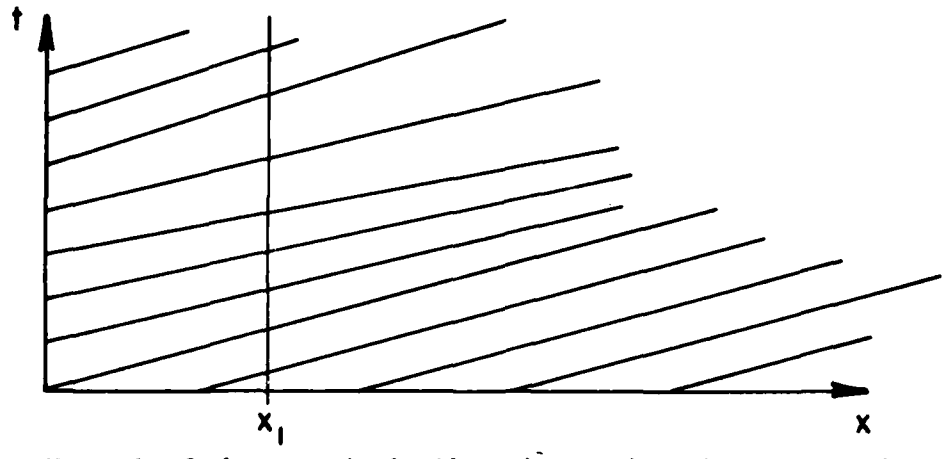

Fig. 6. Network of characteristic lines in a prismatic channel with no tributary inflow.

curves are all straight lines and so form the basis of a very simple computational technique. With Q(A) known, w is known for every point on the inflow hydrograph and (straight) characteristic curves may be drawn extending from the t axis as shown in Fig. 6. Along any one of those lines, Q remains constant at the value set by the inflow hydrograph, at the point of emanation of the line from the t axis. Thus the hydrograph at stations such as x_1 can be computed.

5.4.2 Kinematic shocks.

Evidently, with a rising inflow hydrograph and $w = \partial Q/\partial A$ an increasing function of Q, the characteristic lines converge, and if the channel is long enough, intersect. Such an intersection constitutes a kinematic shock. From the standpoint of kinematic-wave theory, i.e., with strict adherence to the Q(A) relationship given a priori, a kinematic shock is simply a discontinuity in water-surface elevation and discharge--an abrupt wave front moving at the velocity

$$w_{s_{12}} = \frac{Q_2 - Q_1}{A_2 - A_1} \tag{84}$$

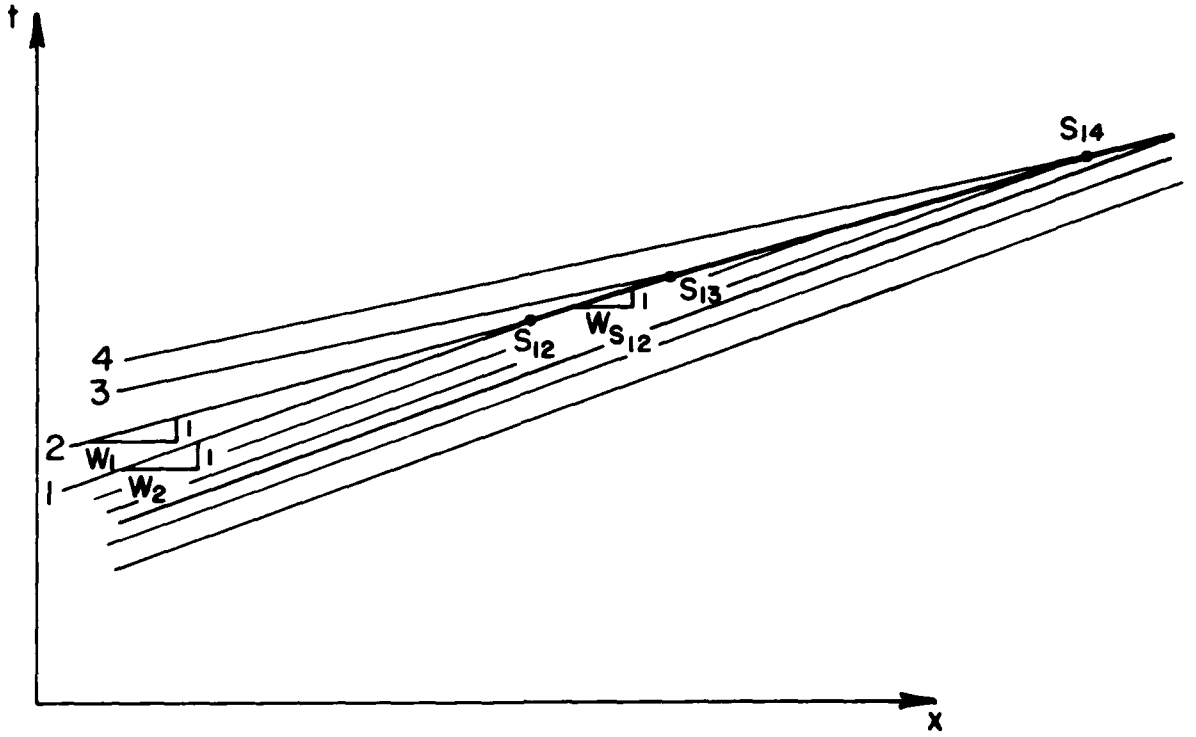

Fig. 7. Formation and propagation of a kinematic shock.

as found from elementary mass-conservation considerations. The subscripts 2 and 1 refer to the high and low sides of the shock, respectively, as in Fig. 7. As can be seen from Fig. 7a, the shock speed lies between the individual velocities of propagation of the two component discharges

$$w_1 < w_s < w_2 \tag{85}$$

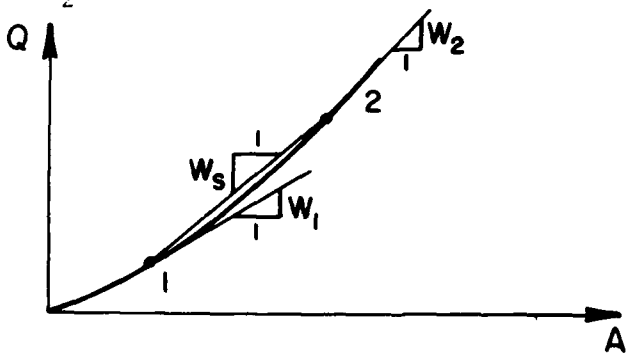

Fig. 7a. Shock speed w_s compared to wave speed w.

The discontinuity propagates at this speed, intersecting, successively, characteristics each carrying its own value of discharge. Thus, in Fig. 7, between points S_{12} and S_{13}, the discontinuity has Q_1 on its low (downstream) side and Q_2 on its high (upstream) side. Between S_{13} and S_{14}, it has Q_1 on its low side and Q_3 on the high side; Q_2 has disappeared from the wave. With $Q_4 < Q_3$, representing the falling limb of the hydrograph, it is apparent that the peak value Q_3 has disappeared from the floodwave by point S_{14}. In this way it is seen that kinematic waves can attenuate, as they propagate, through the mechanism of the kinematic shock.

This phenomenon is complicated by the presence of flood plains. A typical Q(A) relation for this case can be seen in Fig. 8.

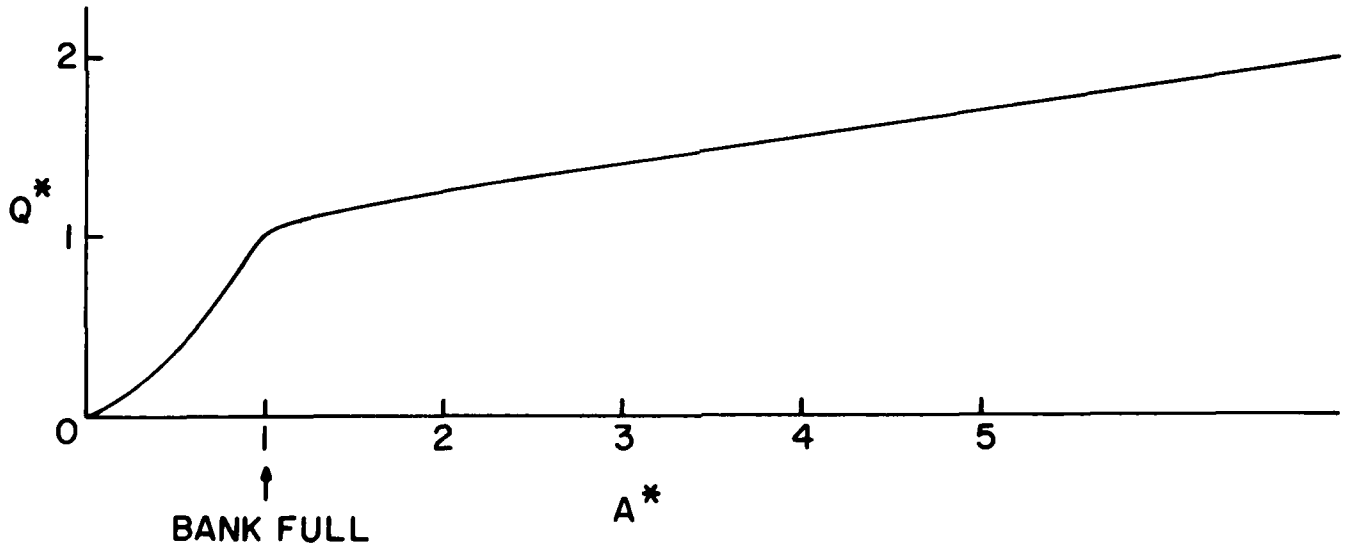

Fig. 8. Discharge-area relation for channel with floodplains.

The resulting array of characteristic lines is seen in Fig. 9. Evident are both the extreme dispersal of the wave as it enters the flood plains and the two shocks, one positive, one negative.

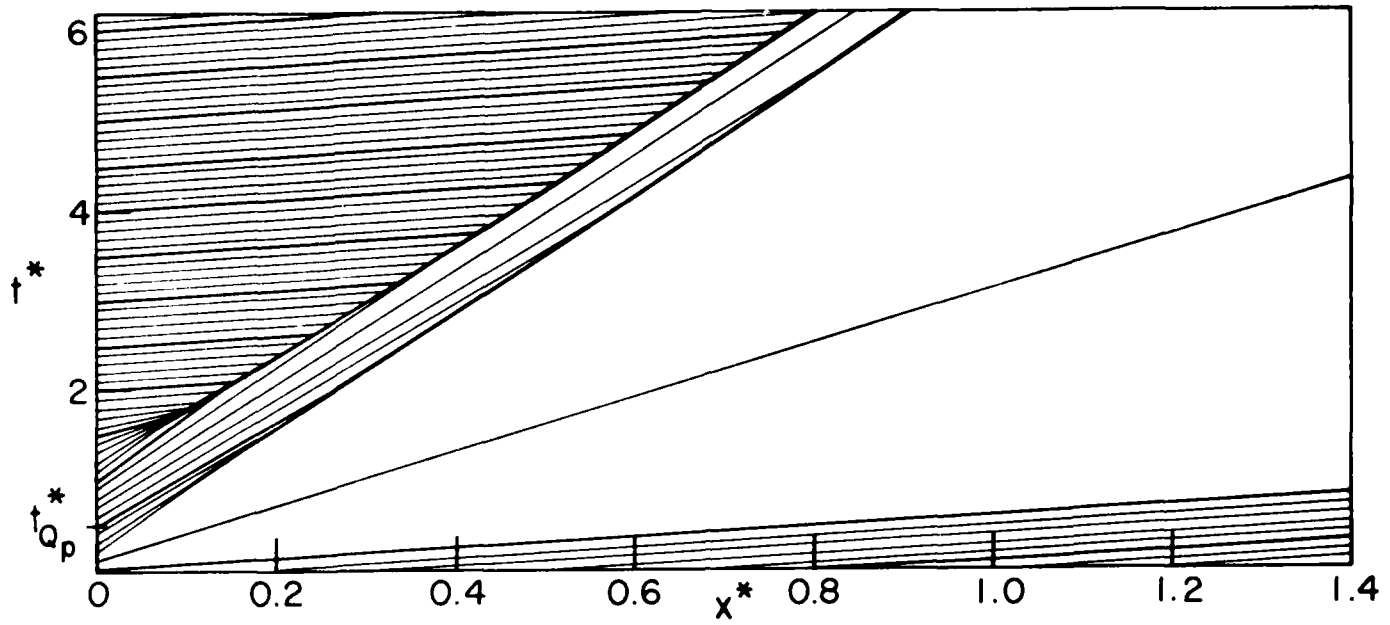

Fig. 9. Characteristics and shock trajectories in channel with floodplains.

5.5 Modified-Puls technique.

The Modified-Puls technique couples a given relationship between storage S in a reach and outflow Q_R from the reach with an expression of mass conservation in the reach. The latter, nothing more than an integral of Eq. 66 over the length of the reach, and over an increment of time δt, can be written

$$\left[\theta(Q_L - Q_R) + (1 - \theta)(Q_J - Q_M)\right]\delta t = S_{LR} - S_{JM} \tag{86}$$

In Eq. 86 S_{LR} is the storage in the reach at the end of the time increment, and S_{JM} is the storage at the beginning of the time increment; the weighting factor θ is normally taken $\theta = 1/2$. The quantities Q_J, Q_M, and S_{JM} are known from initial conditions or from computation of the previous time step. The inflow hydrograph gives Q_L, and the given storage-outflow relation yields the necessary equation to close the system

$$S_{LR} = S(Q_R) \tag{87}$$

allowing solution for Q_R.

The form of these governing equations is unaffected if the symbols are meant to represent dimensionless rather than dimensioned quantities.

In a variation of the scheme, L and R, and J and M, represent cross sections bounding a subreach. Then a sequence of solutions of Eqs. 86 and 87 is made at each time step, starting with the upstream-most subreach and progressing to the last one in the reach, Q_R of one subreach comprising Q_L of its downstream neighbor.

In the particular variant used in this study, total reach storage was computed for reach outflow, and this total storage was apportioned uniformly amongst the subreaches, all of equal length. When the water-surface profile from which reach storage was determined corresponded to uniform flow--a normal condition for long, prismatic reaches--the Modified-Puls equations 86 and 87 agree with the kinematic-wave equations 72 and 71 with no tributary inflow; the latter are then simply differential forms of the former.

6. Graphical Presentation of Data

6.1 Organization.

Results of the routing analyses are shown on Figs. 10-27. All of the graphs are in terms of dimensionless time, flow, and discharge as described in sections 2 through 4. Peak discharges (Q_m^*) are plotted on Figs. 10-15, peak stages (y_m^*) on Figs. 16-21, and time of arrival of peak discharge ($t_{Q_m}^*$) on Figs. 22-27. These variables are plotted vs. distance down the channel (x^*). Within each set, the first three figures are for the rectangular channel, and the second three for the channel with flood plains. Within each group of three, the first is for a normal depth downstream boundary condition, the second for a weir downstream boundary condition, and the third for a free-overfall downstream boundary condition. There are several graphs for each channel configuration representing various inflow hydrograph rise times ($t_{Q_p}^*$); these are distinguished by a letter (e.g., 10c). Table 2 provides a convenient way of identifying which conditions are presented on which graphs.

6.2 Contents.

Plotted on each graph are one or more continuous lines which depict the solution of the full St. Venant equations for various Froude numbers (F^*). These lines represent the "true" solutions at different Froude numbers. Note that, by definition, the $F^* = 0.0$ line depicts the "zero inertia" solution. When solutions with different Froude numbers are indistinguishable, a single solution curve is shown and identified by all the Froude numbers for which it was calculated. Absence of a parameter value implies use of the standard value $F^* = 0.2$ (see, e.g., Fig. 15b,c). Also shown is a line for the kinematic-wave approximation, labeled "kw". Solutions obtained by Modified Puls routing are indicated by symbols (squares, circles, triangles, etc.). Different symbols

represent different numbers (N) of subreaches for the Modified Puls technique. Also shown are the corresponding dimensionless subreach lengths (δx^*). When a Modified Puls result is dependent upon the characteristic Froude number, that number is given followd by "(MP)" (see, e.g., Fig. 11a,c).

All curves end at the downstream channel boundary $x^* = L^*$ (see, e.g., Fig. 14d). Where necessary to prevent confusion, curves are labeled with L^* (see, e.g., Fig. 22d).

The dashed curve labeled "wave speed" in Figs. 23-27 refers to the theoretical time of arrival based on wave velocity as computed by the ratio of incremental change in outflow to incremental change in storage per unit length, all computed under steady flow conditions.

6.3 Variable definitions.

The following variables appear on the graphs:

F^* = Froude number characteristic of base-flow conditions

L^* = dimensionless channel length

N = number of subreaches used in Modified Puls routing

Q_m^* = maximum dimensionless discharge

$t_{Q_m}^*$ = dimensionless time of arrival of Q_m^*

$t_{Q_p}^*$ = dimensionless rise time of the inflow hydrograph

x^* = dimensionless distance down the channel

δx^* = dimensionless subreach length

y_m^* = dimensionless maximum stage

Refer to Sections 2 through 4 for definition and discussion of the dimensionless variables.

6.4 Discussion.

Interpretation and discussion of the results presented on Figs. 10-27 may be found in Section 4, "Analysis of Results".

Table 2. Summary of Conditions Presented on the Figures

Channel Shape	Type of Downstream Boundary Condition	Distance Downstream vs:		
		Peak Discharge	Peak Stage	Arrival Time of Peak Discharge
Rectangular	Normal Depth	Fig. 10a-10g	Fig. 16a-16g	Fig. 22a-22g
	Weir	Fig. 11a-11f	Fig. 17a-17f	Fig. 23a-23f
	Overfall	Fig. 12a-12d	Fig. 18a-18d	Fig. 24a-24d
Rectangular with Flood Plains	Normal Depth	Fig. 13a-13g	Fig. 19a-19g	Fig. 25a-25g
	Weir	Fig. 14a-14g	Fig. 20a-20g	Fig. 26a-26g
	Overfall	Fig. 15a-15e	Fig. 21a-21e	Fig. 27a-27e

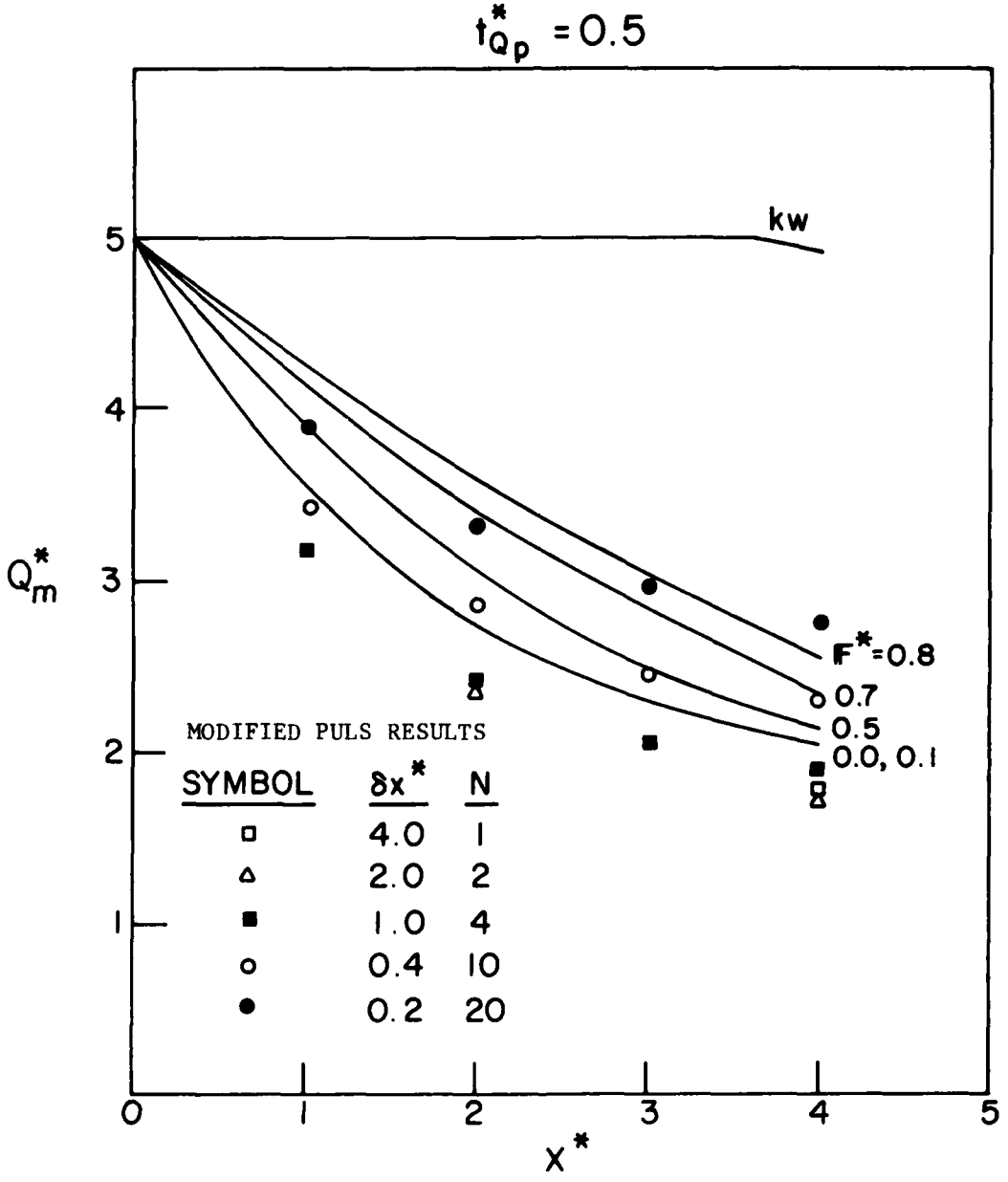

Fig. 10a Attenuation of discharge hydrograph peaks, rectangular channel, normal depth downstream boundary condition.

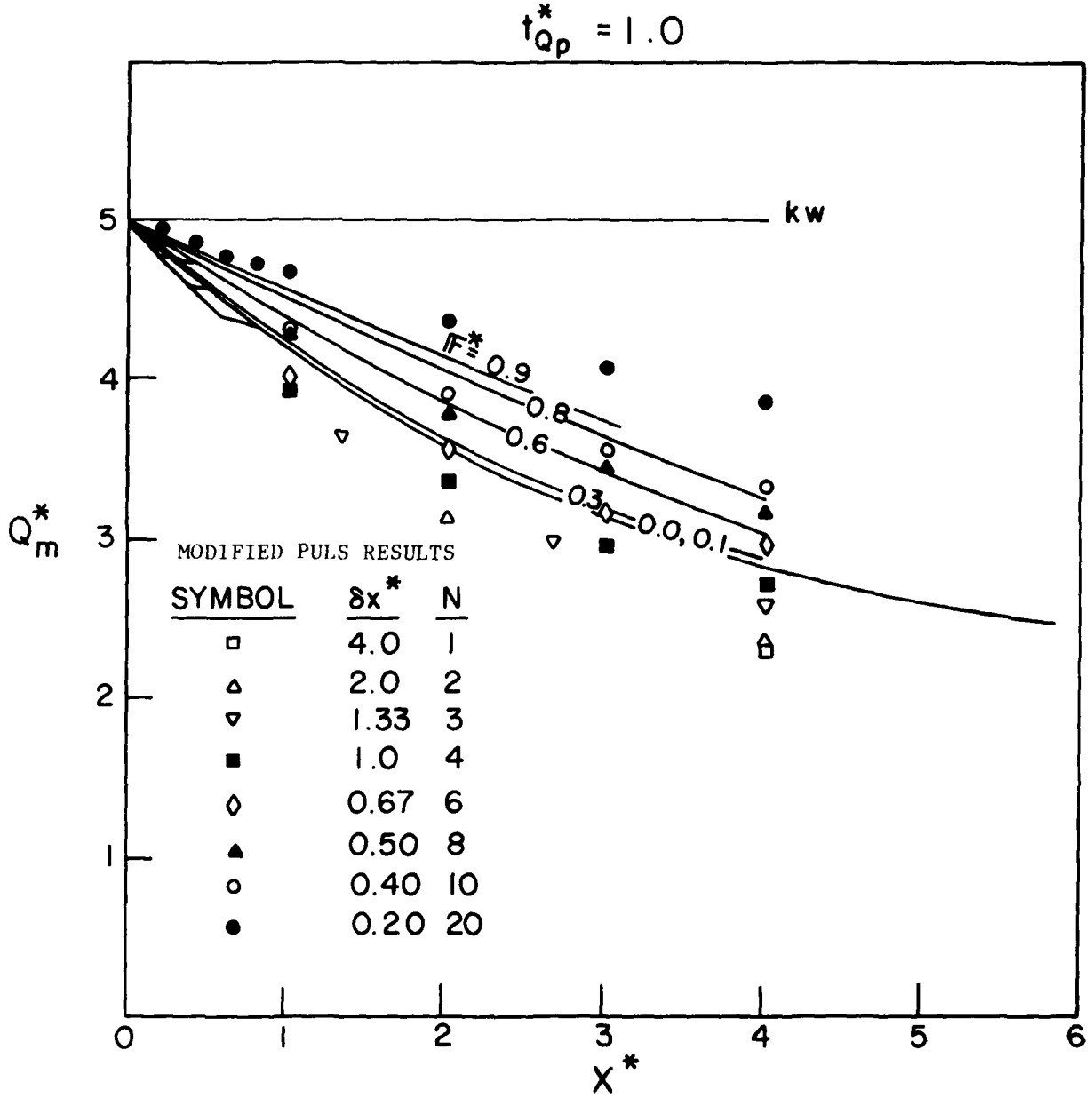

Fig. 10b Attenuation of discharge hydrograph peaks, rectangular channel, normal depth downstream boundary condition.

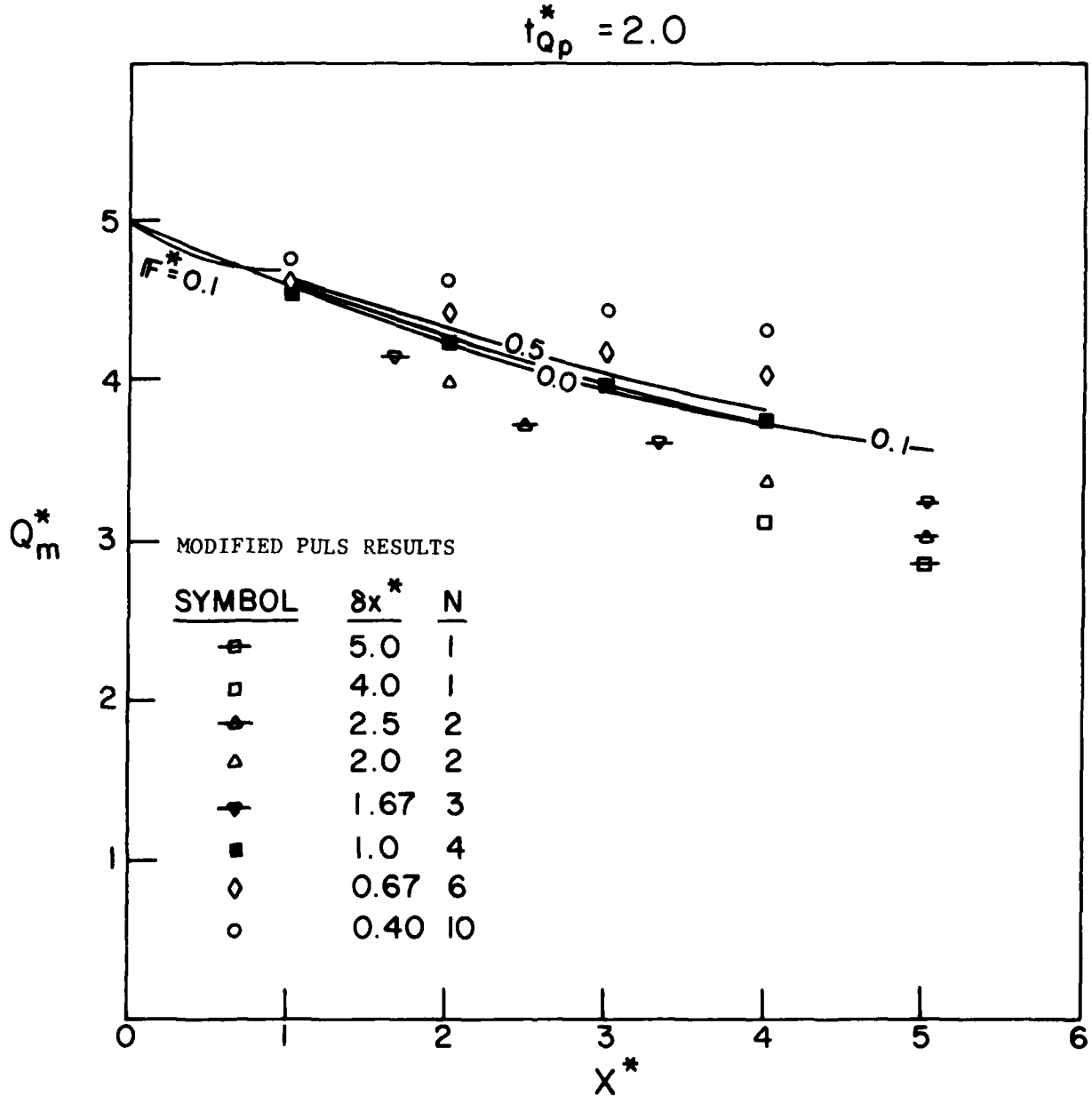

Fig. 10c Attenuation of discharge hydrograph peaks, rectangular channel, normal depth downstream boundary condition.

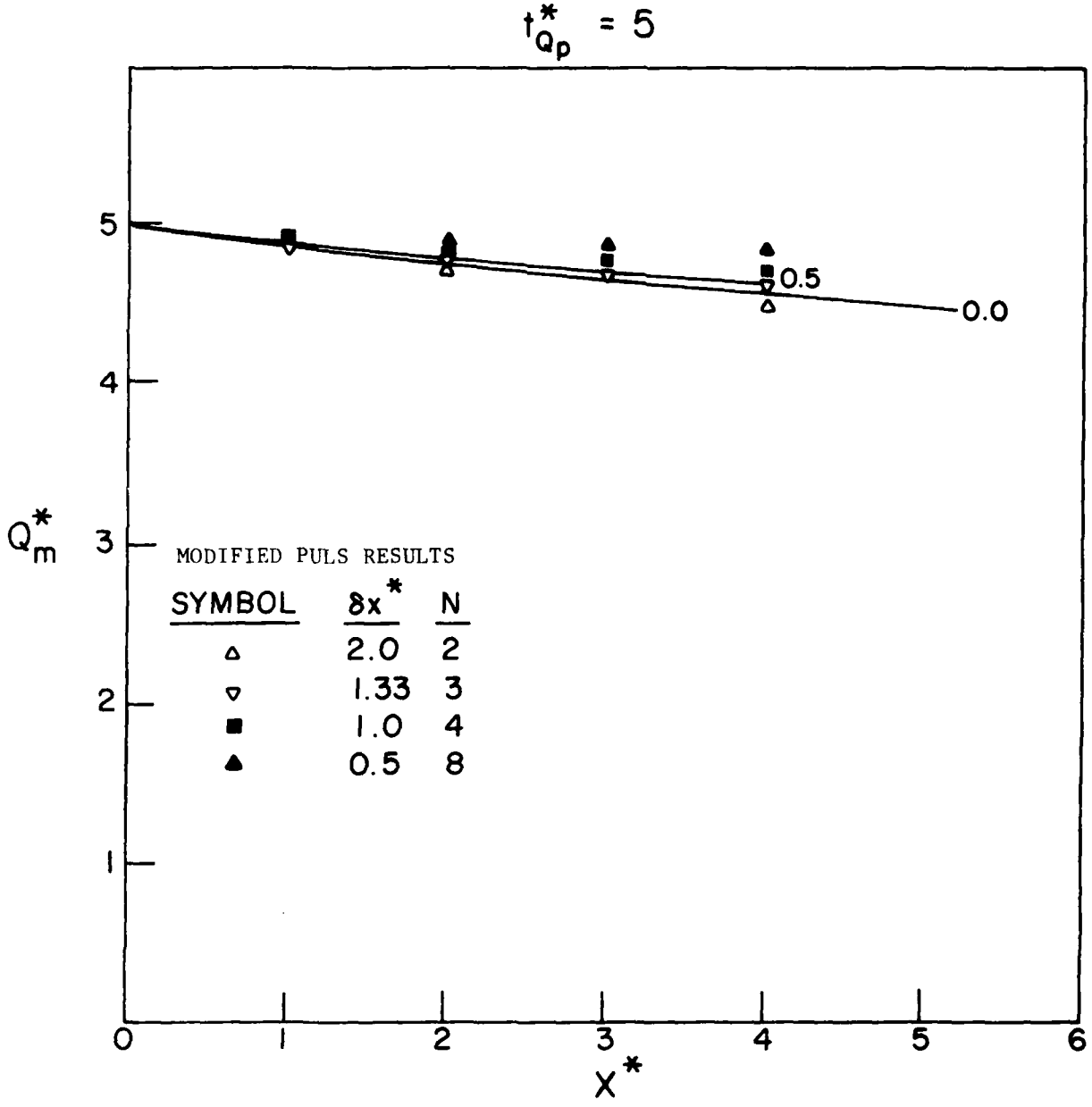

Fig. 10d Attenuation of discharge hydrograph peaks, rectangular channel, normal depth downstream boundary condition.

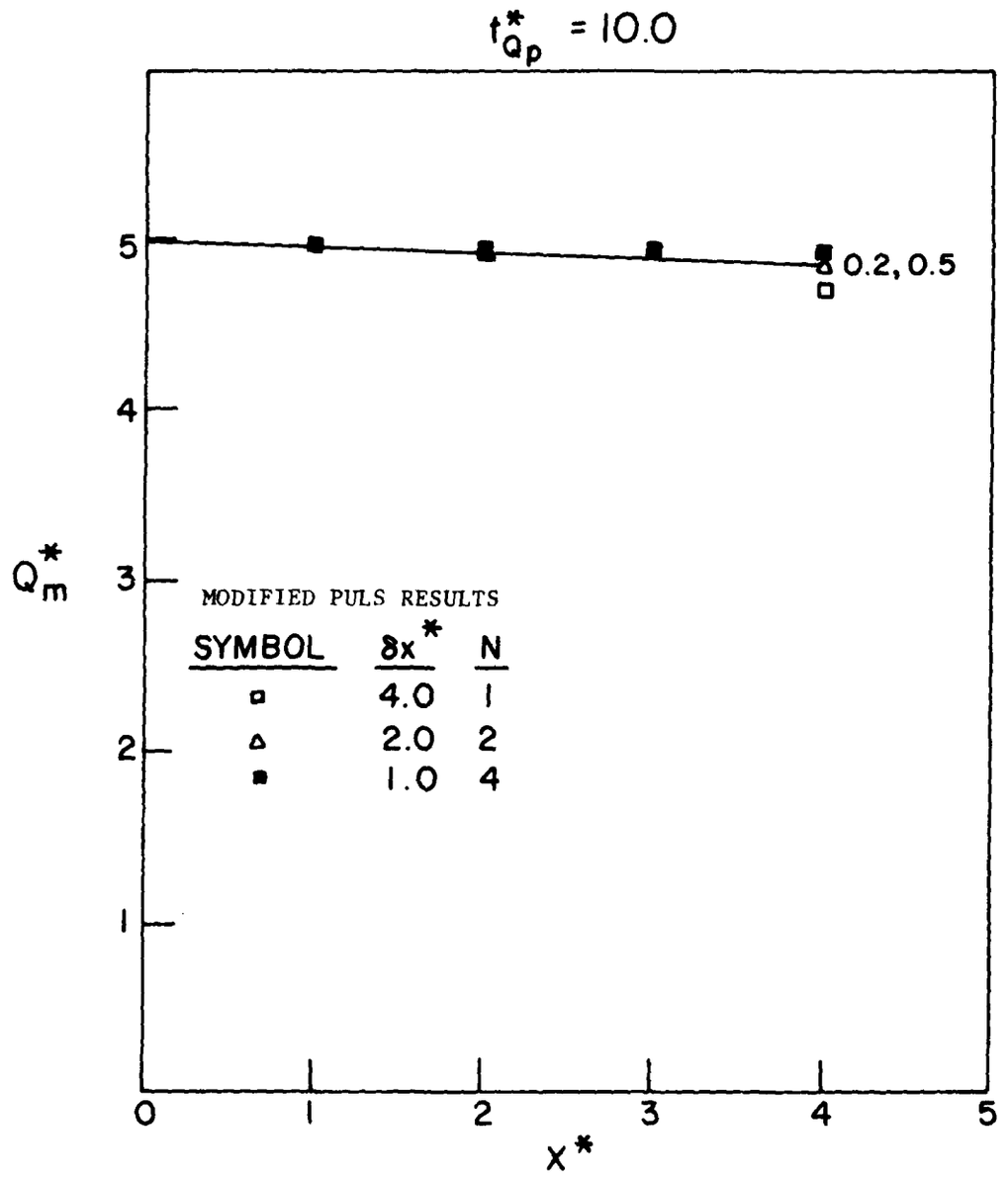

Fig. 10e Attenuation of discharge hydrograph peaks, rectangular channel, normal depth downstream boundary condition.

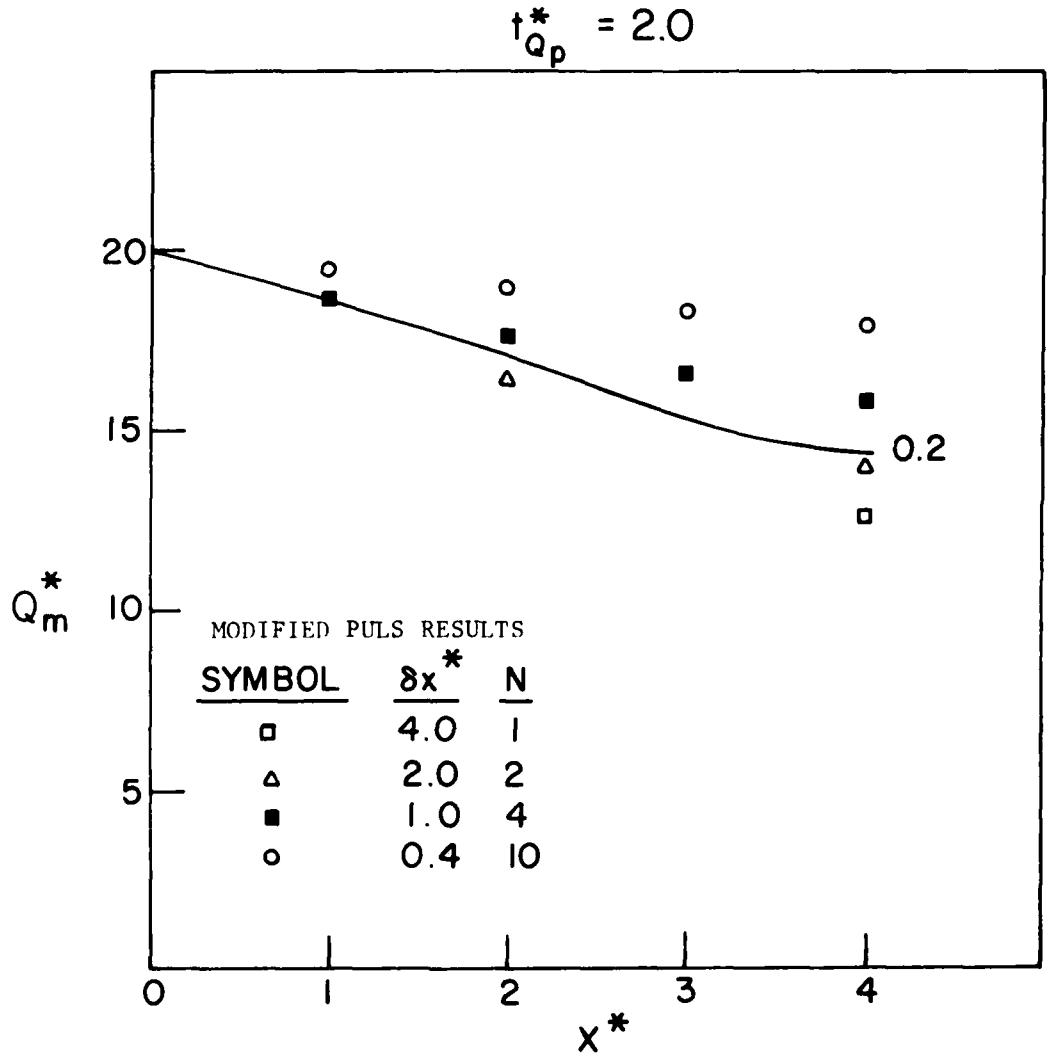

Fig. 10f Attentuation of discharge hydrograph peaks, rectangular channel, normal depth downstream boundary condition.

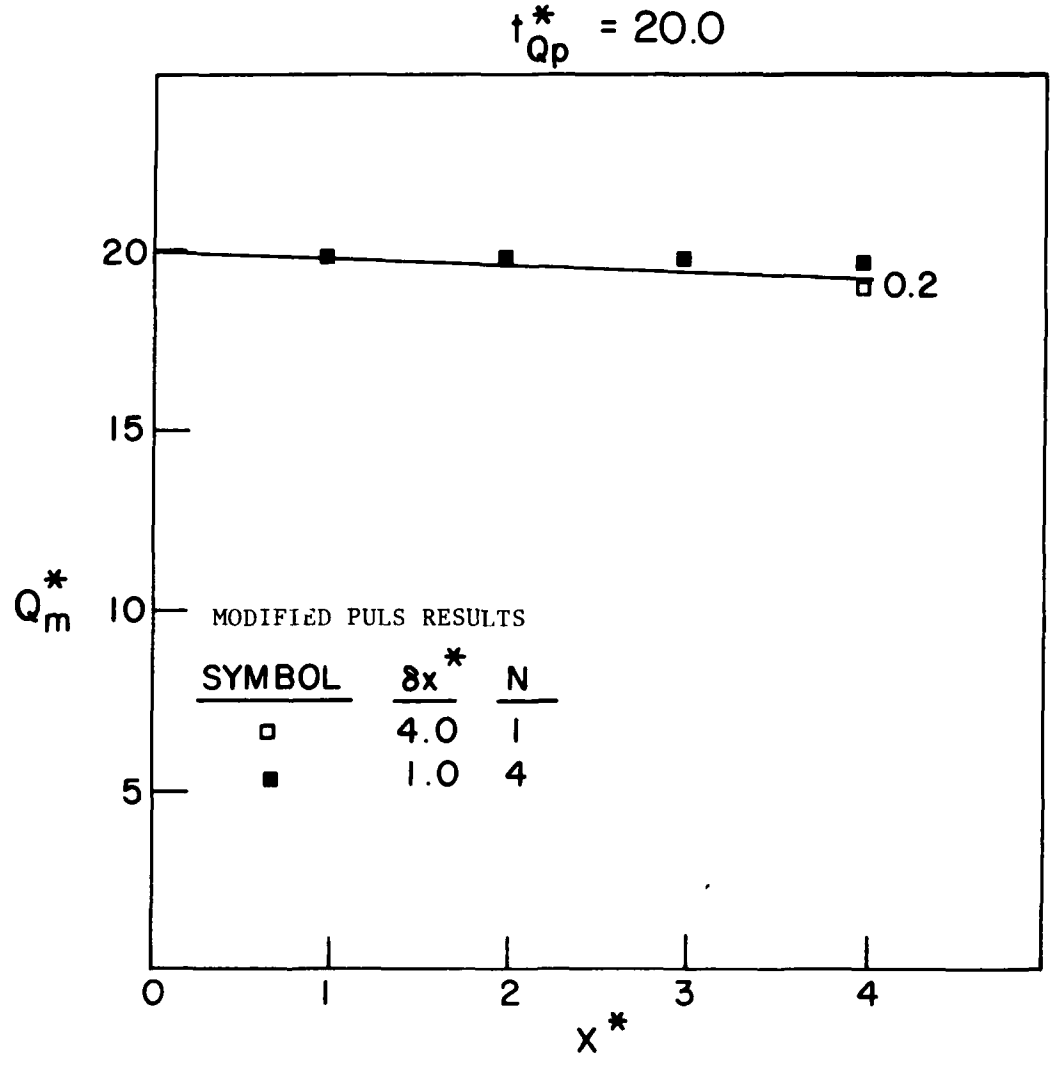

Fig. 10g Attenuation of discharge hydrograph peaks, rectangular channel, normal depth downstream boundary condition.

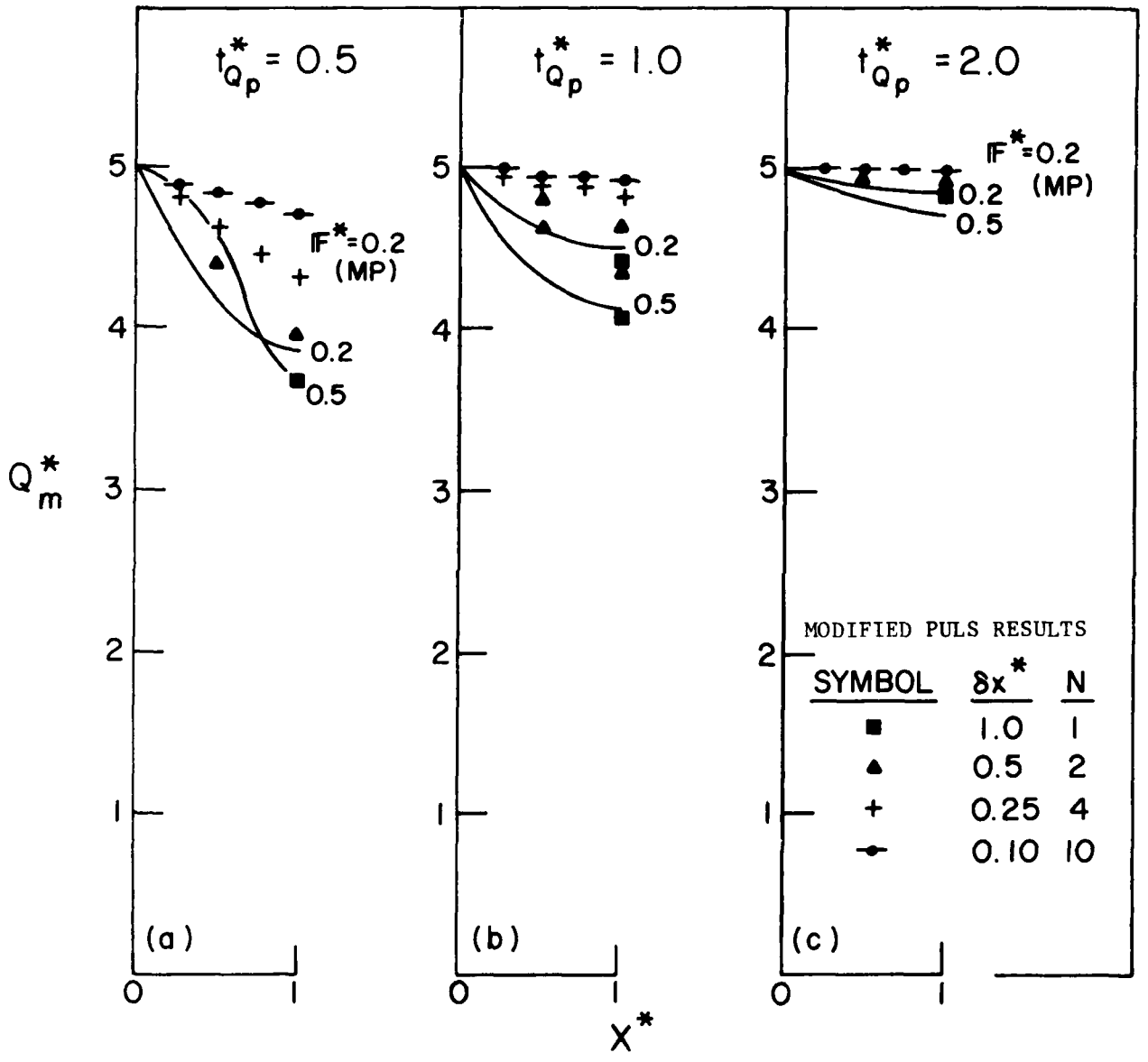

Fig. 11 a-c Attenuation of discharge hydrograph peaks, rectangular channel, weir downstream boundary condition.

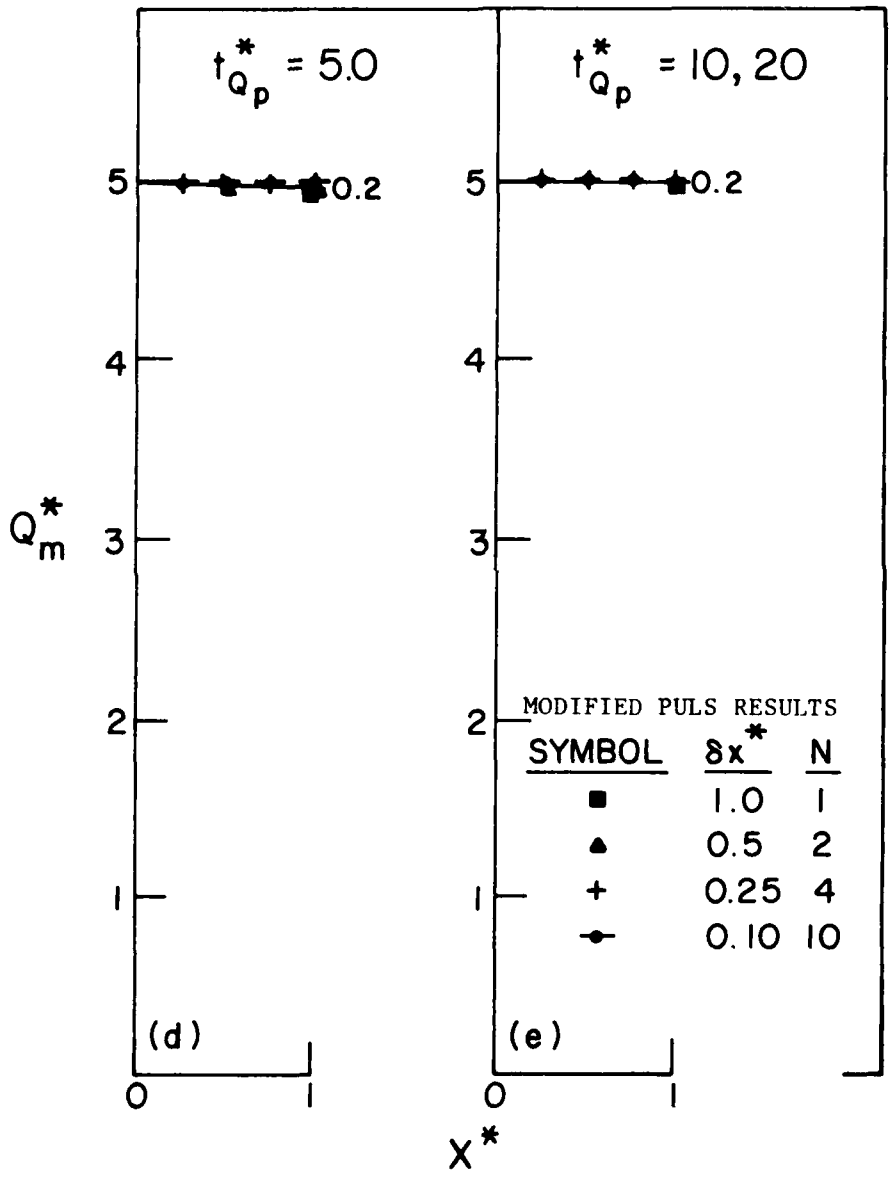

Fig. 11 d-e Attenuation of discharge hydrograph peaks, rectangular channel, weir downstream boundary condition.

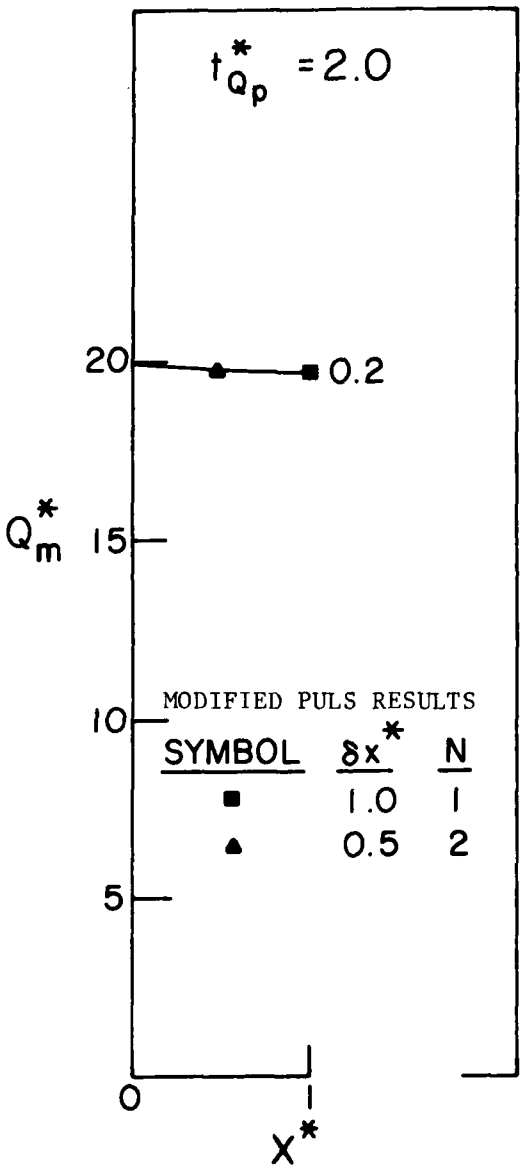

Fig. 11f Attenuation of discharge hydrograph peaks, rectangular channel, weir downstream boundary condition.

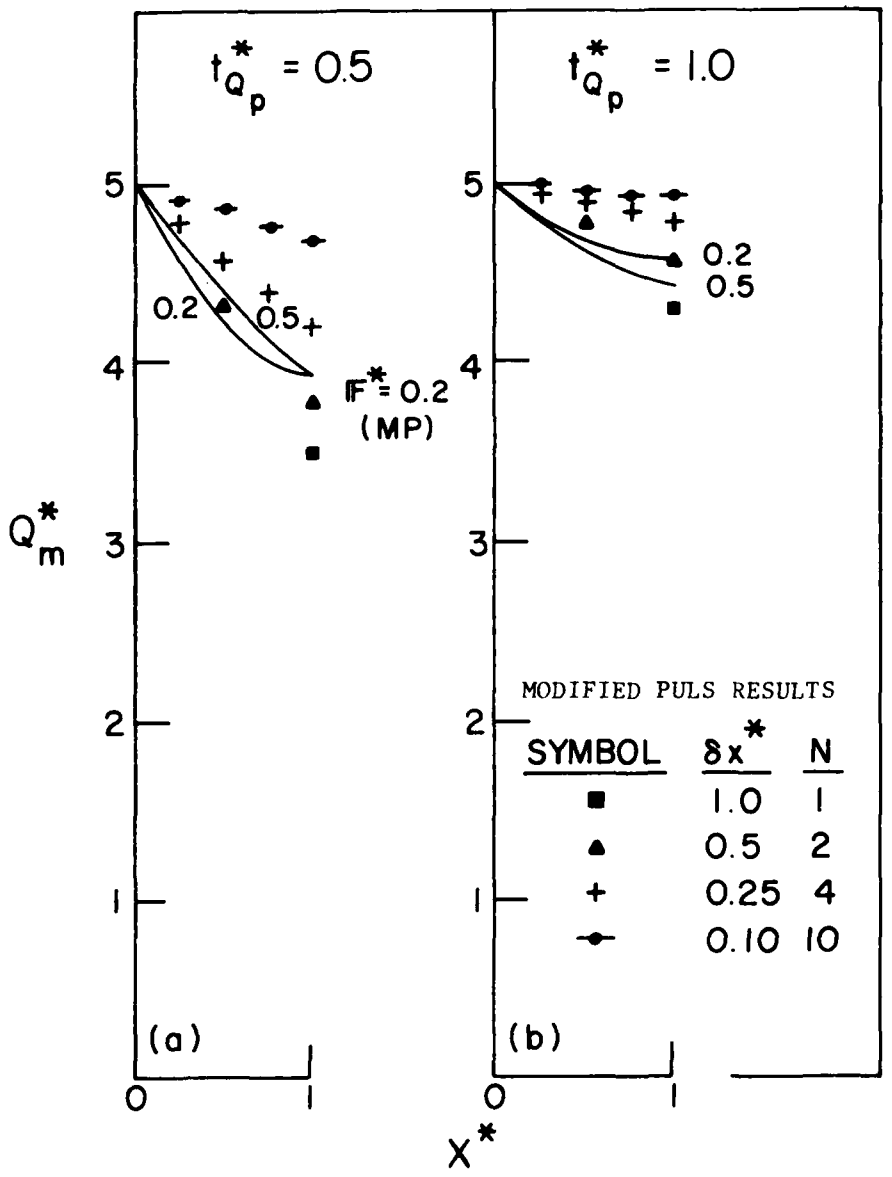

Fig. 12 a-b Attenuation of discharge hydrograph peaks, rectangular channel, overfall downstream boundary condition.

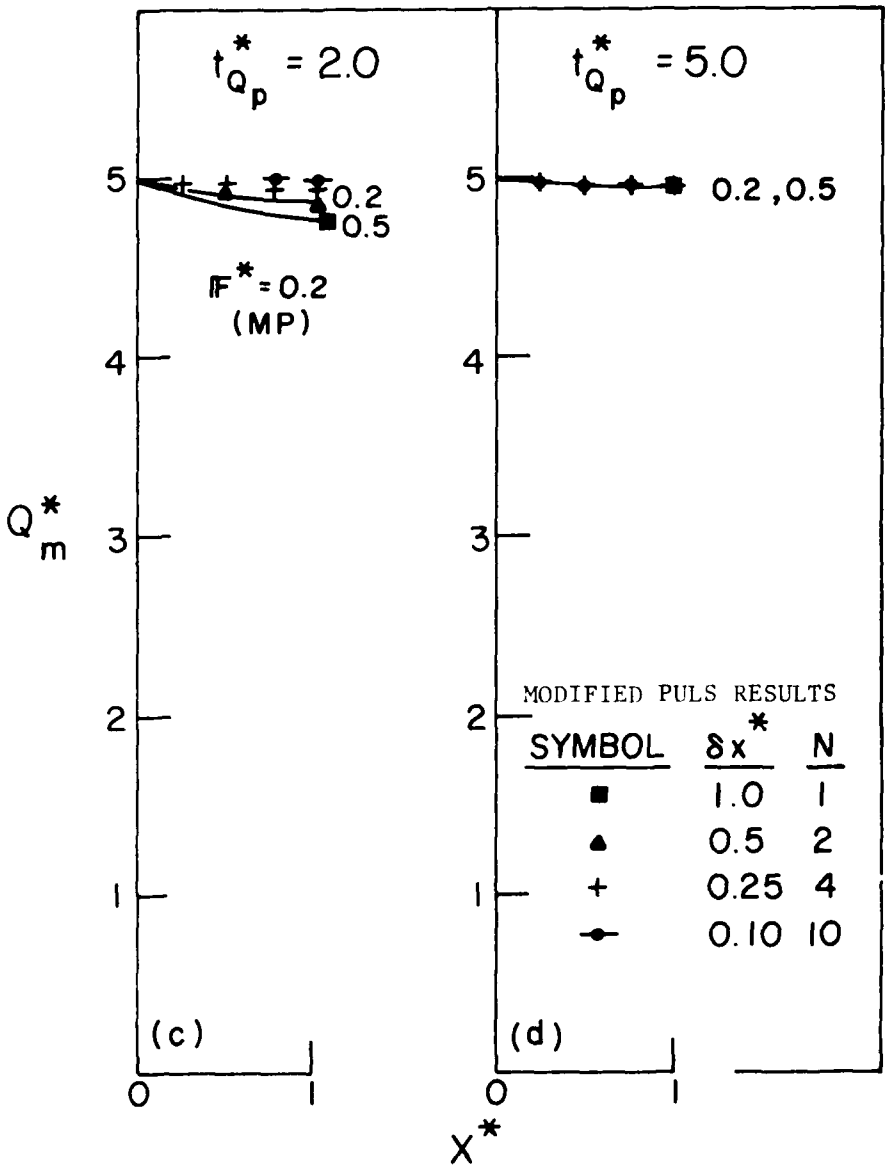

Fig. 12 c-d Attenuation of discharge hydrograph peaks, rectangular channel, overfall downstream boundary condition.

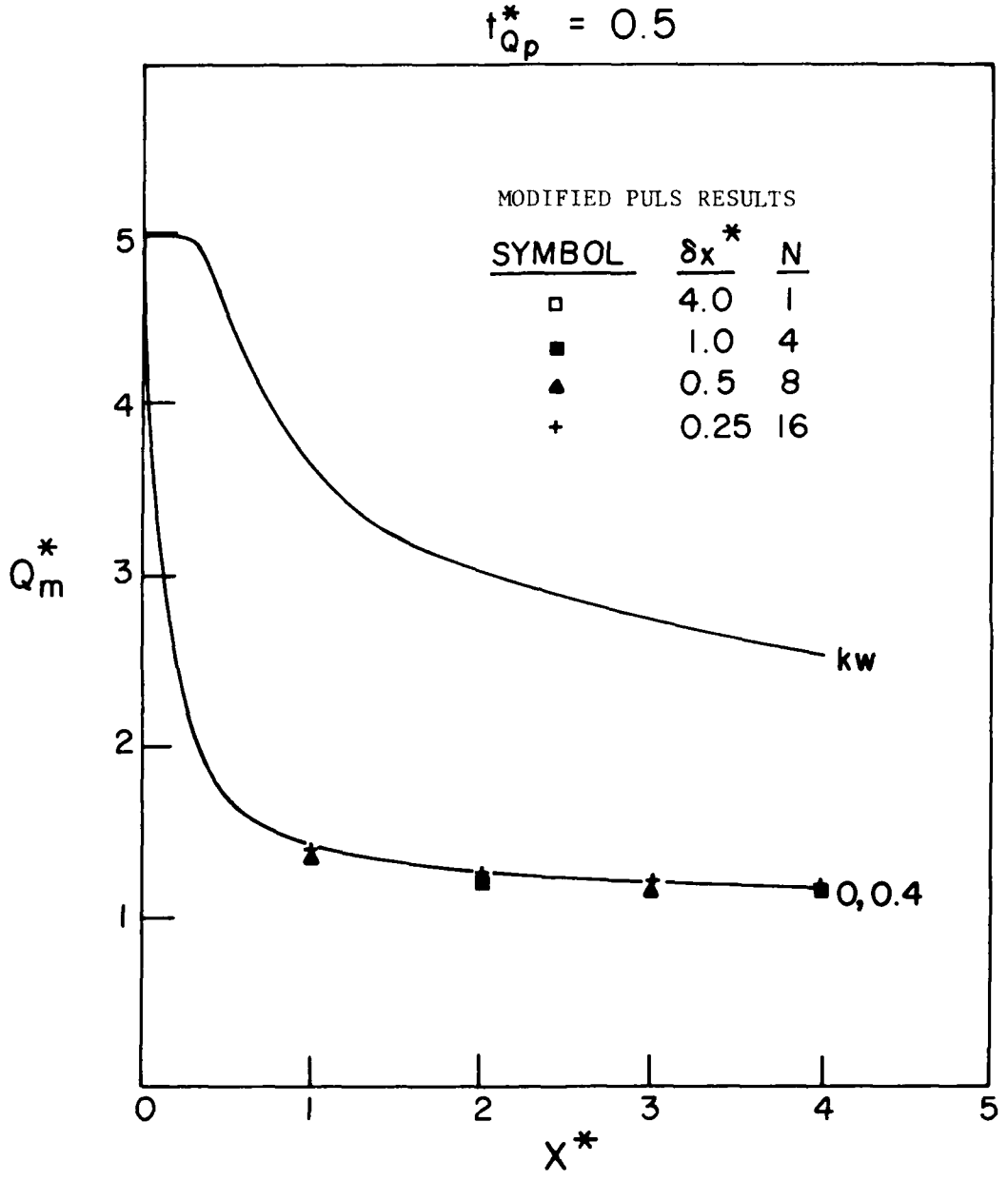

Fig. 13a Attenuation of discharge hydrograph peaks, channel with floodplain, normal depth downstream boundary condition.

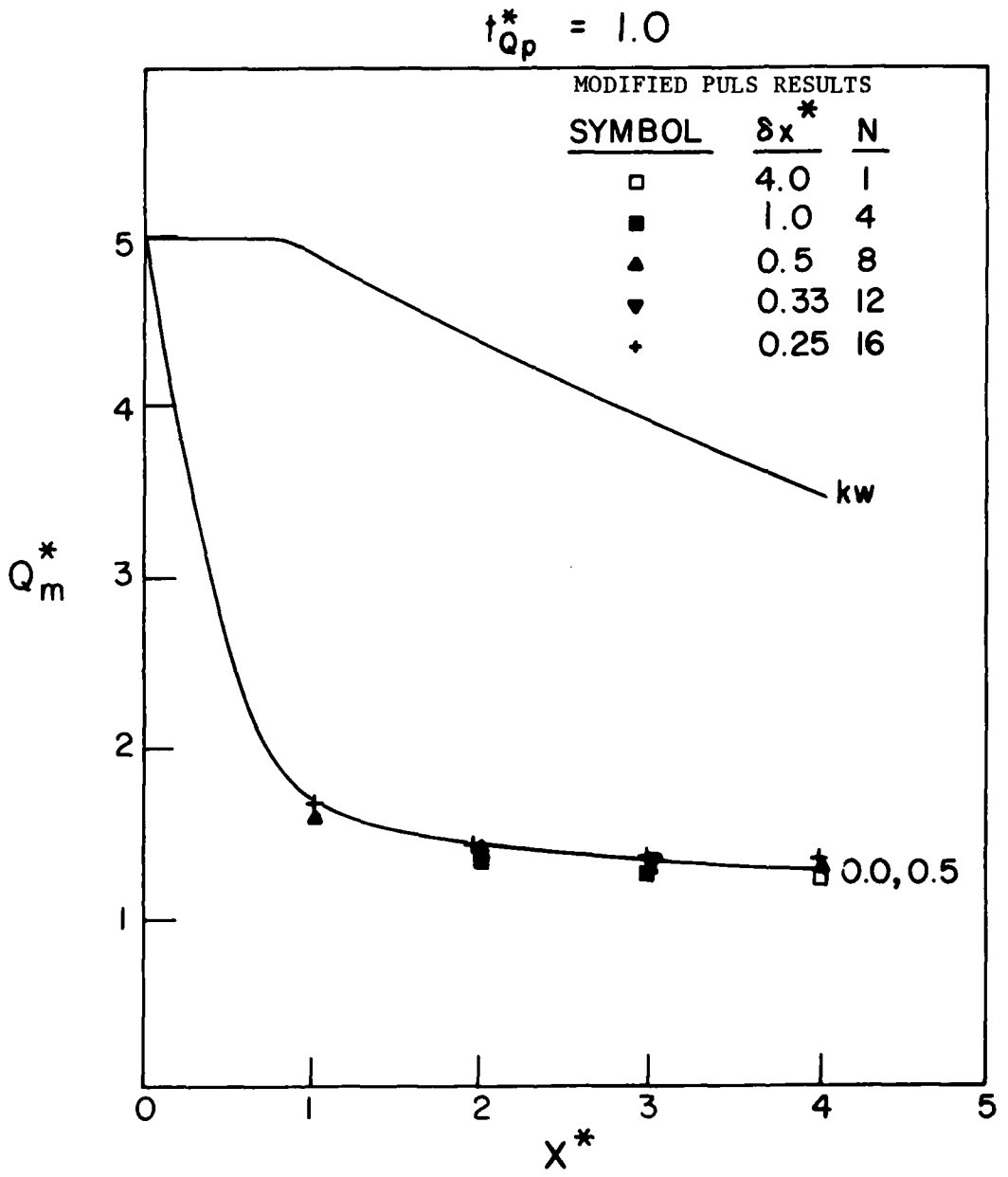

Fig 13b Attenuation of discharge hydrograph peaks, channel with floodplain, normal depth downstream boundary condition.

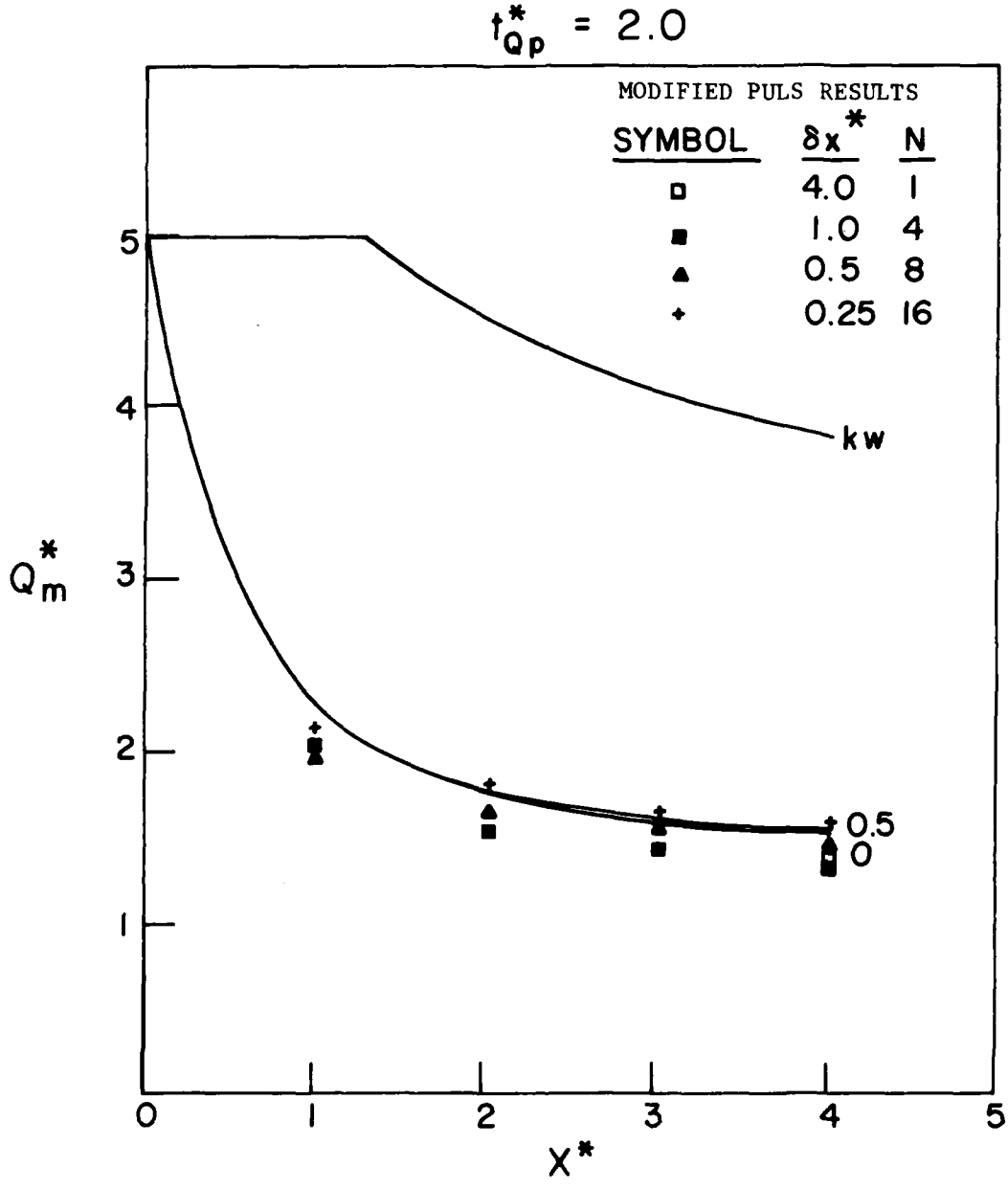

Fig. 13c Attenuation of discharge hydrograph peaks, channel with floodplain, normal depth downstream boundary condition.

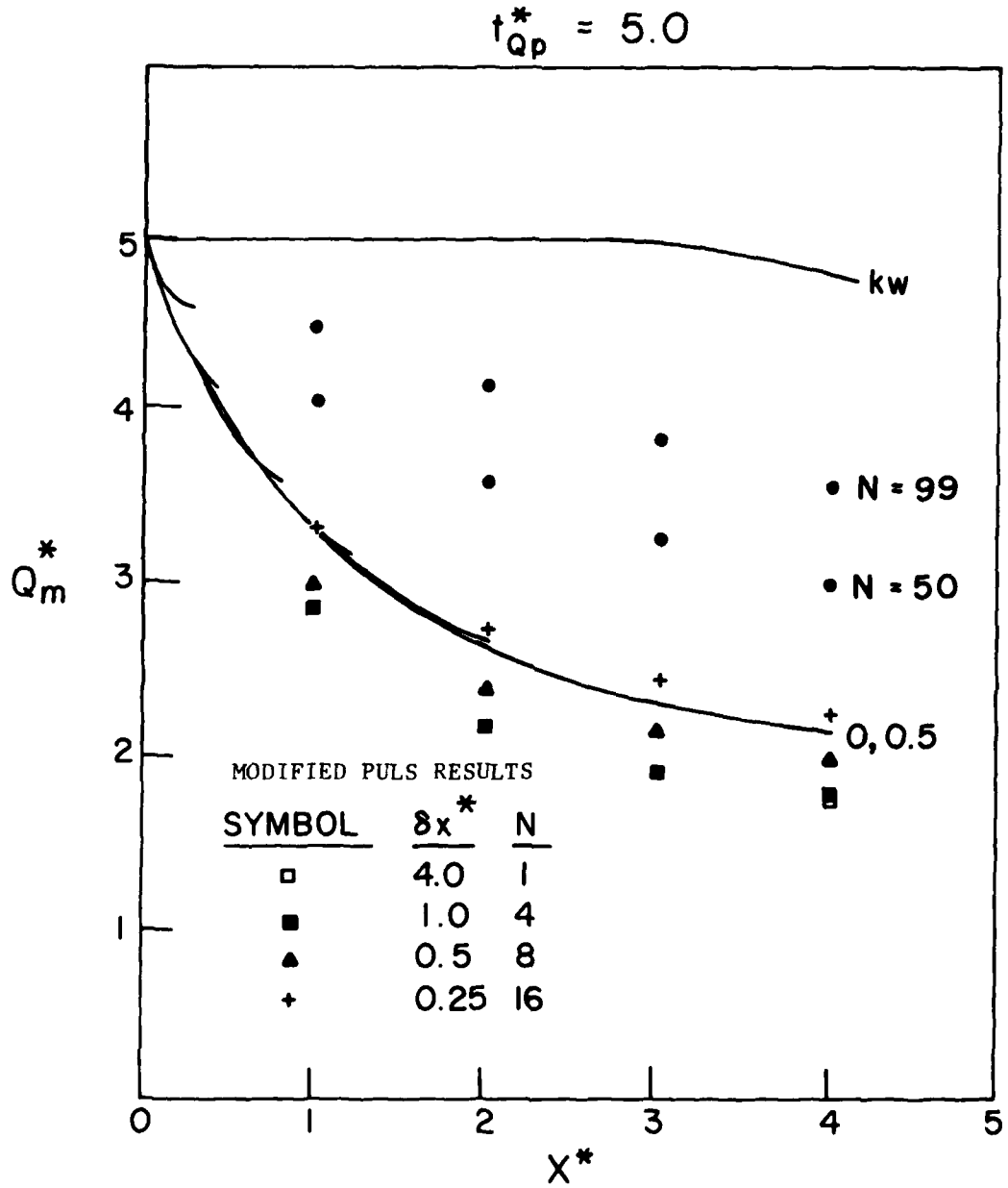

Fig. 13d Attenuation of discharge hydrograph peaks, channel with floodplain, normal depth downstream boundary condition.

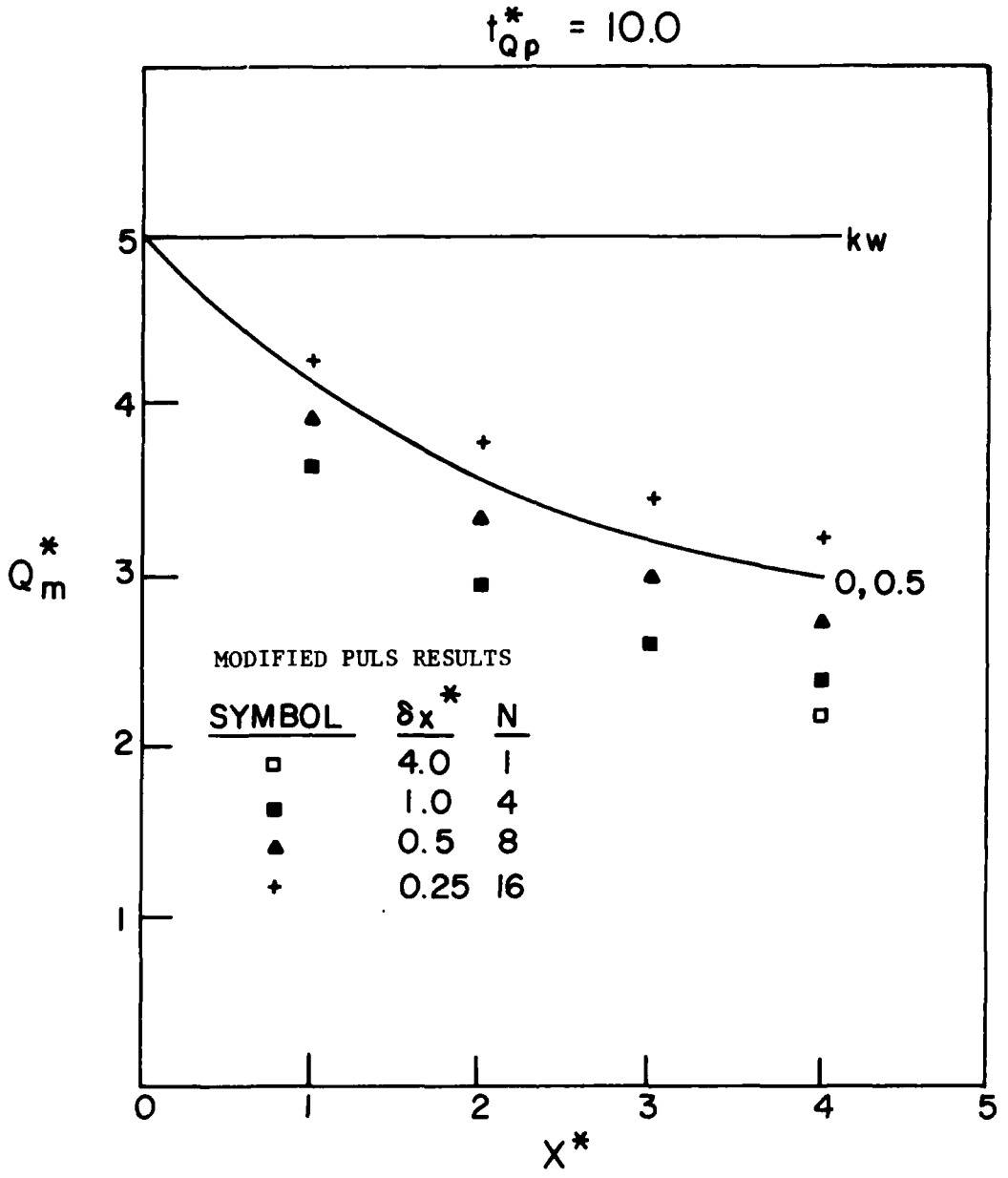

Fig. 13e Attenuation of discharge hydrograph peaks, channel with floodplain, normal depth downstream boundary condition.

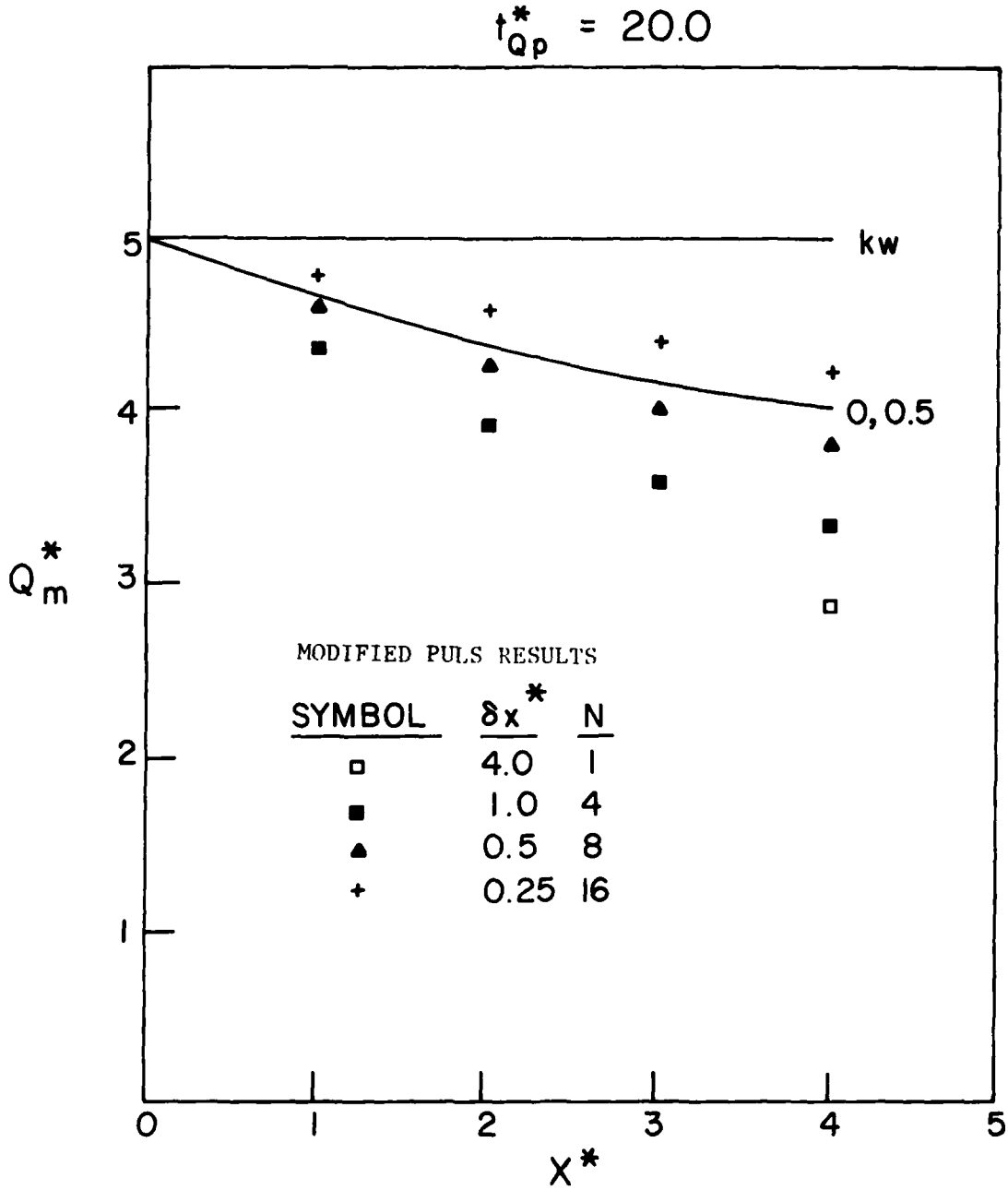

Fig. 13f Attenuation of discharge hydrograph peaks, channel with floodplain, normal depth downstream boundary condition.

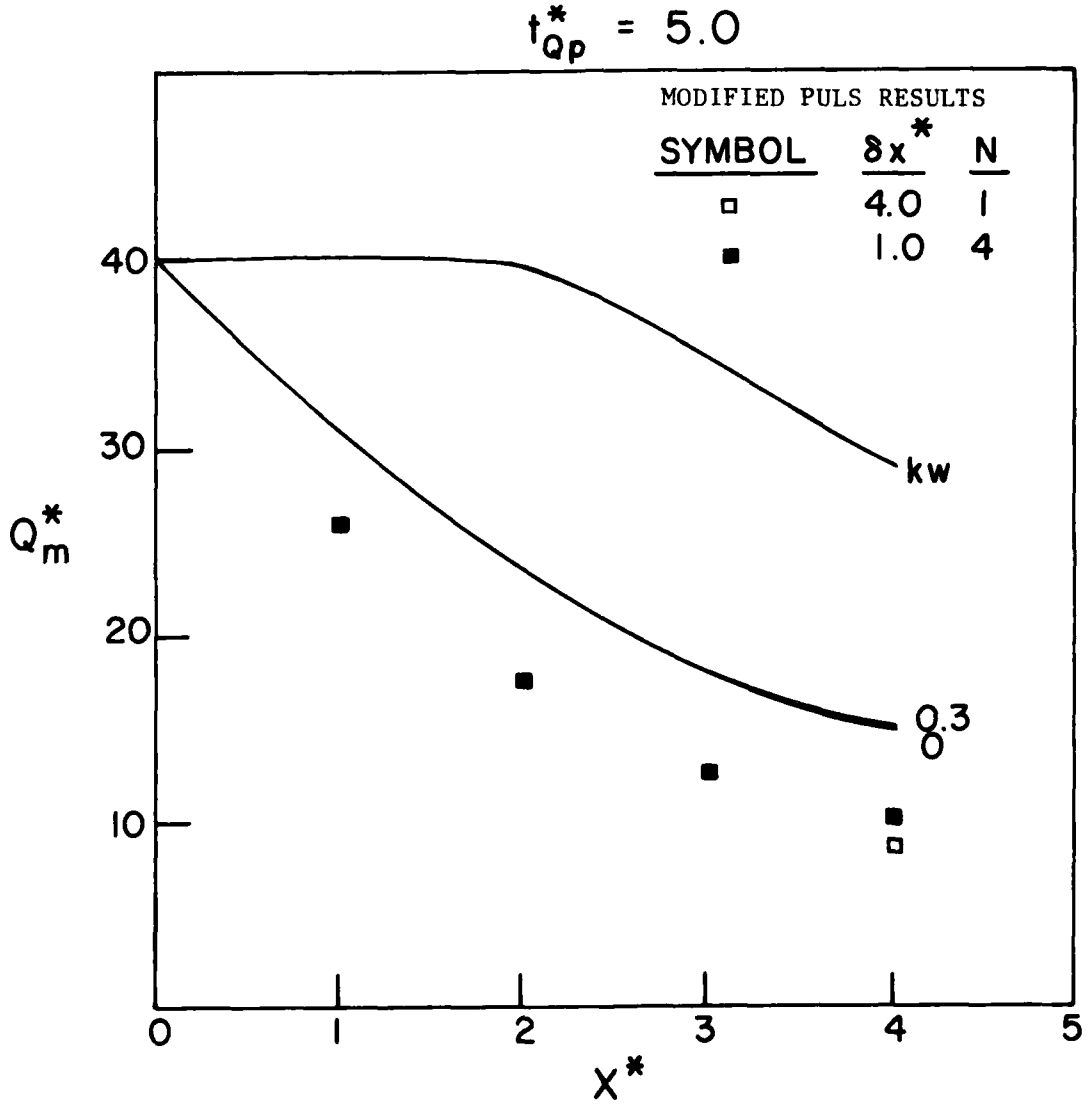

Fig. 13g Attenuation of discharge hydrograph peaks, channel with floodplain, normal depth downstream boundary condition.

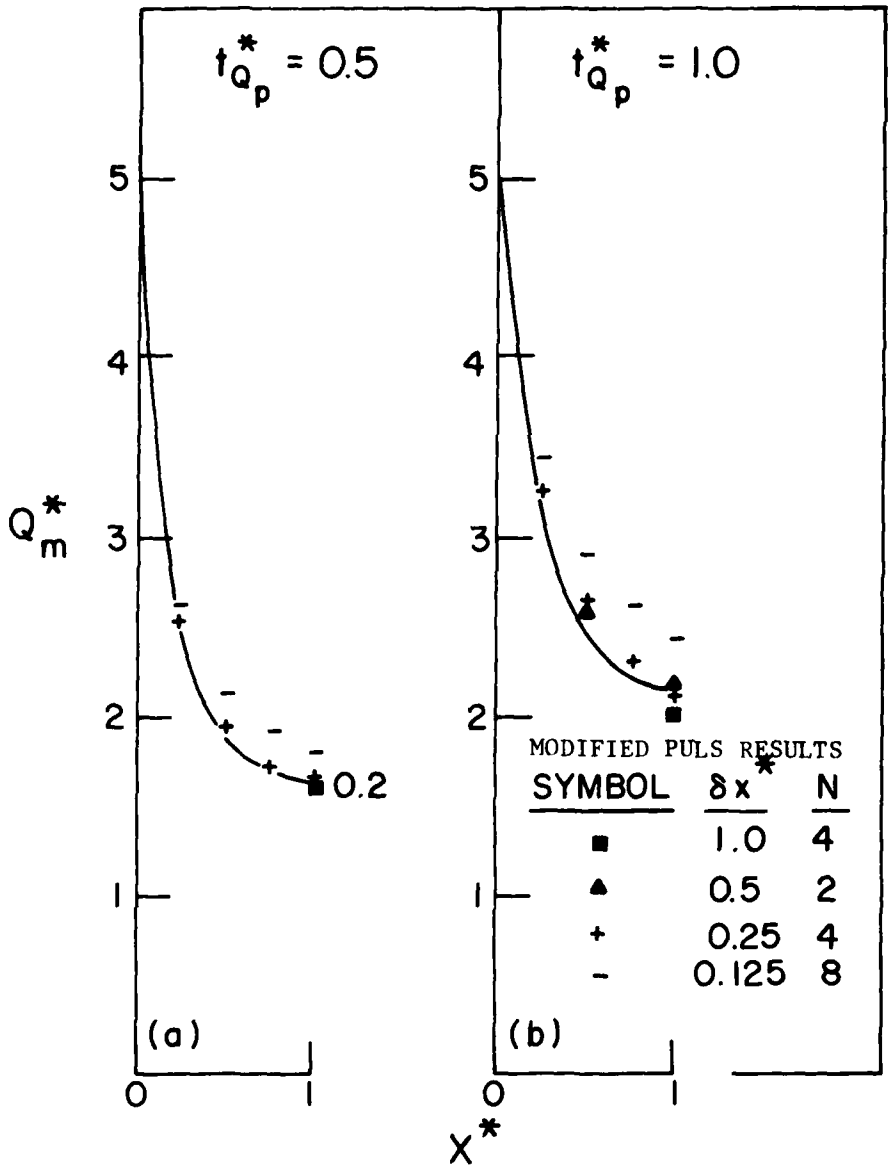

Fig. 14a-b Attenuation of discharge hydrograph peaks, channel with floodplain, weir downstream boundary condition.

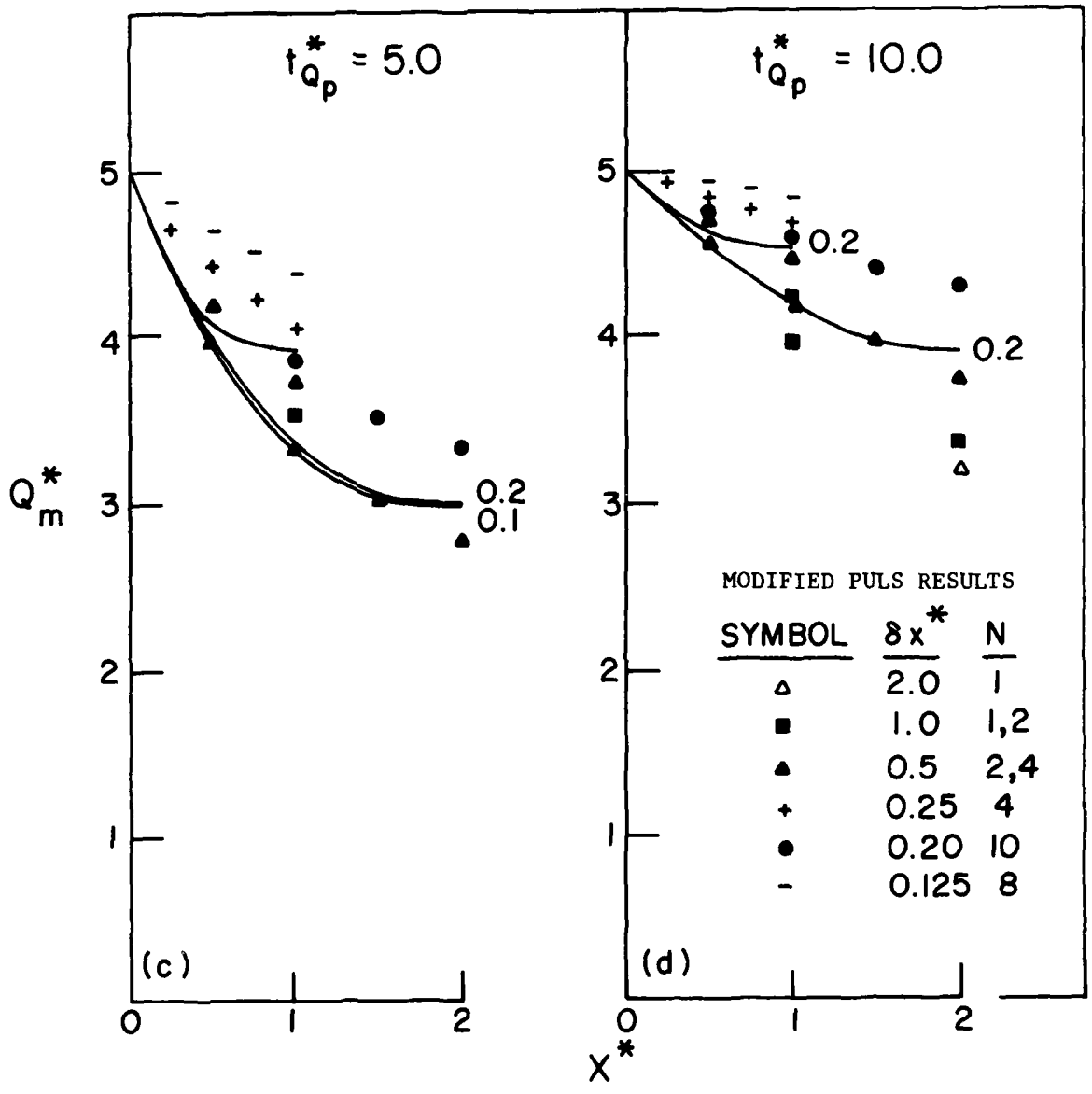

Fig. 14c-d Attenuation of discharge hydrograph peaks, channel with floodplain, weir downstream boundary condition.

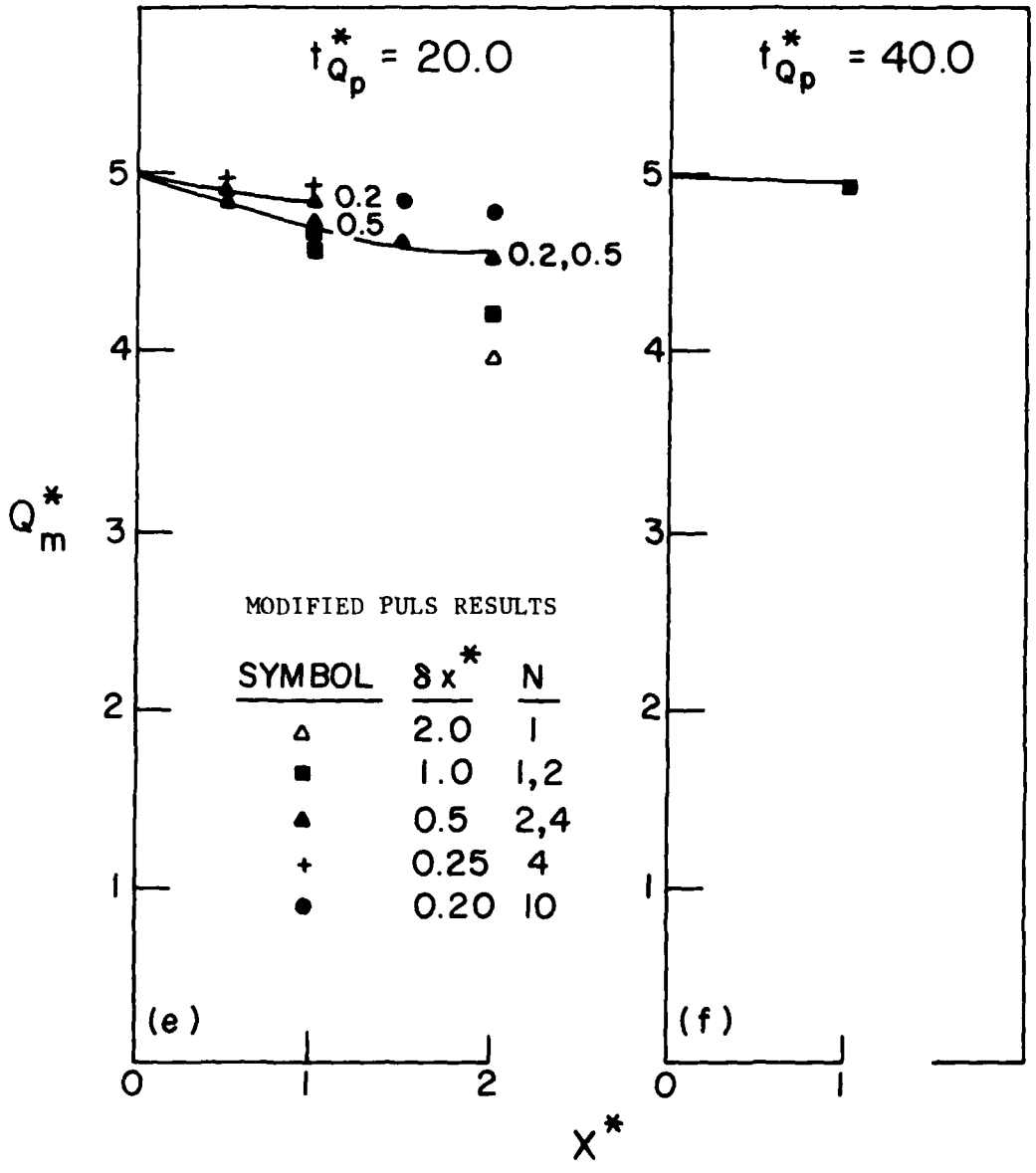

Fig. 14 e-f Attenuation of discharge hydrograph peaks, channel with floodplain, weir downstream boundary condition.

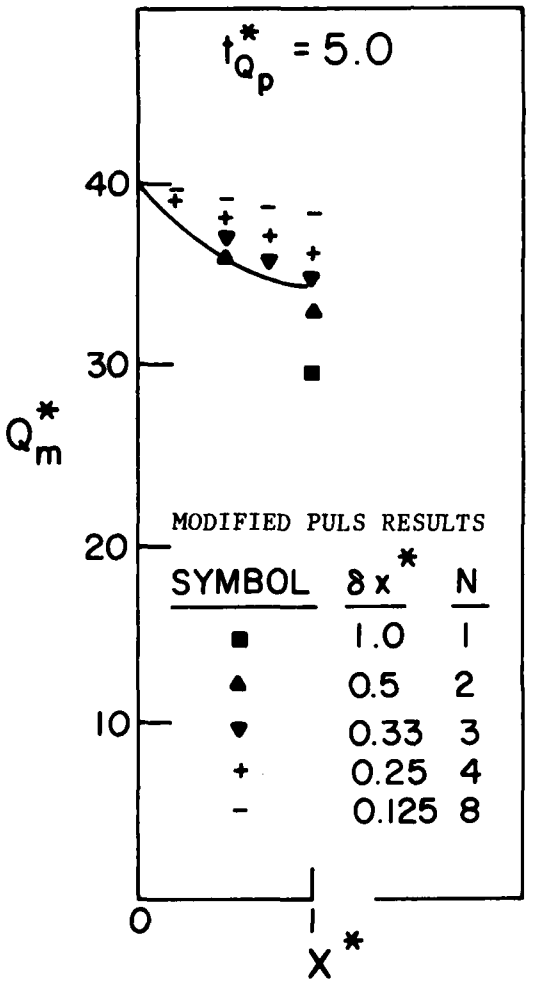

Fig. 14g Attenuation of discharge hydrograph peaks, channel with floodplain, weir downstream boundary condition.

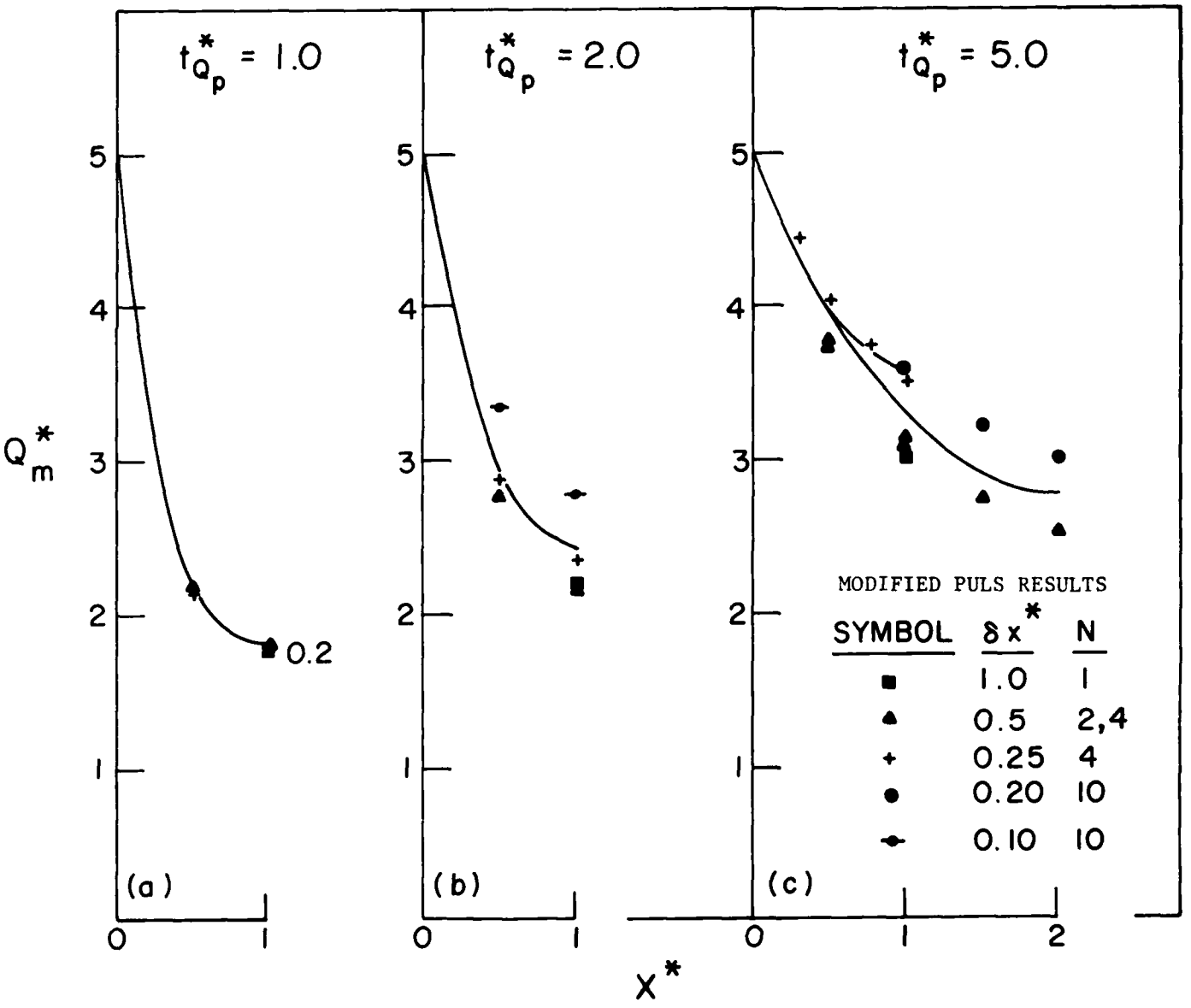

Fig. 15 a-c Attenuation of discharge hydrograph peaks, channel with floodplain, overfall downstream boundary condition.

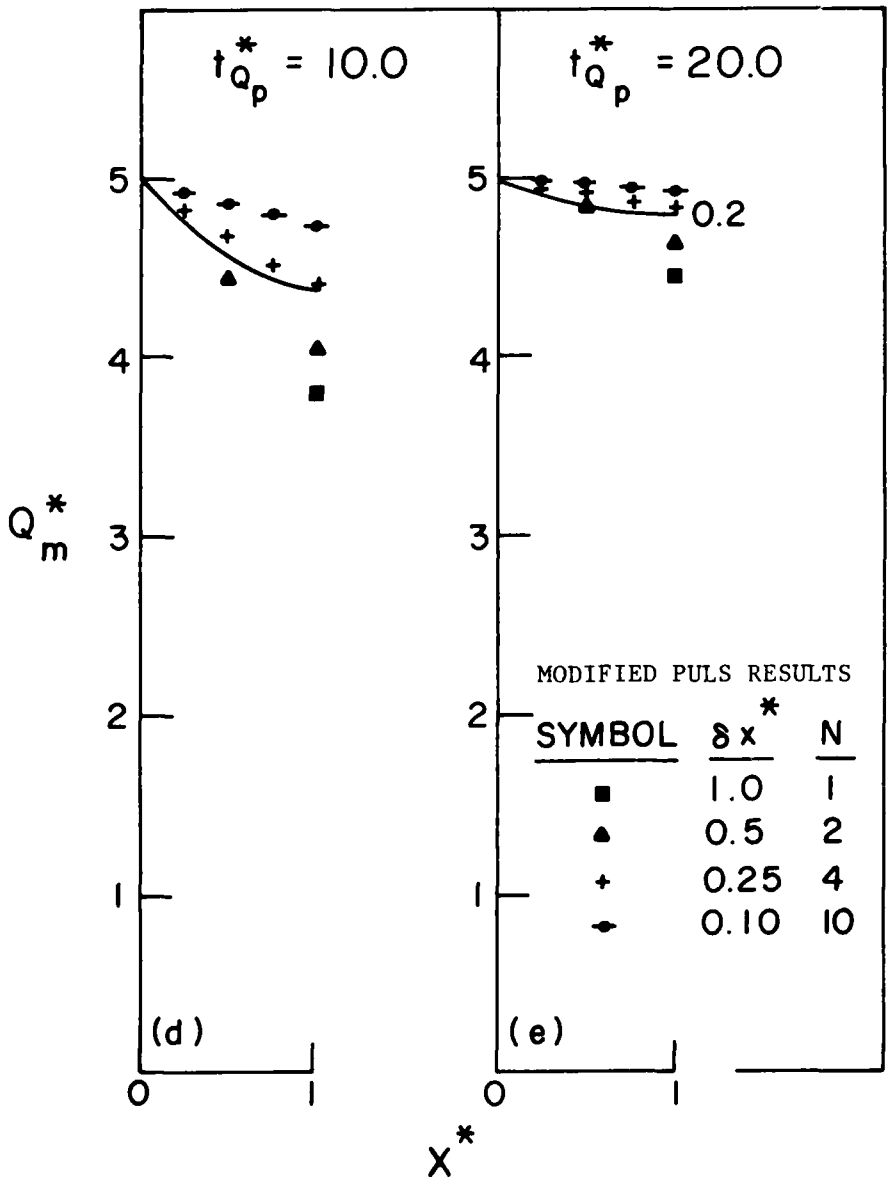

Fig. 15 d-e Attenuation of discharge hydrograph peaks, channel with floodplain, overfall downstream boundary condition.

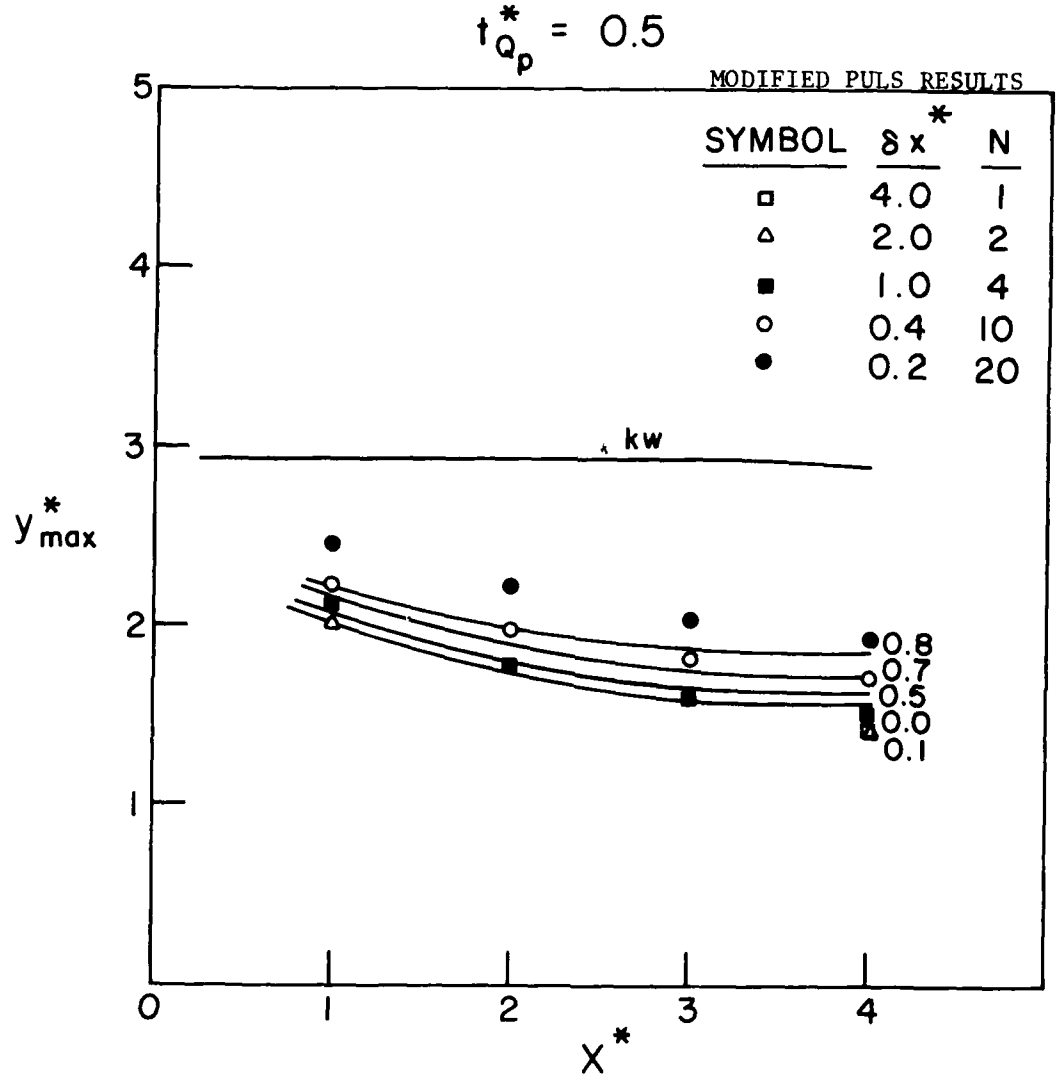

Fig. 16a Attenuation of stage hydrograph peaks, rectangular channel, normal depth downstream boundary condition.

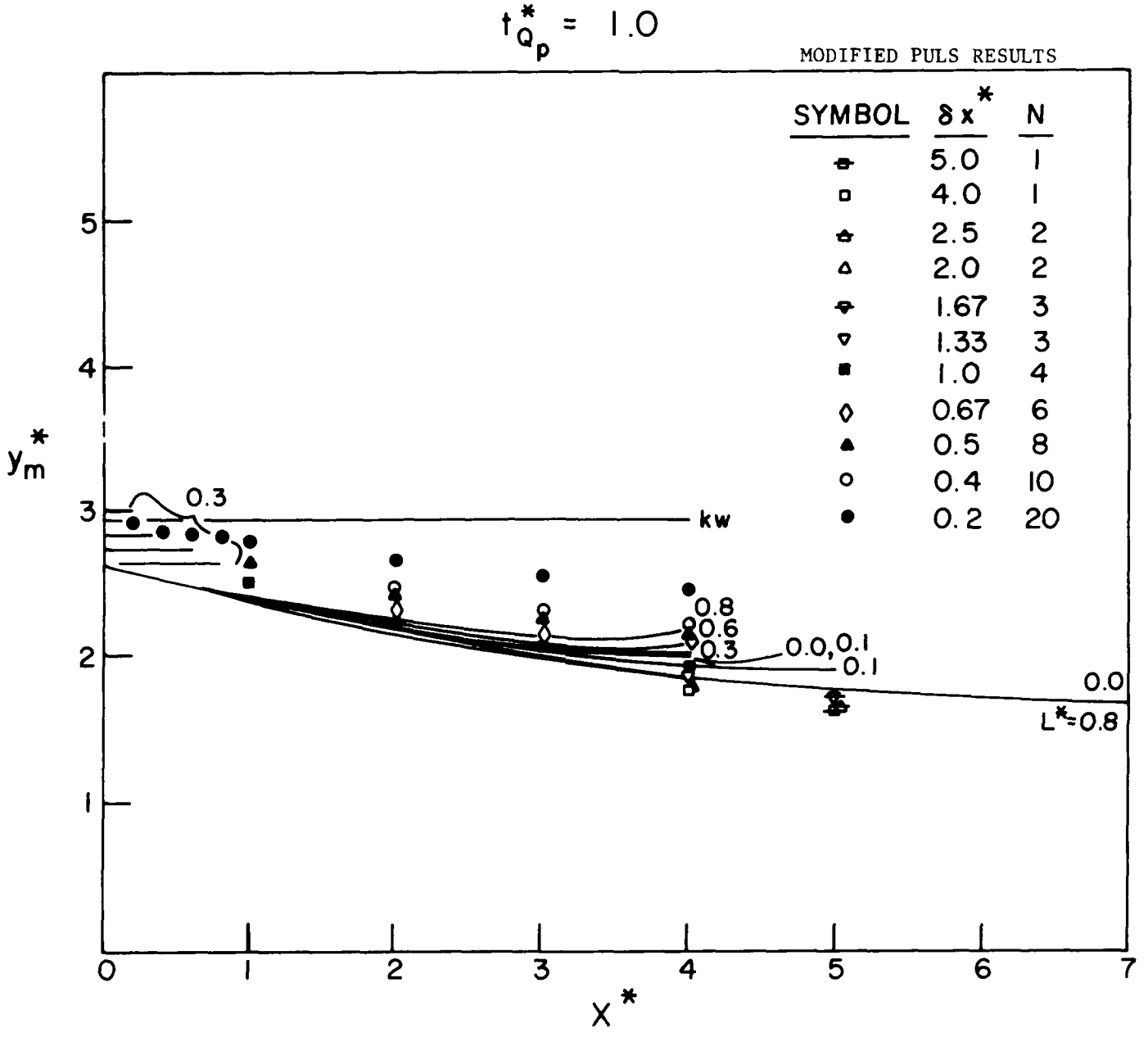

Fig. 16b Attenuation of stage hydrograph peaks, rectangular channel, normal depth downstream boundary condition.

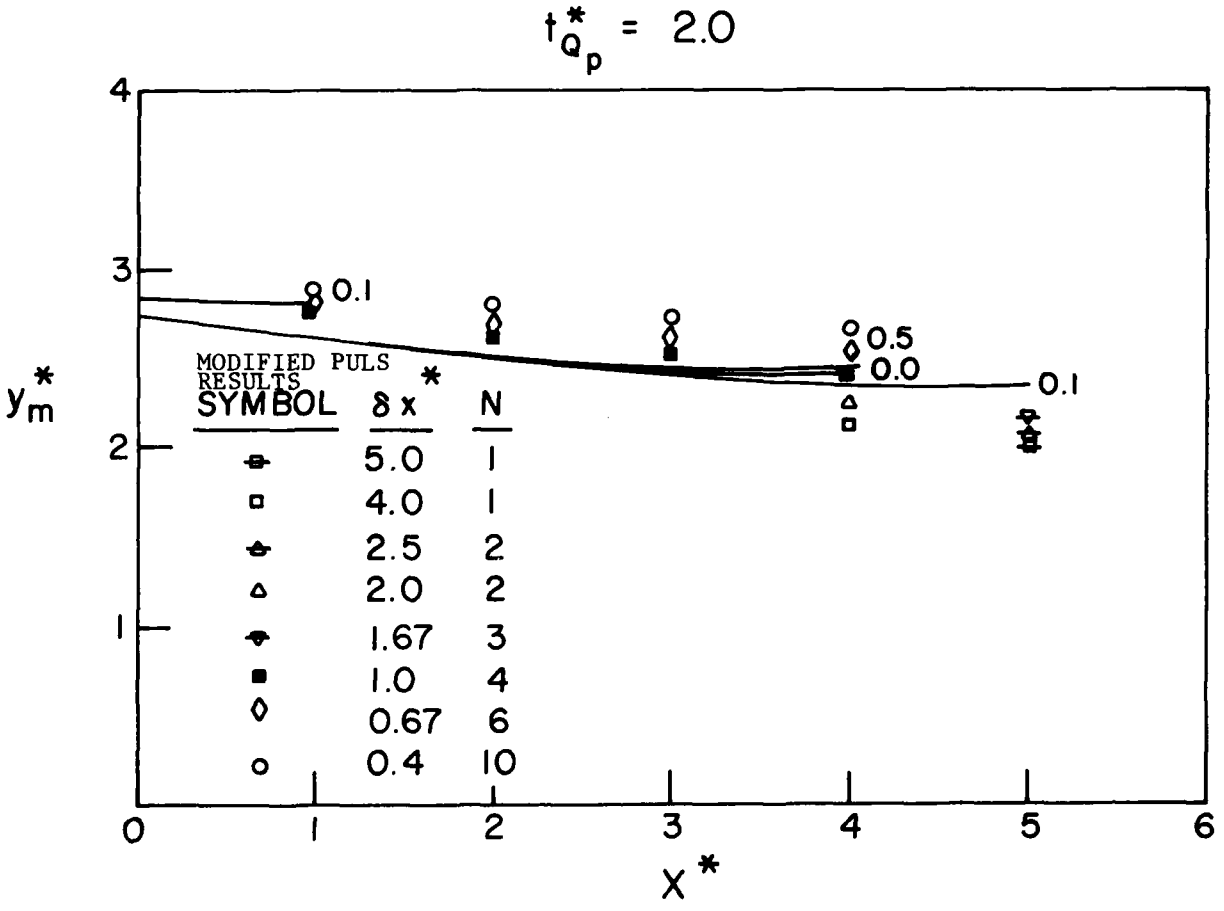

Fig. 16c Attenuation of stage hydrograph peaks, rectangular channel, normal depth downstream boundary condition.

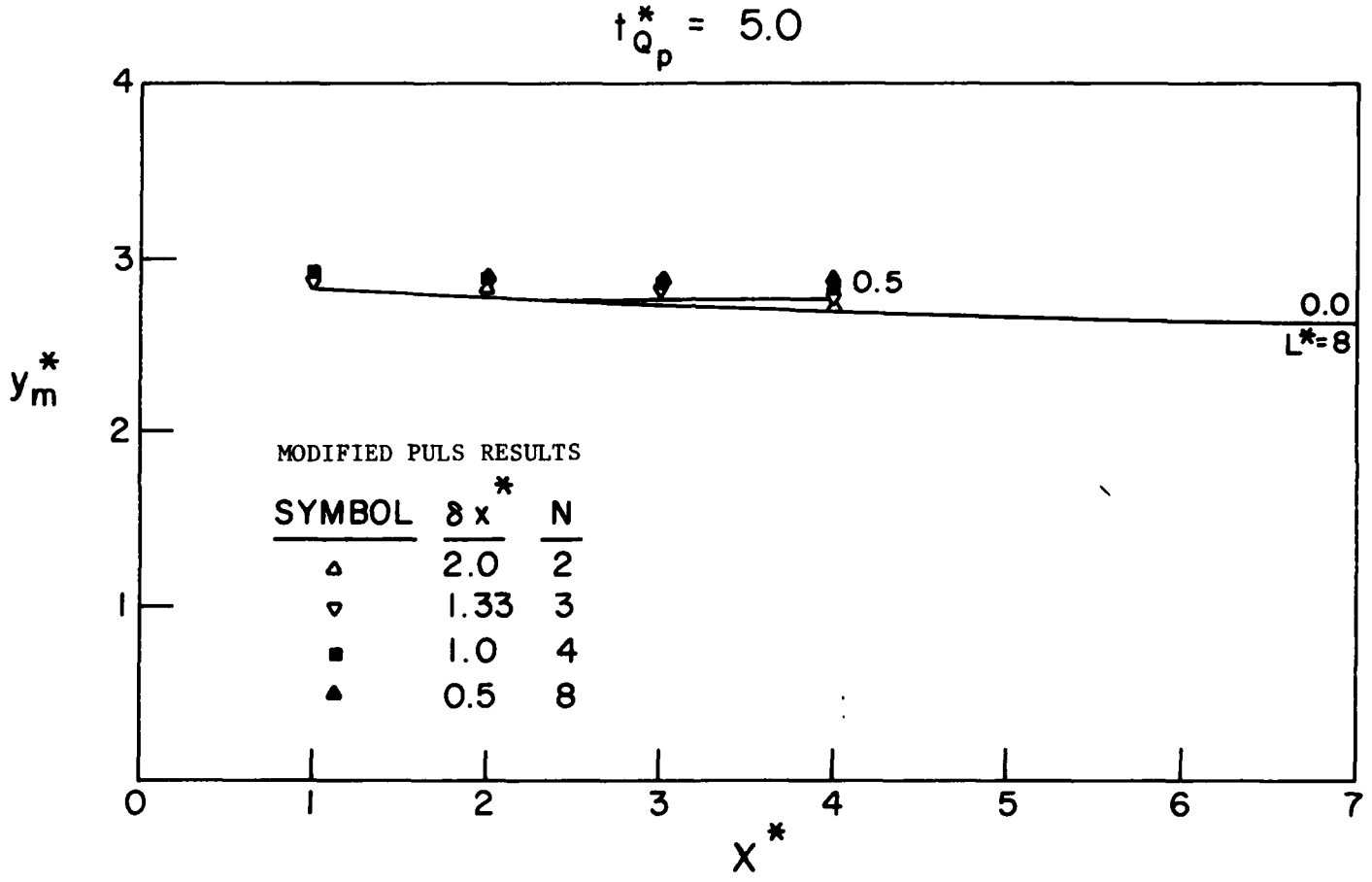

Fig. 16d Attenuation of stage hydrograph peaks, rectangular channel, normal depth downstream boundary condition.

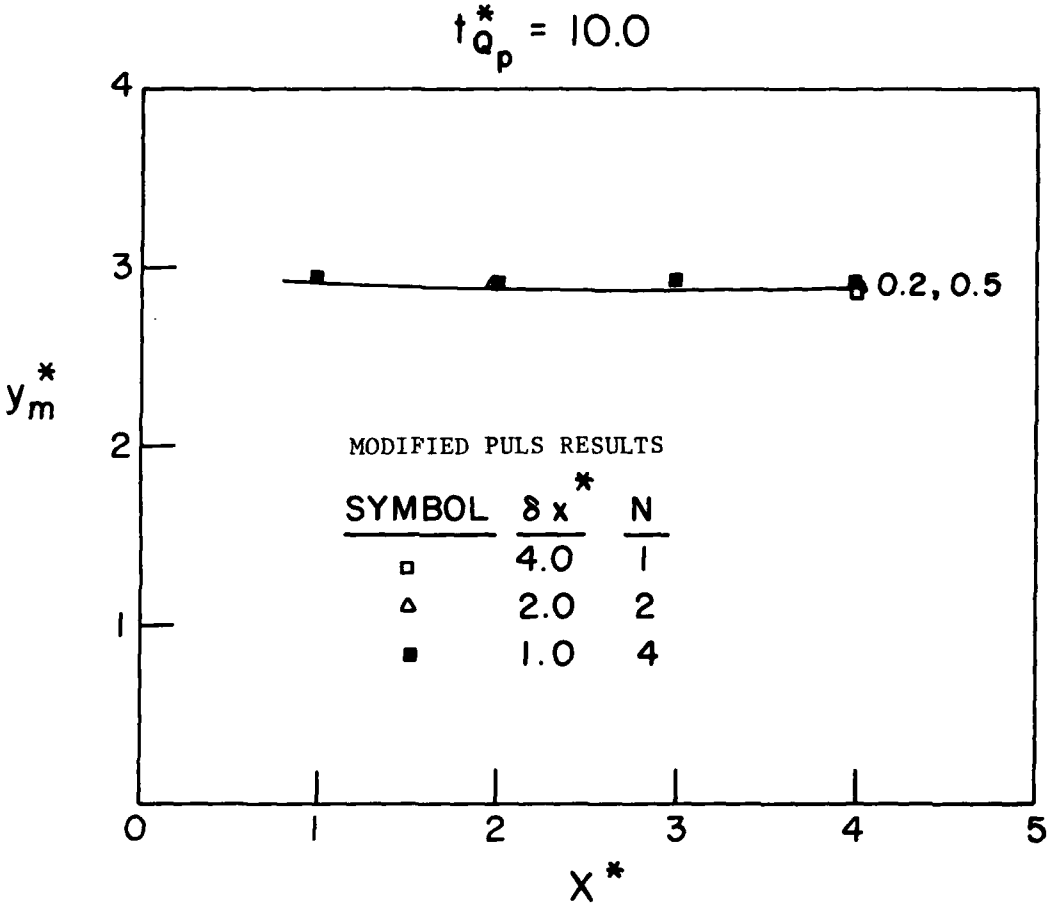

Fig. 16e Attenuation of stage hydrograph peaks, rectangular channel, normal depth downstream boundary condition.

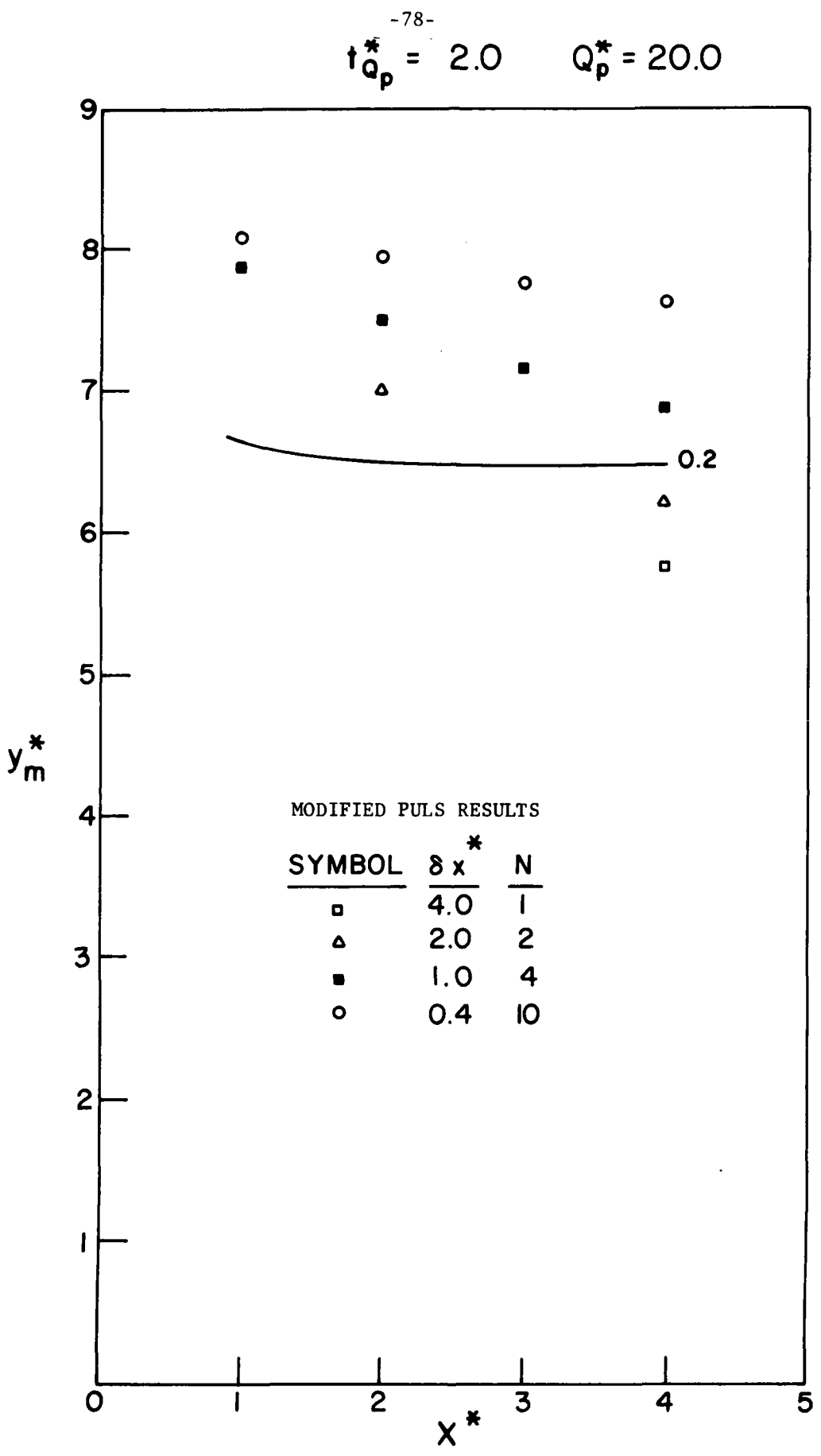

Fig. 16f Attenuation of stage hydrograph peaks, rectangular channel, normal depth downstream boundary condition.

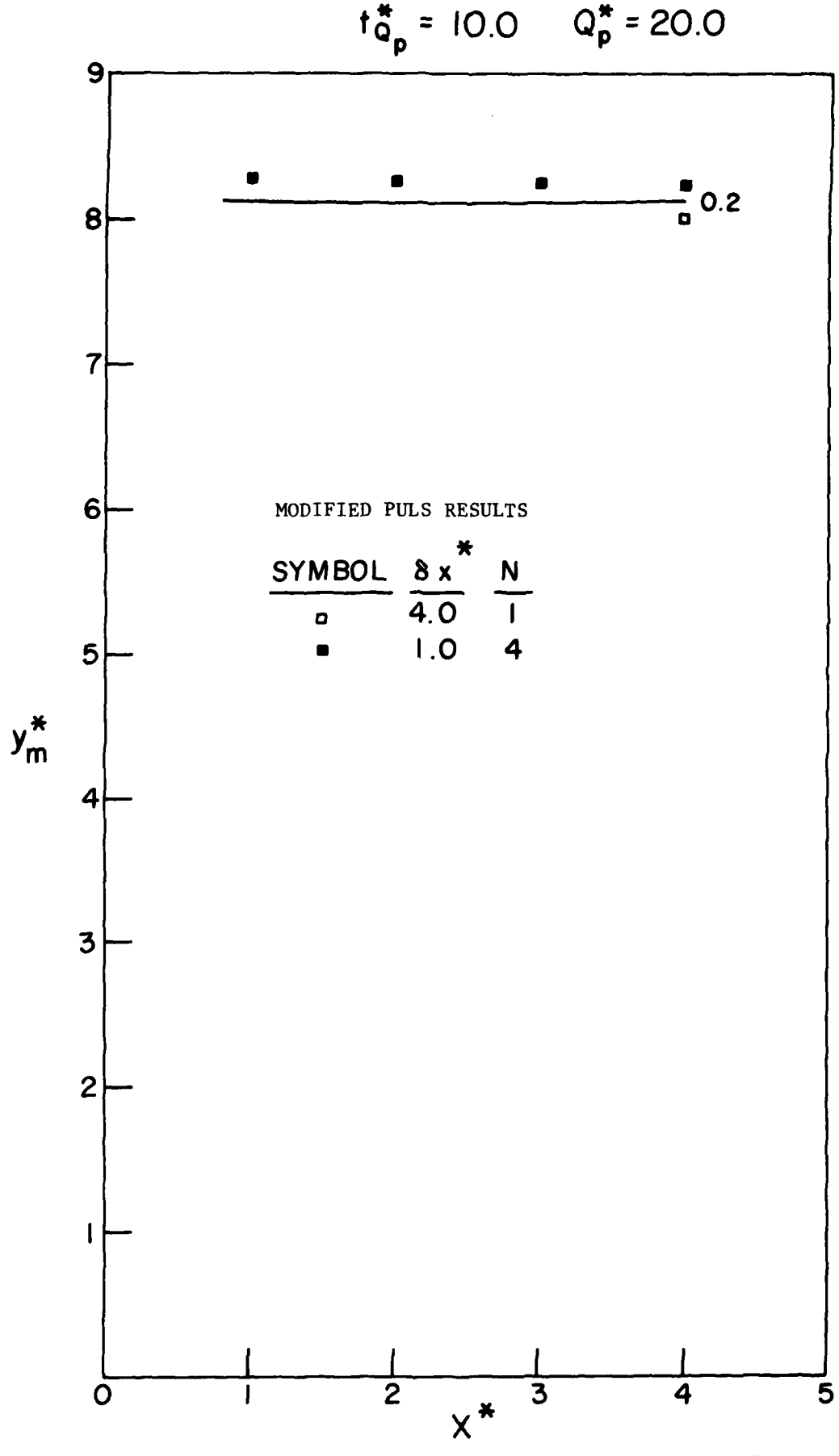

Fig. 16g Attenuation of stage hydrograph peaks, rectangular channel, normal depth downstream boundary condition.

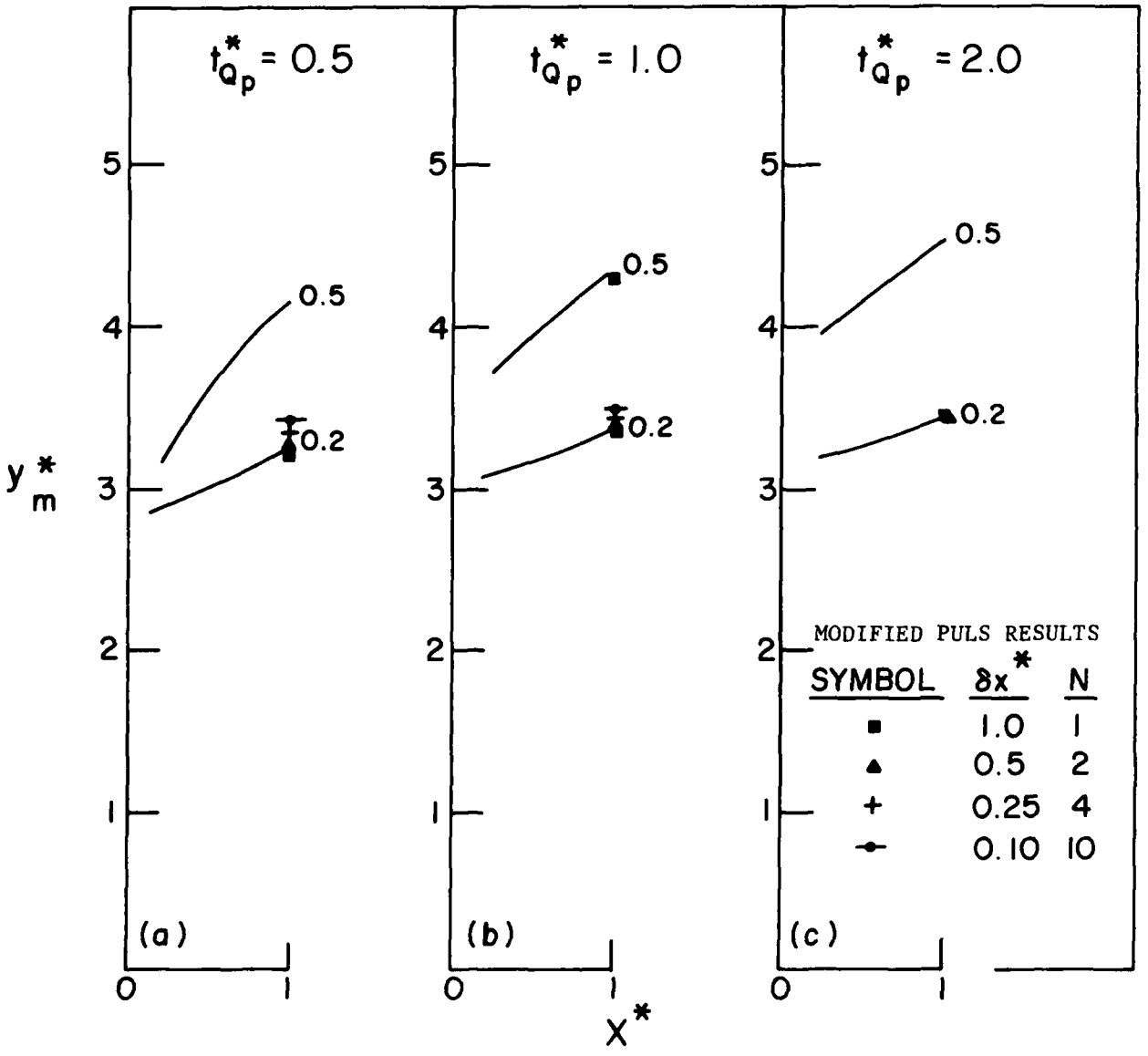

Fig. 17a-c Attenuation of stage hydrograph peaks, rectangular channel, weir downstream boundary condition.

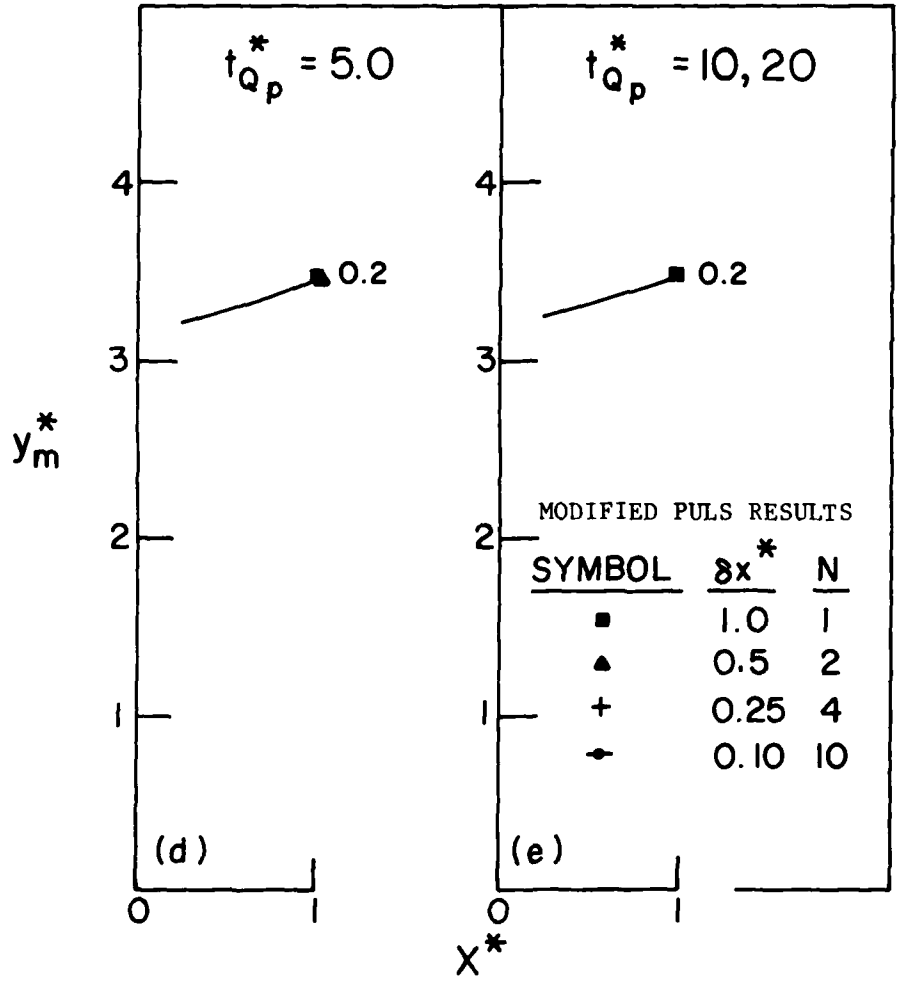

Fig. 17_{d-e} Attenuation of stage hydrograph peaks, rectangular channel, weir downstream boundary condition.

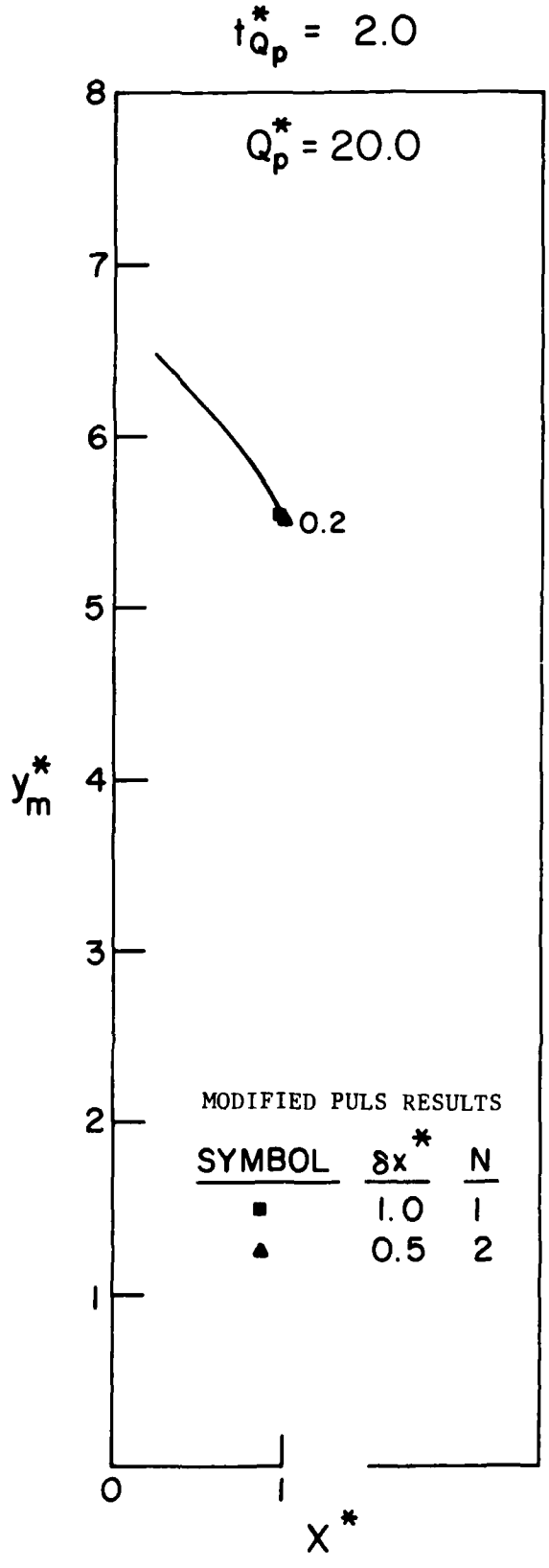

Fig. 17f Attenuation of stage hydrograph peaks, rectangular channel, weir downstream boundary condition.

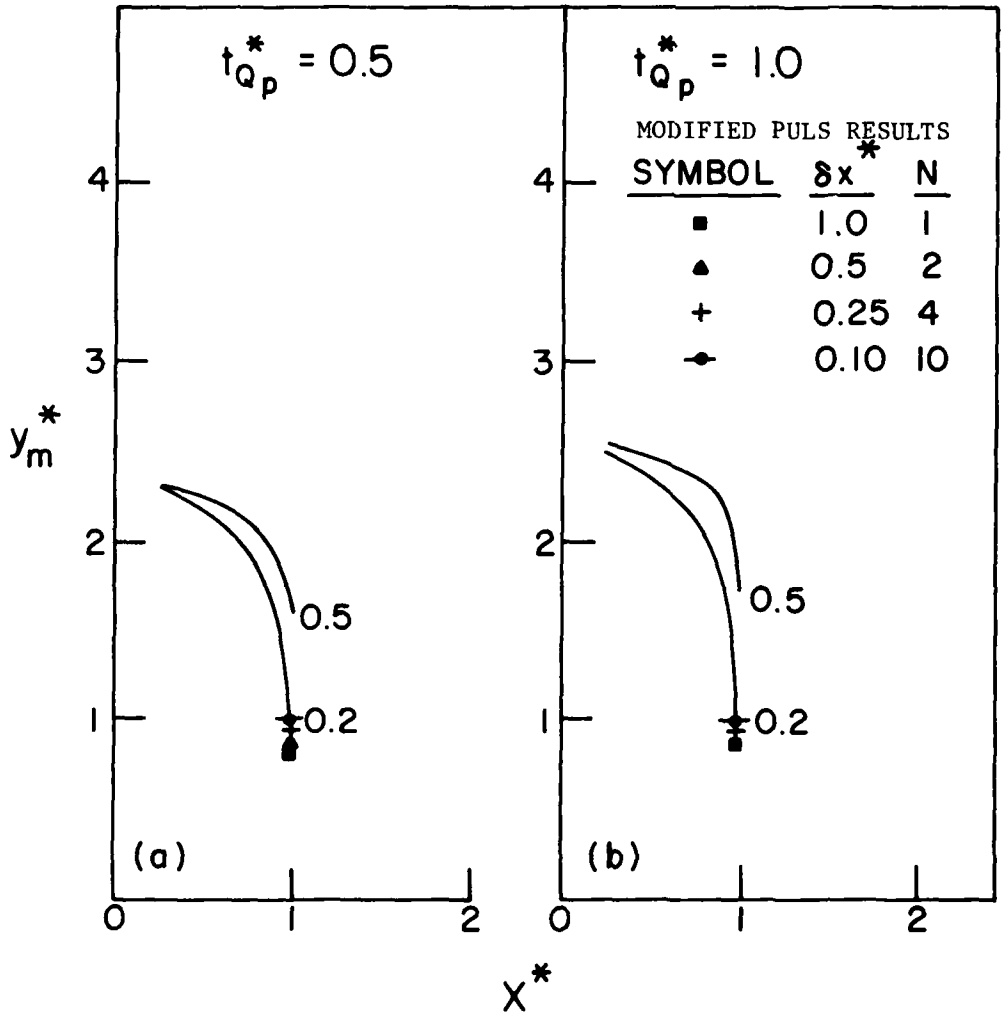

Fig. 18 a-b Attenuation of stage hydrograph peaks, rectangular channel, overfall downstream boundary condition.

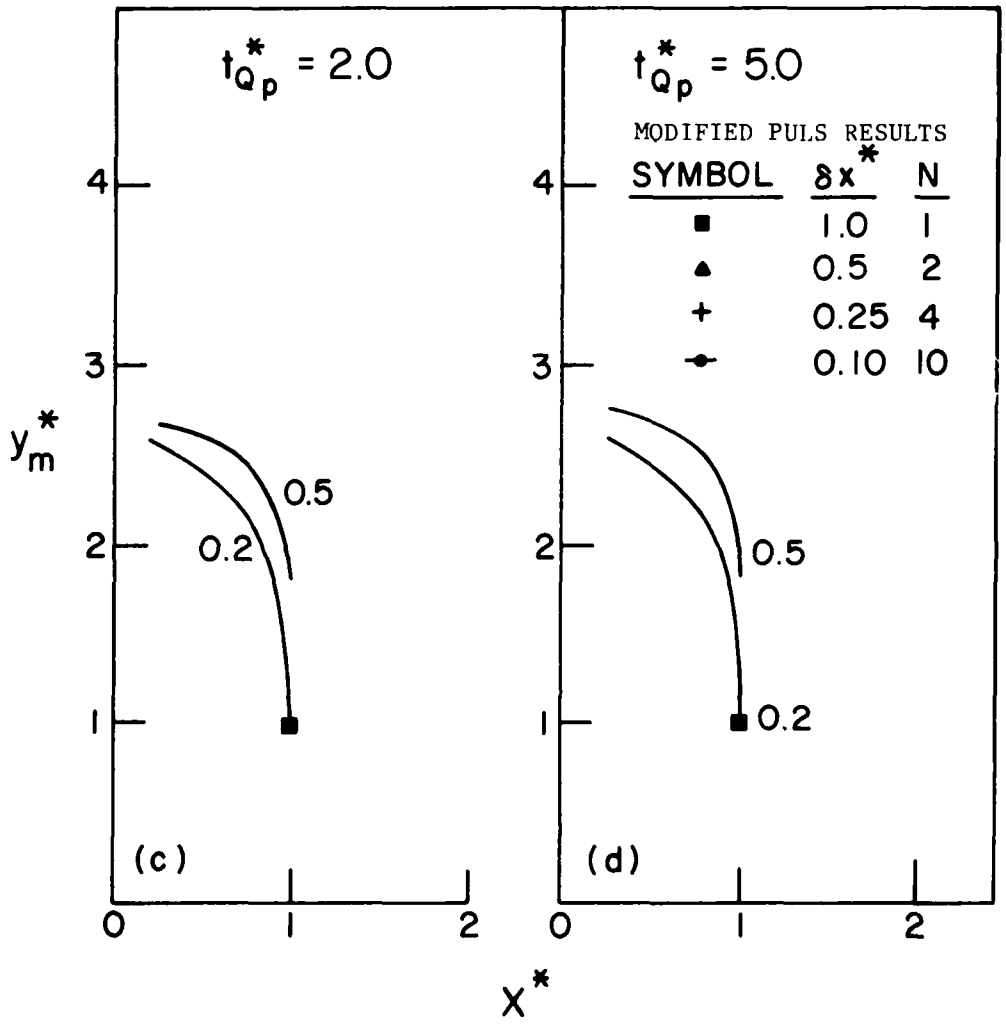

Fig. 18c-d Attenuation of stage hydrograph peaks, rectangular channel, overfall downstream boundary condition.

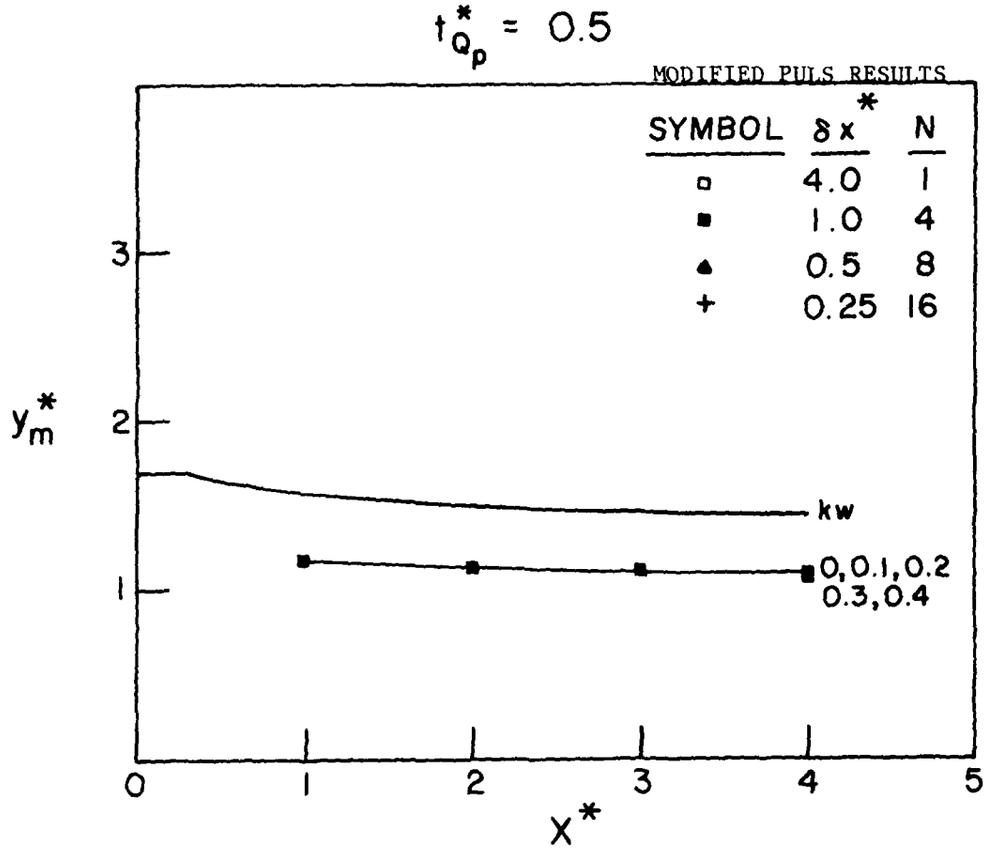

Fig. 19a Attenuation of stage hydrograph peaks, channel with floodplain, normal depth downstream boundary condition.

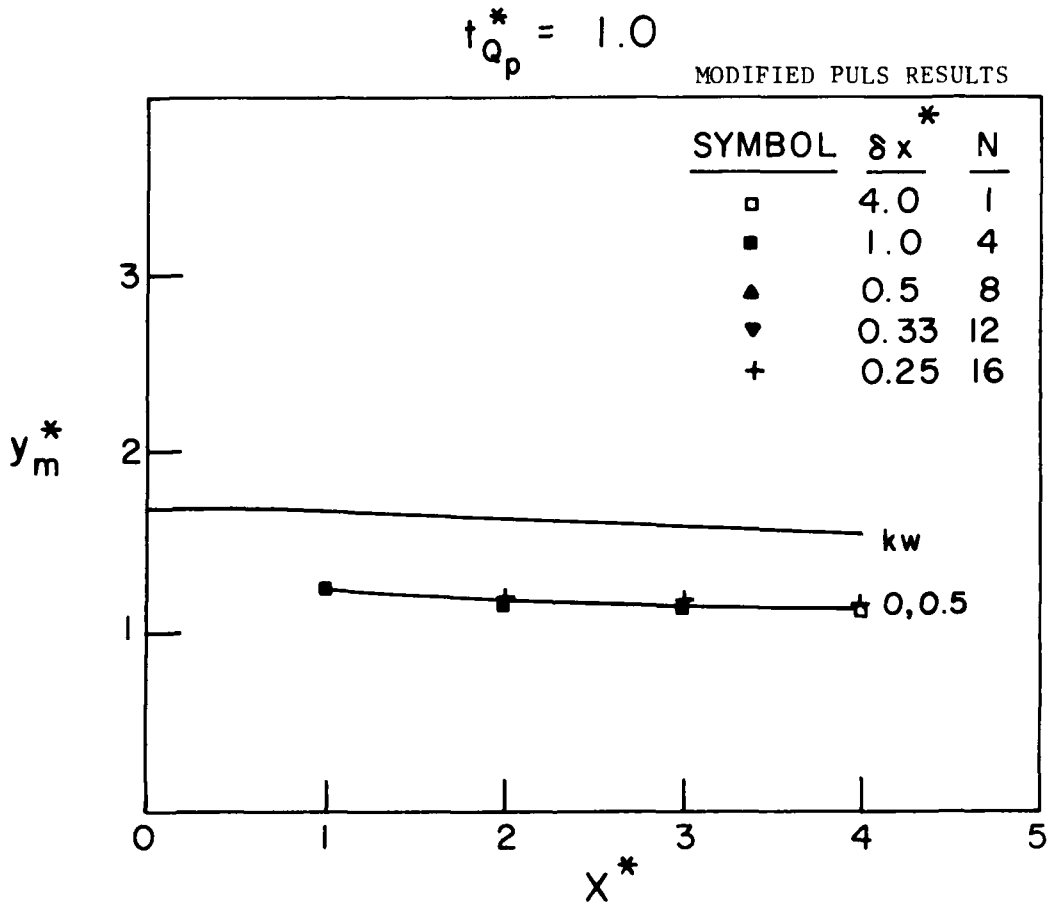

Fig. 19b Attenuation of stage hydrograph peaks, channel with floodplain, normal depth downstream boundary condition.

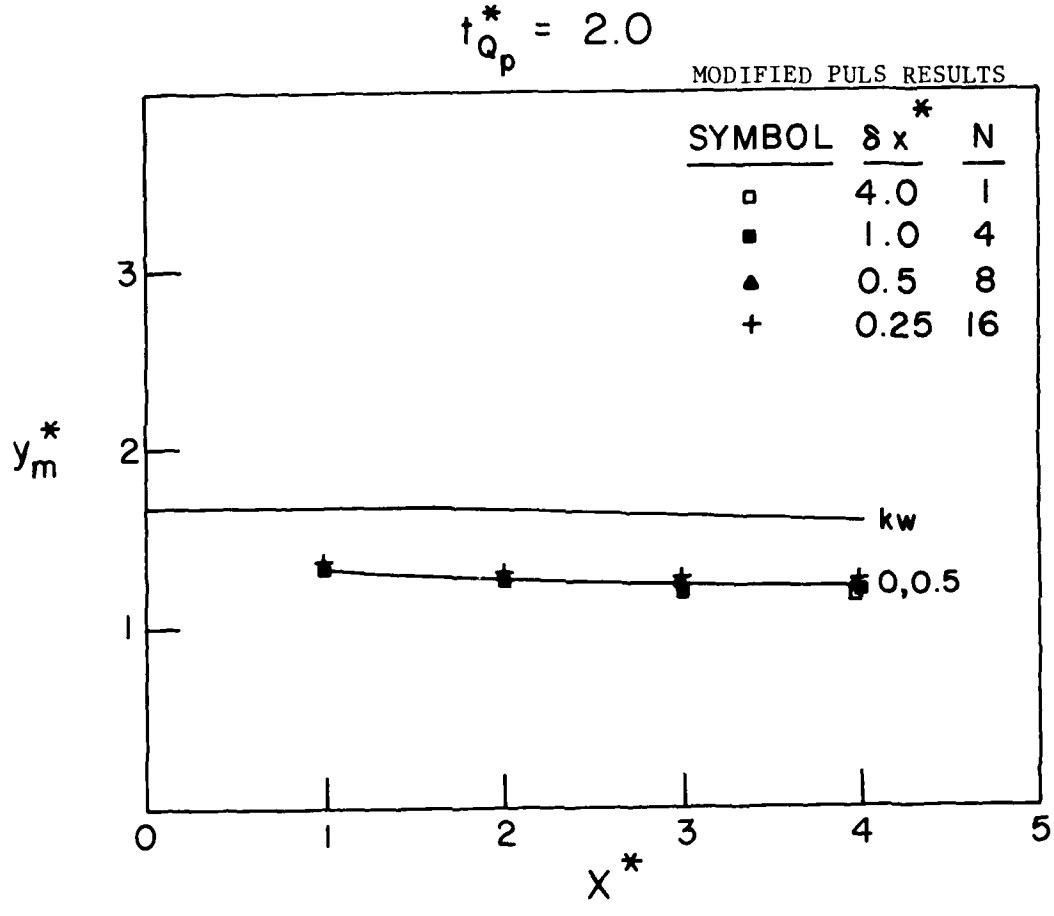

Fig. 19c Attenuation of stage hydrograph peaks, channel with floodplain, normal depth downstream boundary condition.

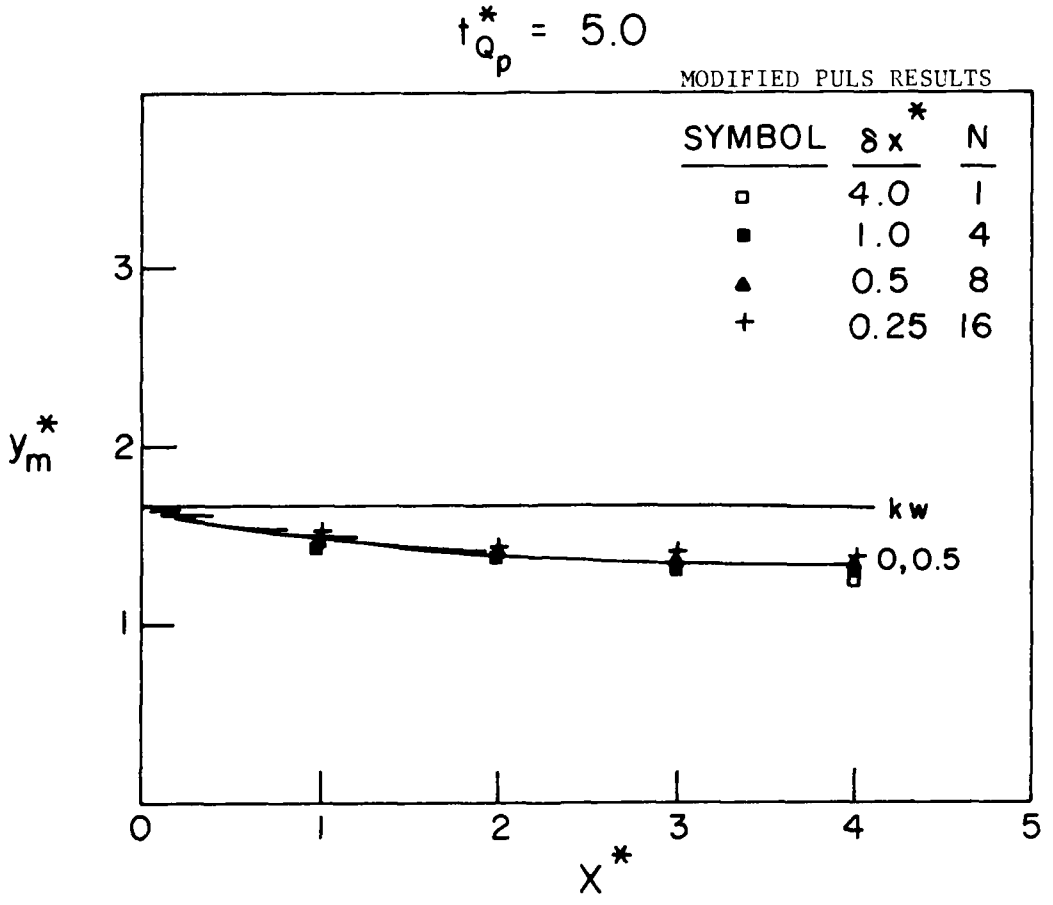

Fig. 19d Attenuation of stage hydrograph peaks, channel with floodplain, normal depth downstream boundary condition.

AD-A158 850 COMPARATIVE ANALYSIS OF FLOOD ROUTING METHODS(U) 2/2
HYDROLOGIC ENGINEERING CENTER DAVIS CA T STRELKOFF
SEP 80 HEC-RD-24

UNCLASSIFIED F/G 13/2 NL

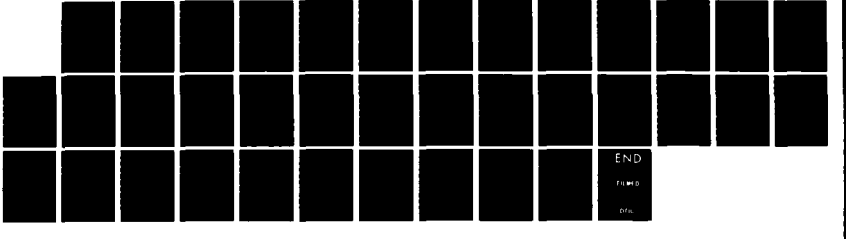

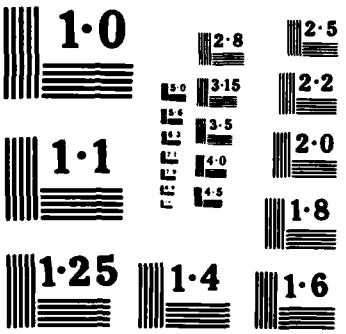

NATIONAL BUREAU OF STANDARDS
MICROCOPY RESOLUTION TEST CHART

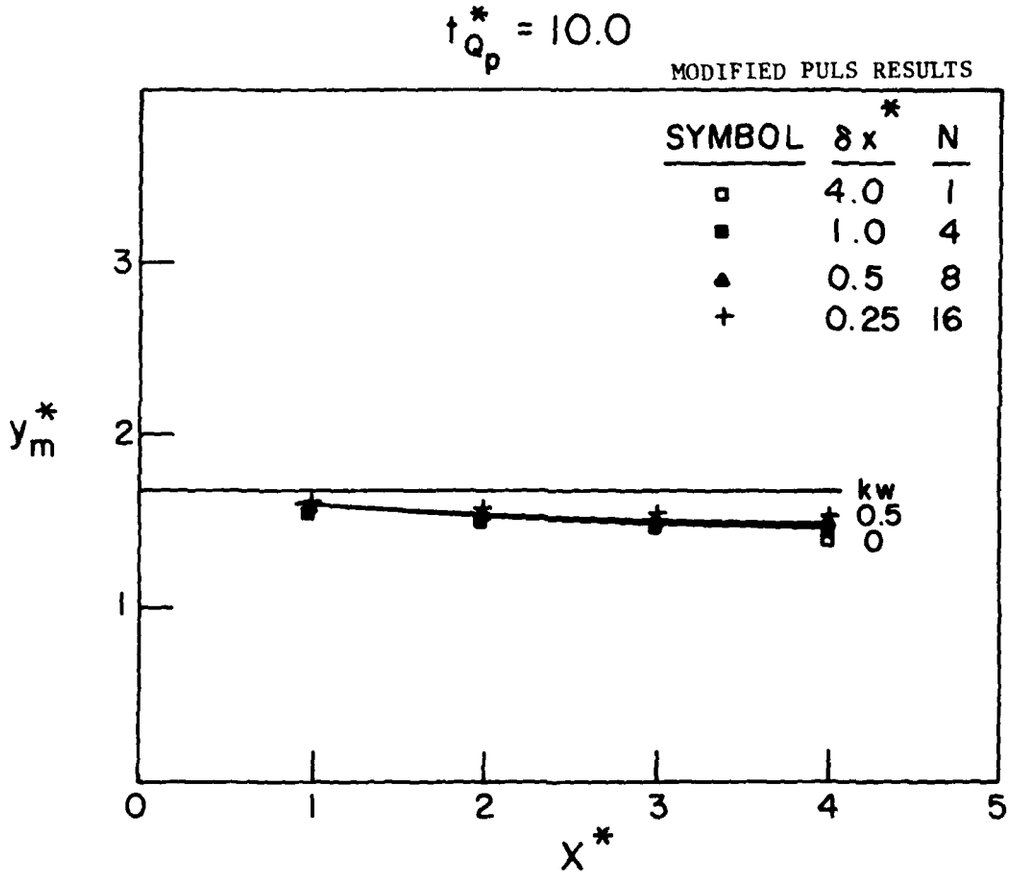

Fig. 19e Attenuation of stage hydrograph peaks, channel with floodplain, normal depth downstream boundary condition.

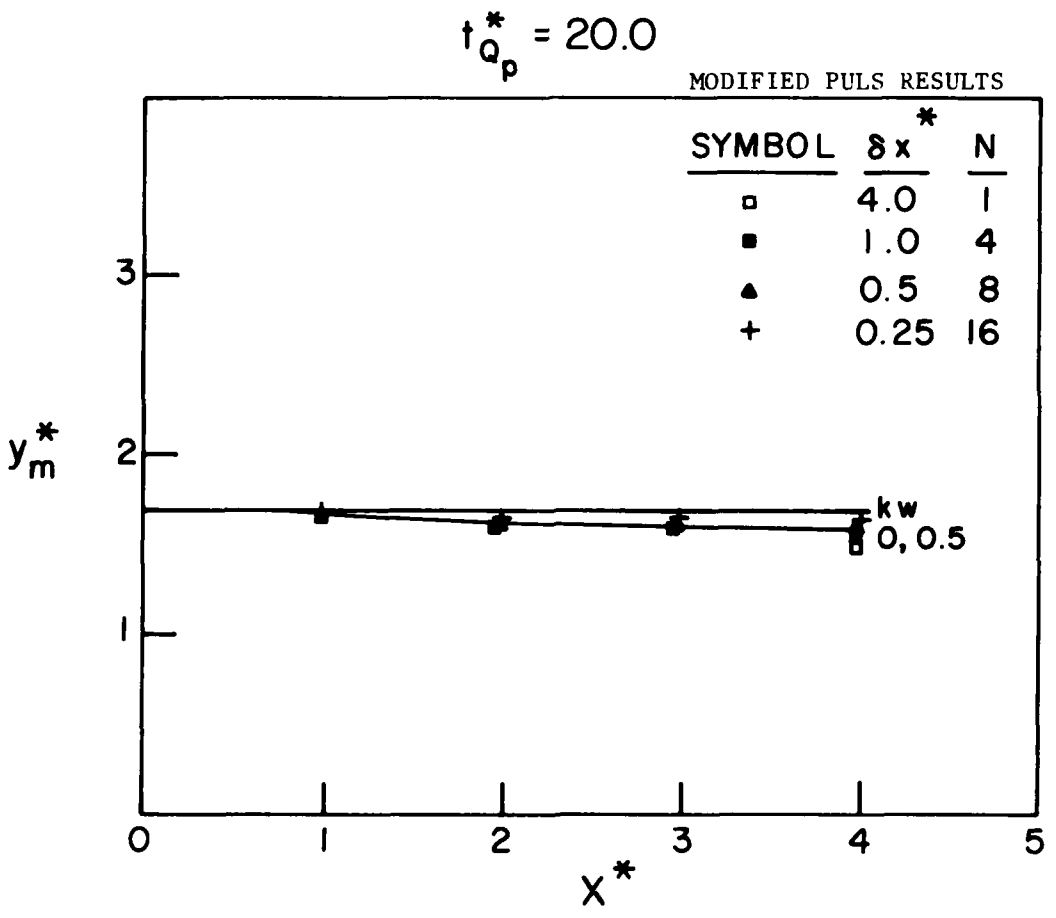

Fig. 19f Attenuation of stage hydrograph peaks, channel with floodplain, normal depth downstream boundary condition.

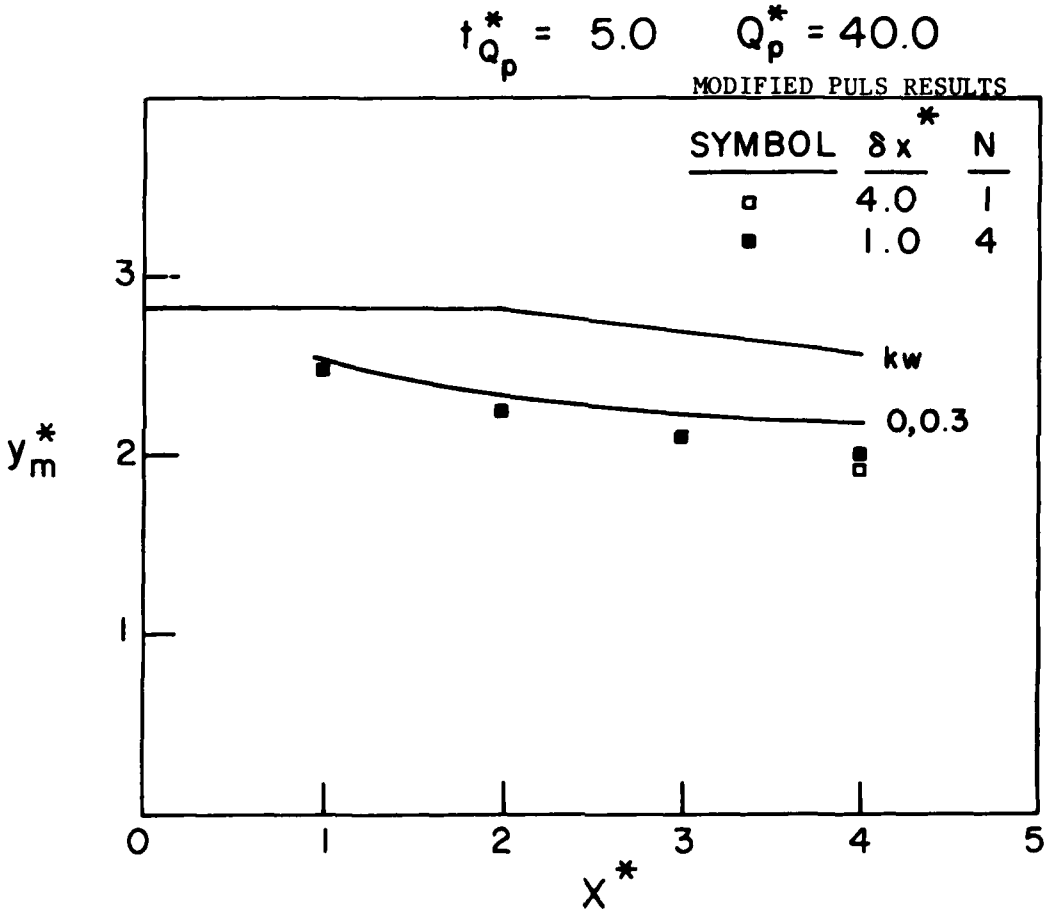

Fig. 19g Attenuation of stage hydrograph peaks, channel with floodplain, normal depth downstream boundary condition.

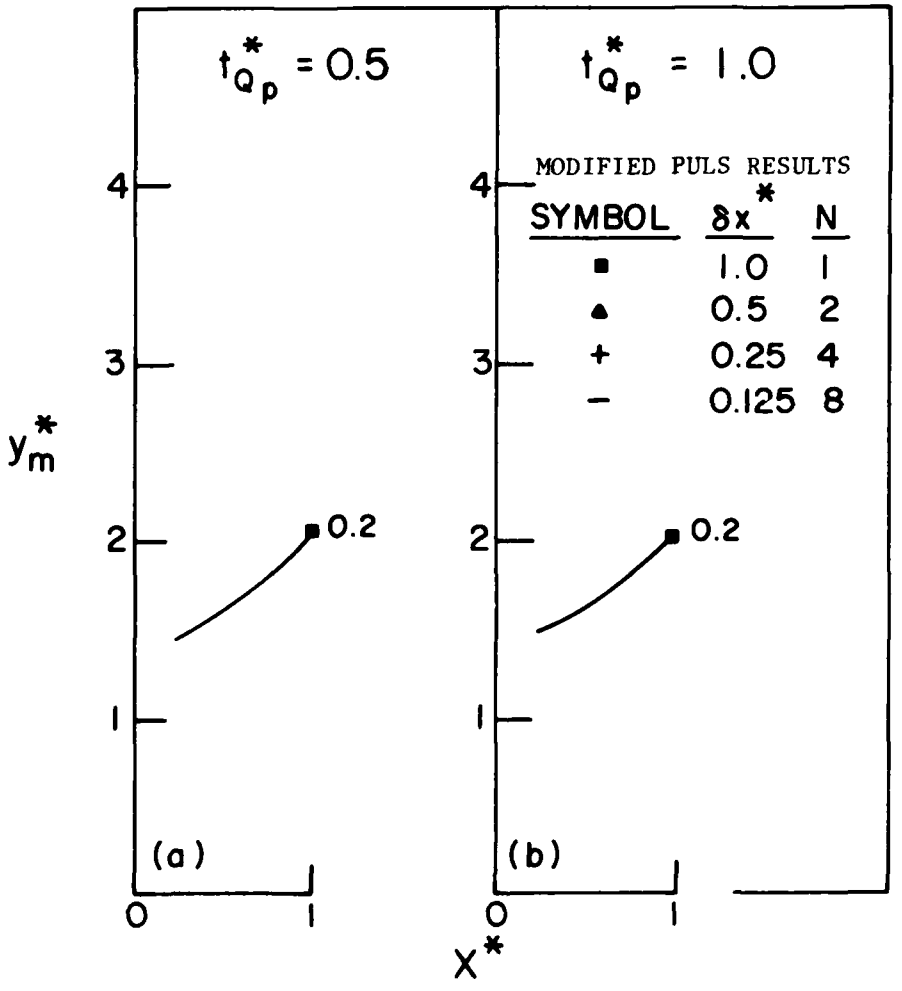

Fig. 20a-b Attenuation of stage hydrograph peaks, channel with floodplain, weir downstream boundary condition.

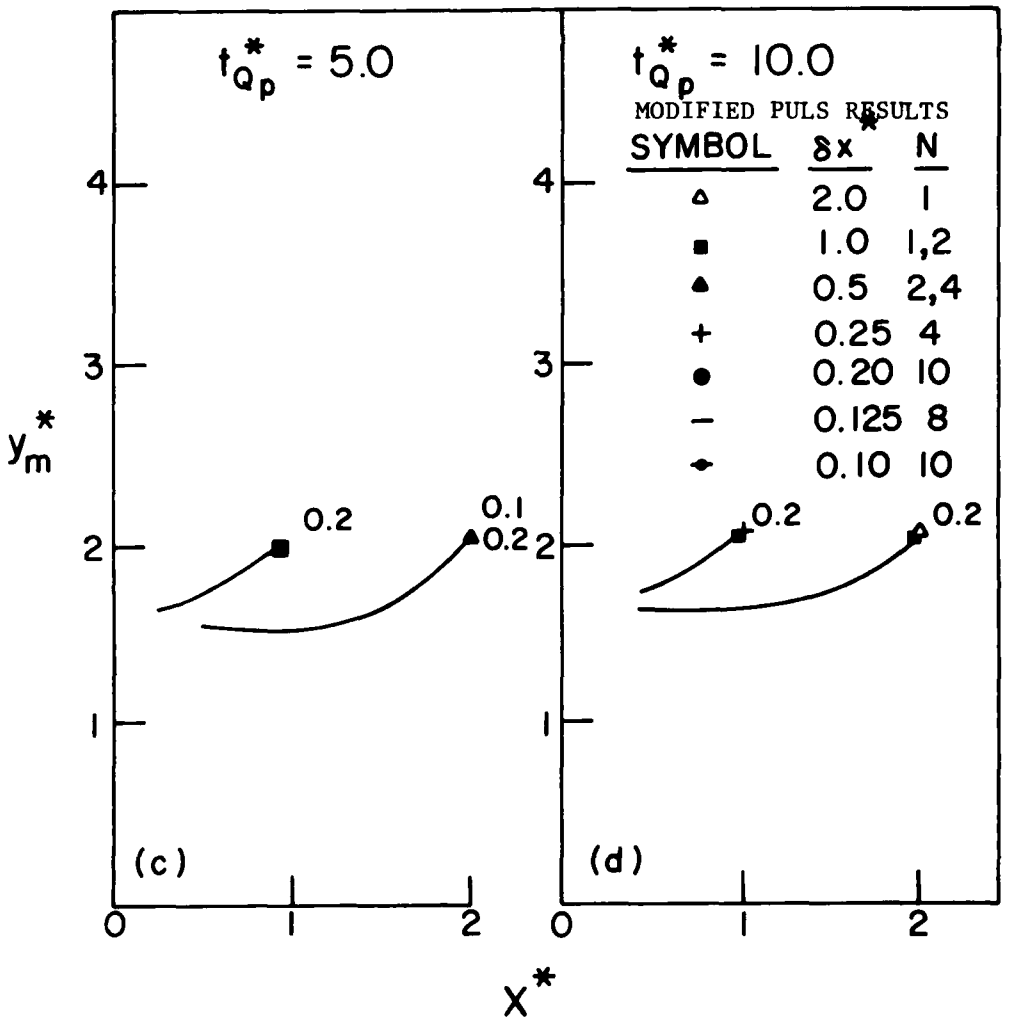

Fig. 20 c-d Attenuation of stage hydrograph peaks, channel with floodplain, weir downstream boundary condition.

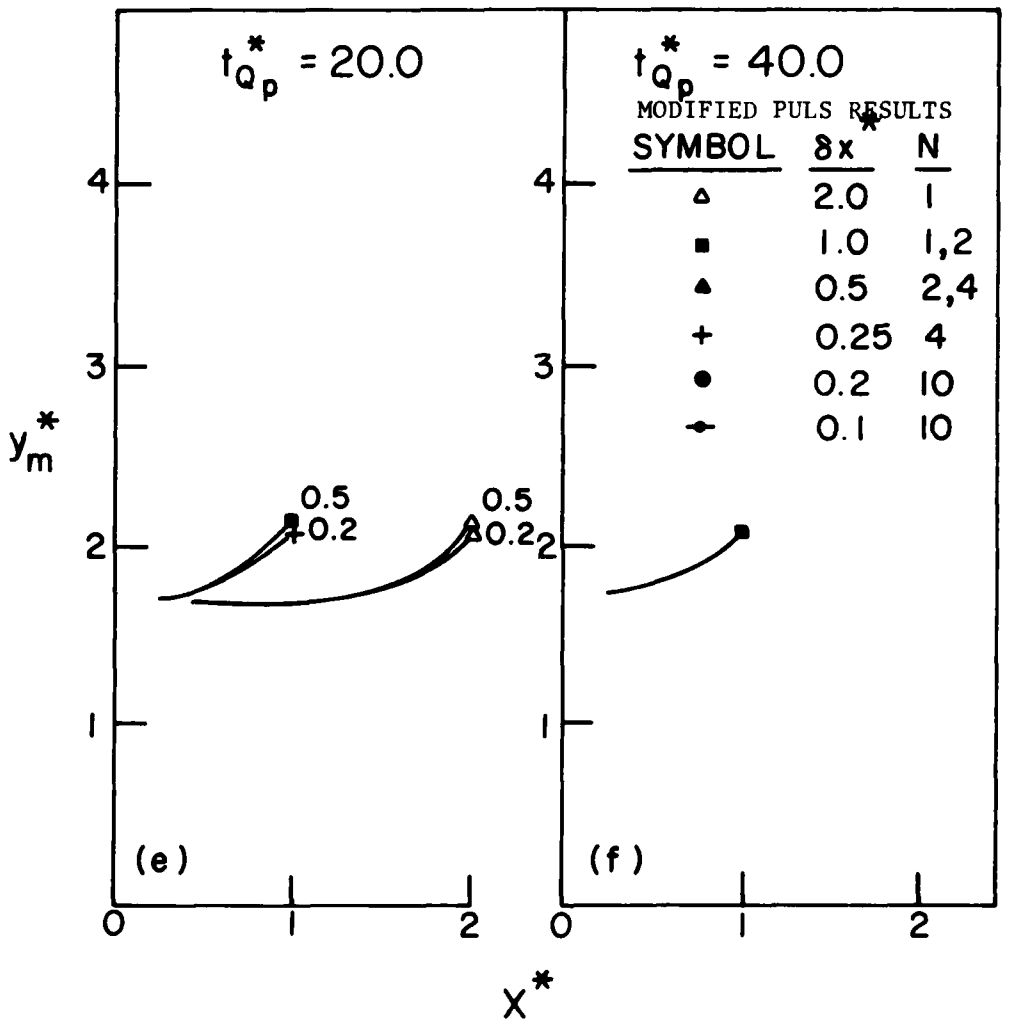

Fig. 20 e-f Attenuation of stage hydrograph peaks, channel with floodplain, weir downstream boundary condition.

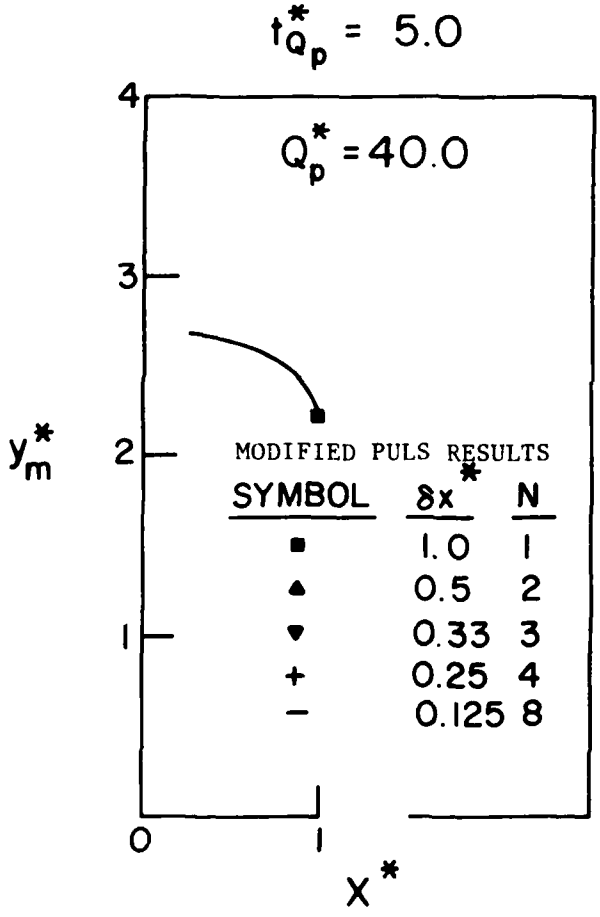

Fig. 20g Attenuation of stage hydrograph peaks, channel with floodplain, weir downstream boundary condition.

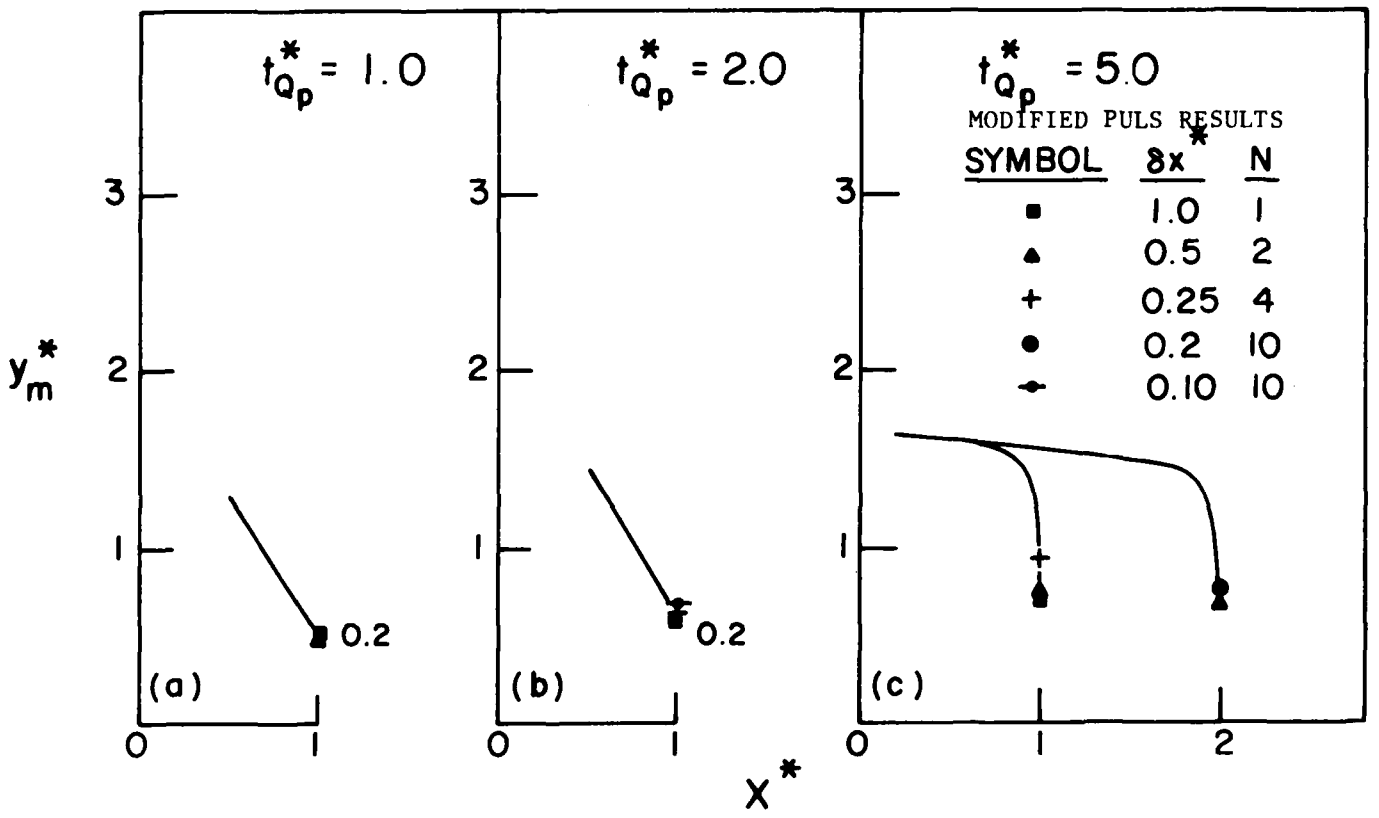

Fig. 21 a-c Attenuation of stage hydrograph peaks, channel with floodplain, overfall downstream boundary condition.

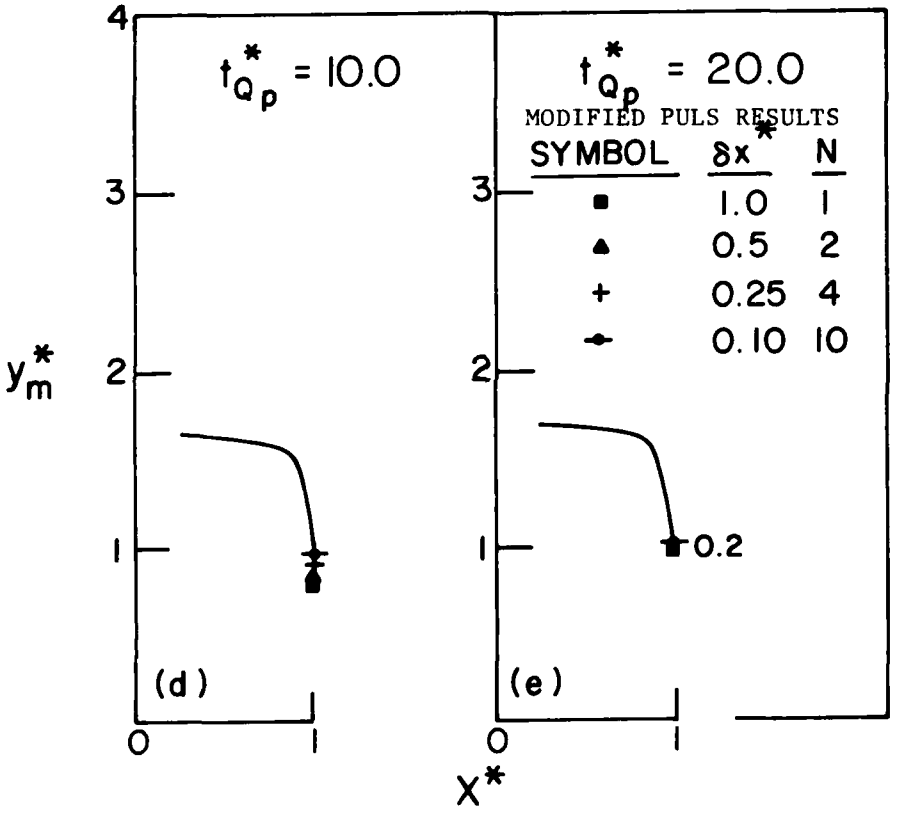

Fig. 21 d-e Attenuation of stage hydrograph peaks, channel with floodplain, overfall downstream boundary condition.

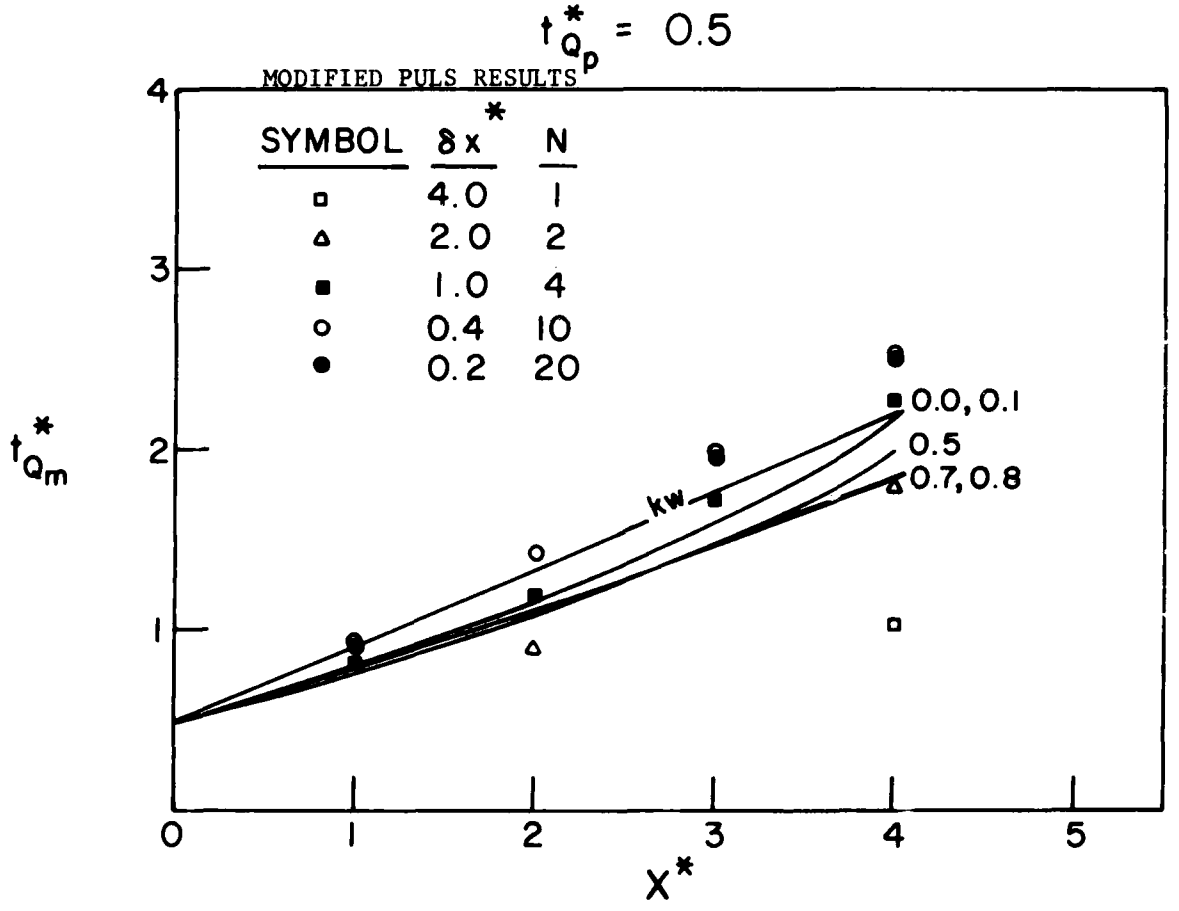

Fig. 22a Time of arrival of peak discharge, rectangular channel, normal depth downstream boundary condition.

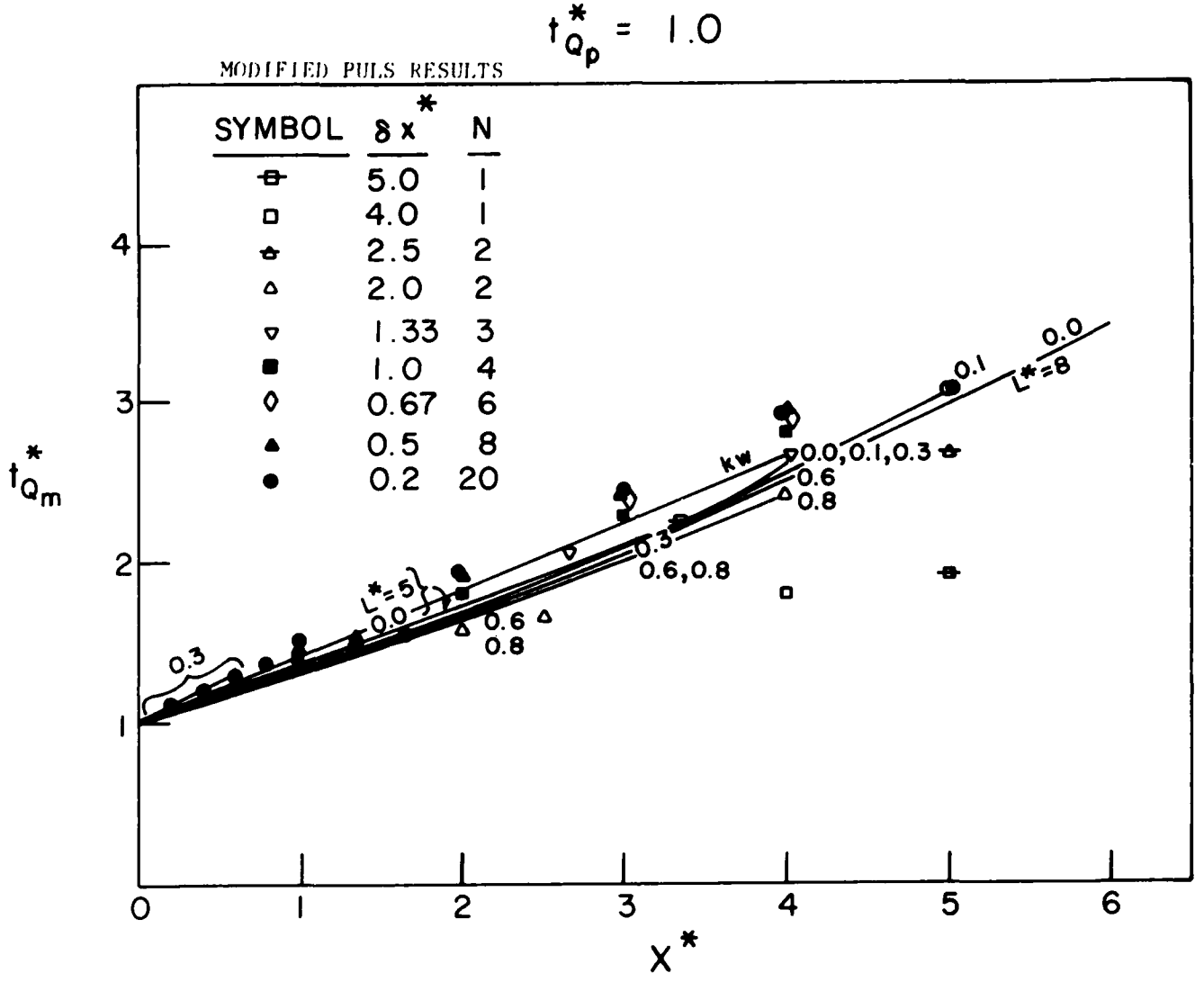

Fig. 22b Time of arrival of peak discharge, rectangular channel, normal depth downstream boundary condition.

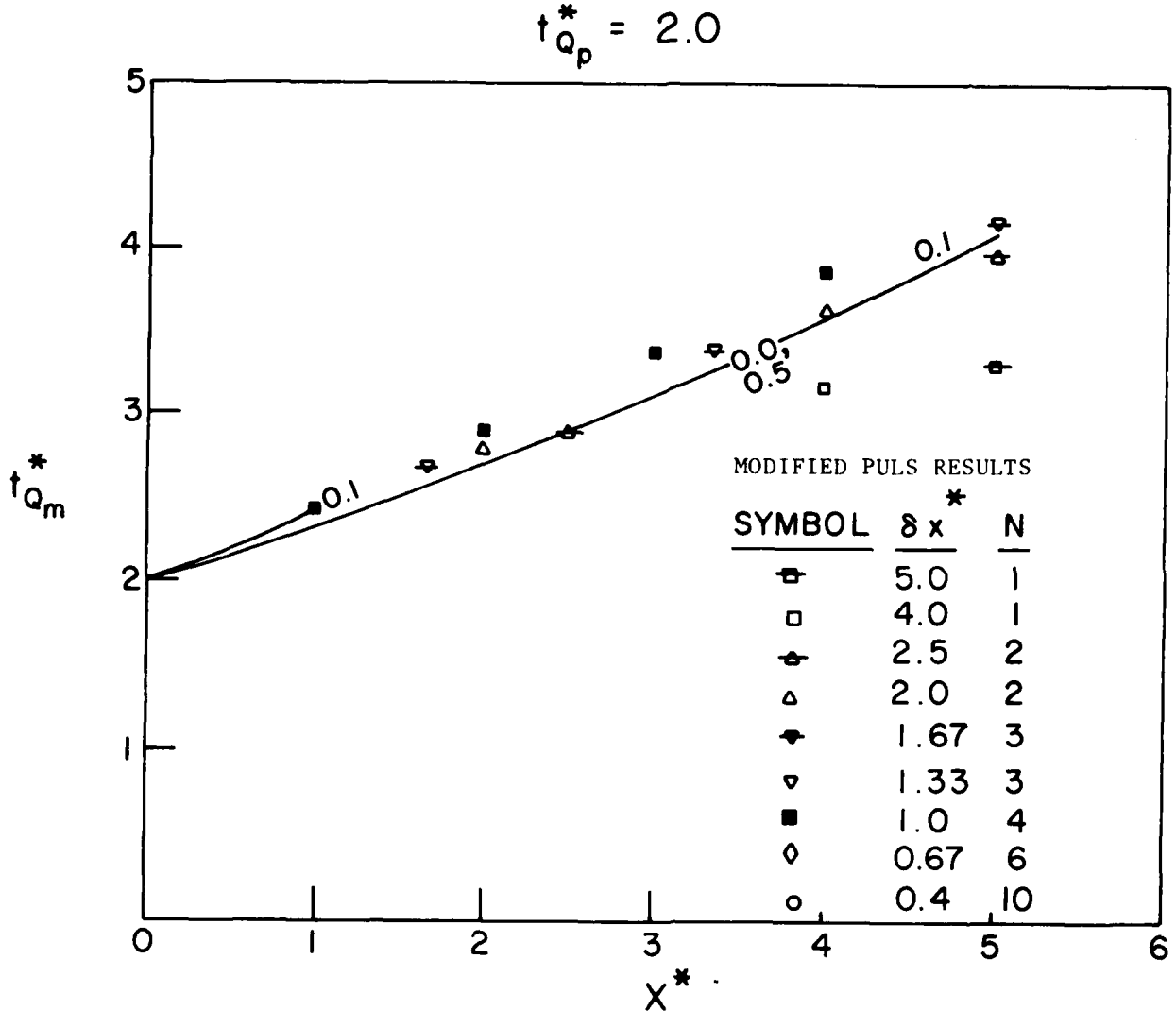

Fig. 22c Time of arrival of peak discharge, rectangular channel, normal depth downstream boundary condition.

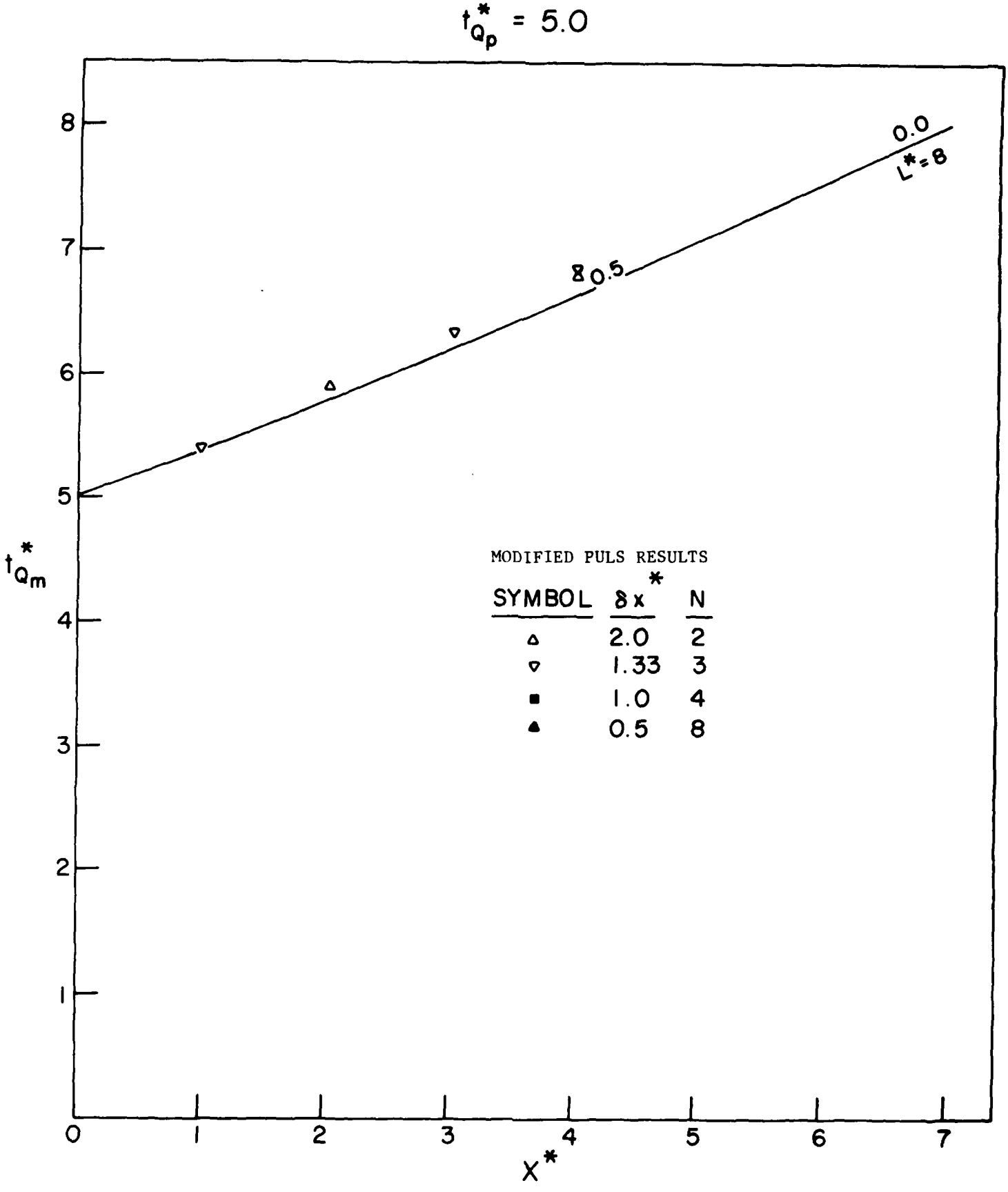

Fig. 22d Time of arrival of peak discharge, rectangular channel, normal depth downstream boundary condition.

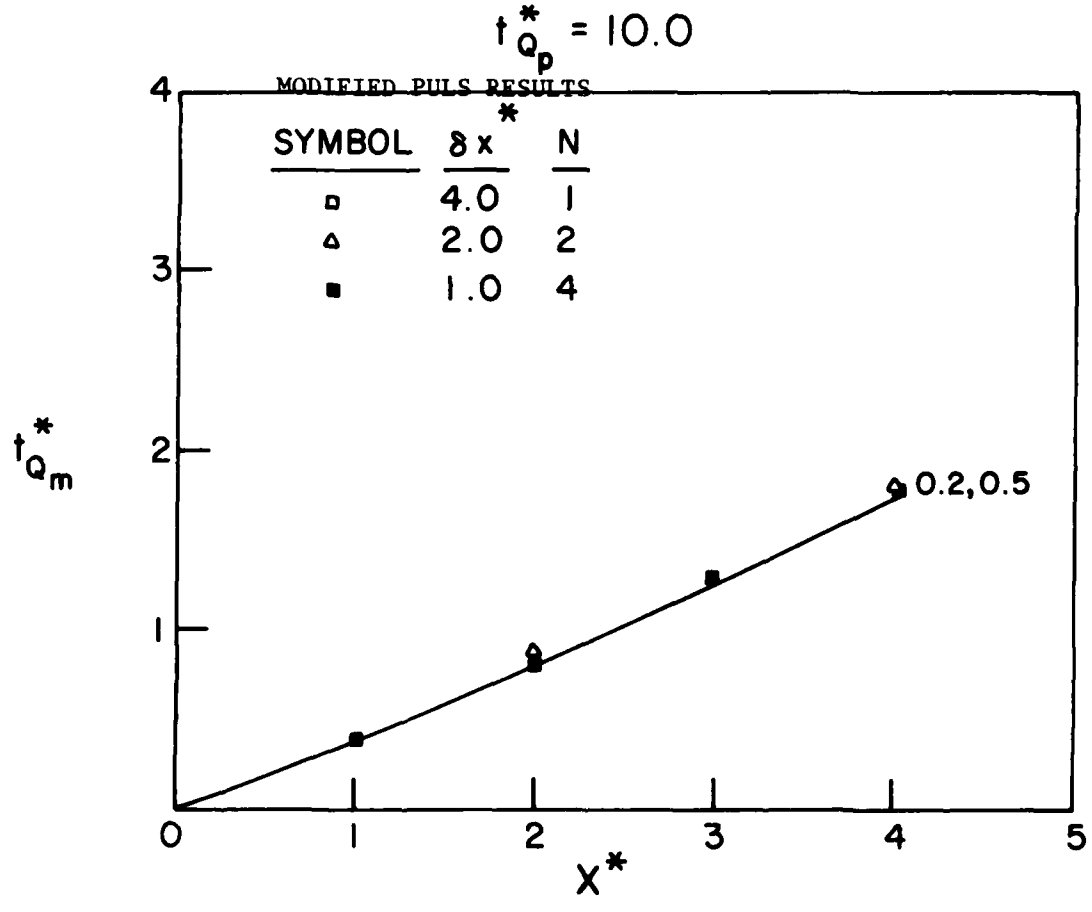

Fig. 22e Time of arrival of peak discharge, rectangular channel, normal depth downstream boundary condition.

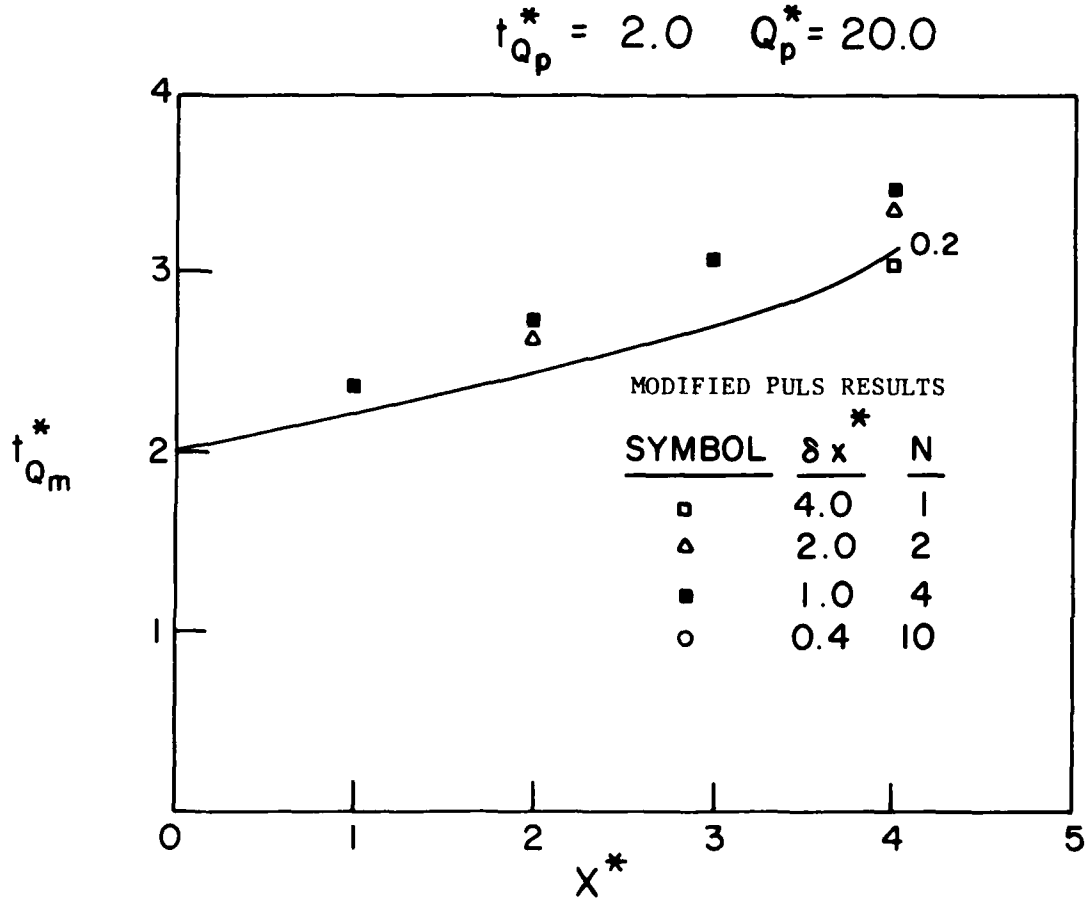

Fig. 22f Time of arrival of peak discharge, rectangular channel, normal depth downstream boundary condition.

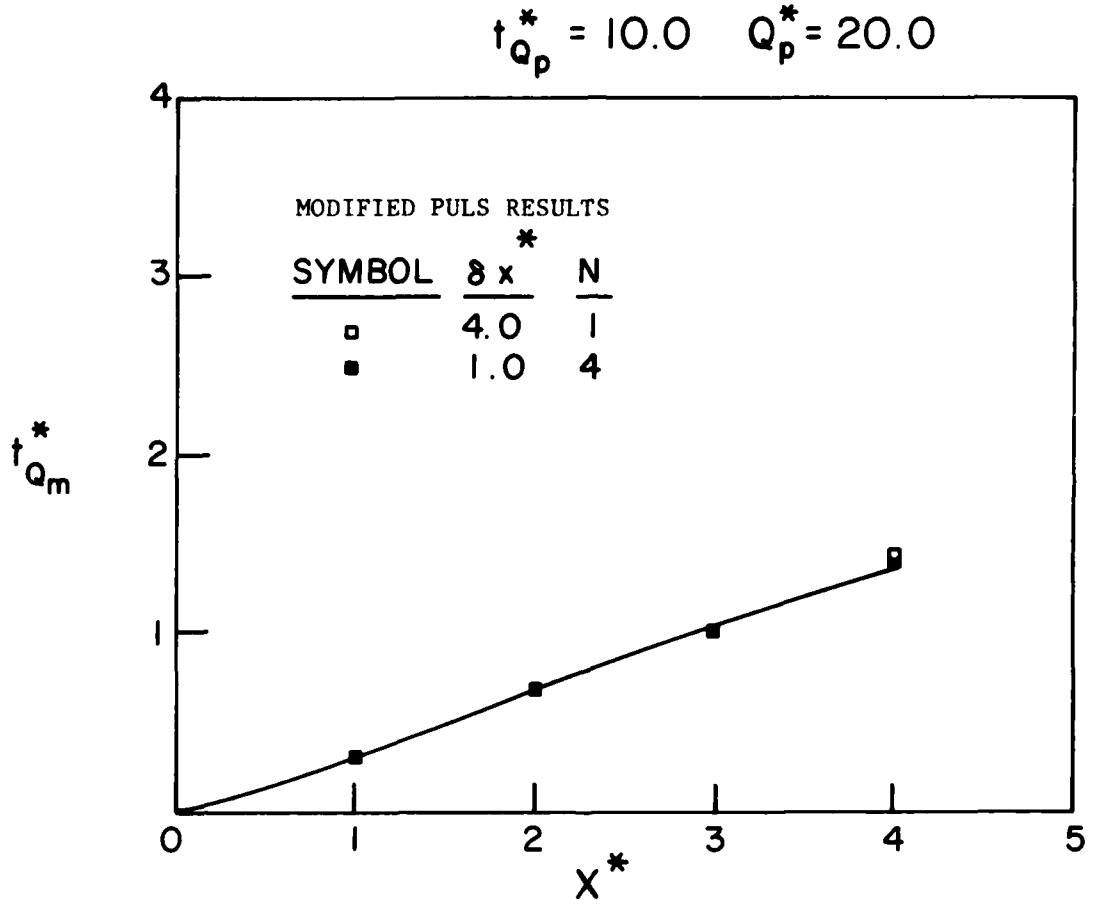

Fig. 22g Time of arrival of peak discharge, rectangular channel, normal depth downstream boundary condition.

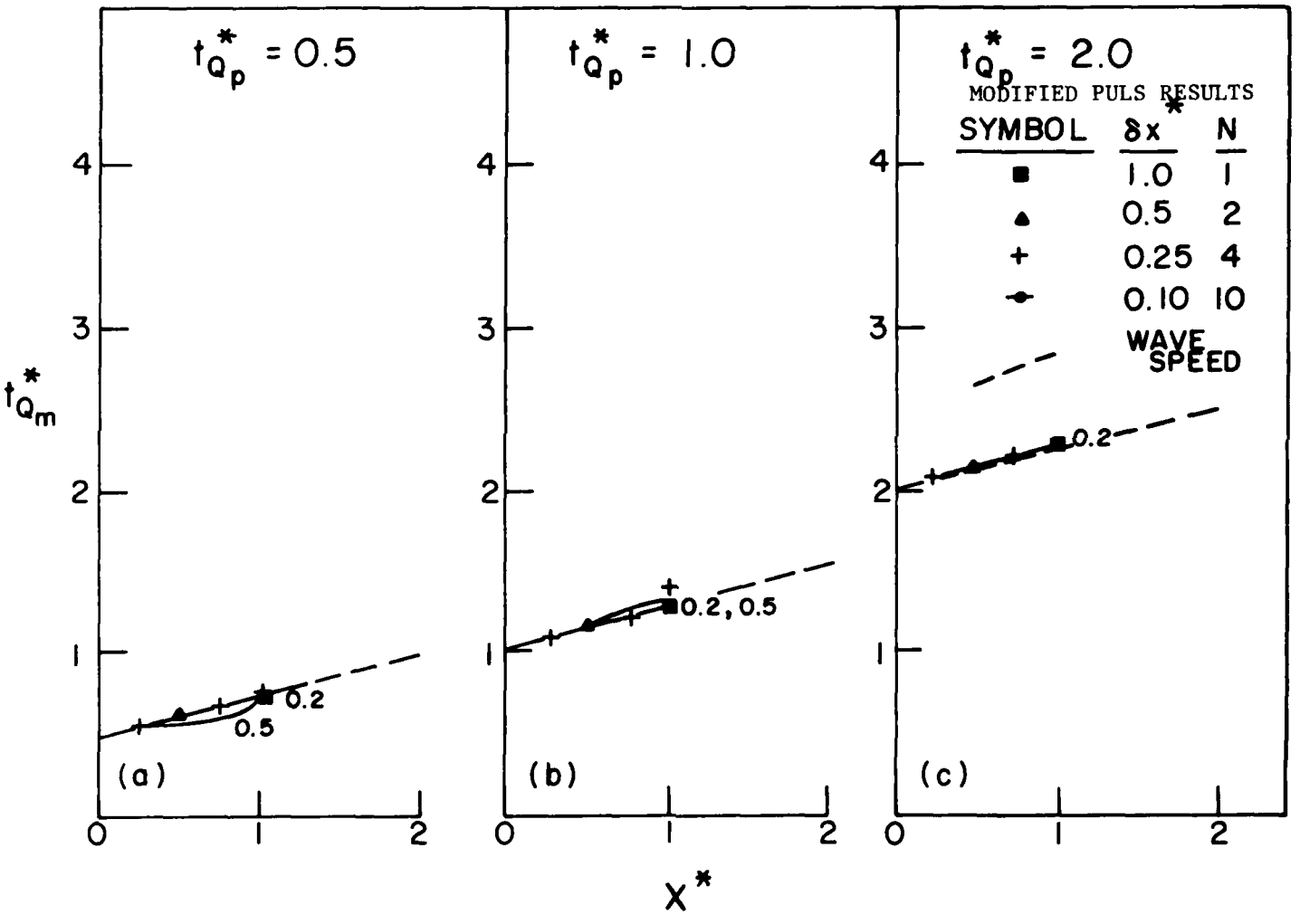

Fig. 23a-c Time of arrival of peak discharge, rectangular channel, weir downstream boundary condition.

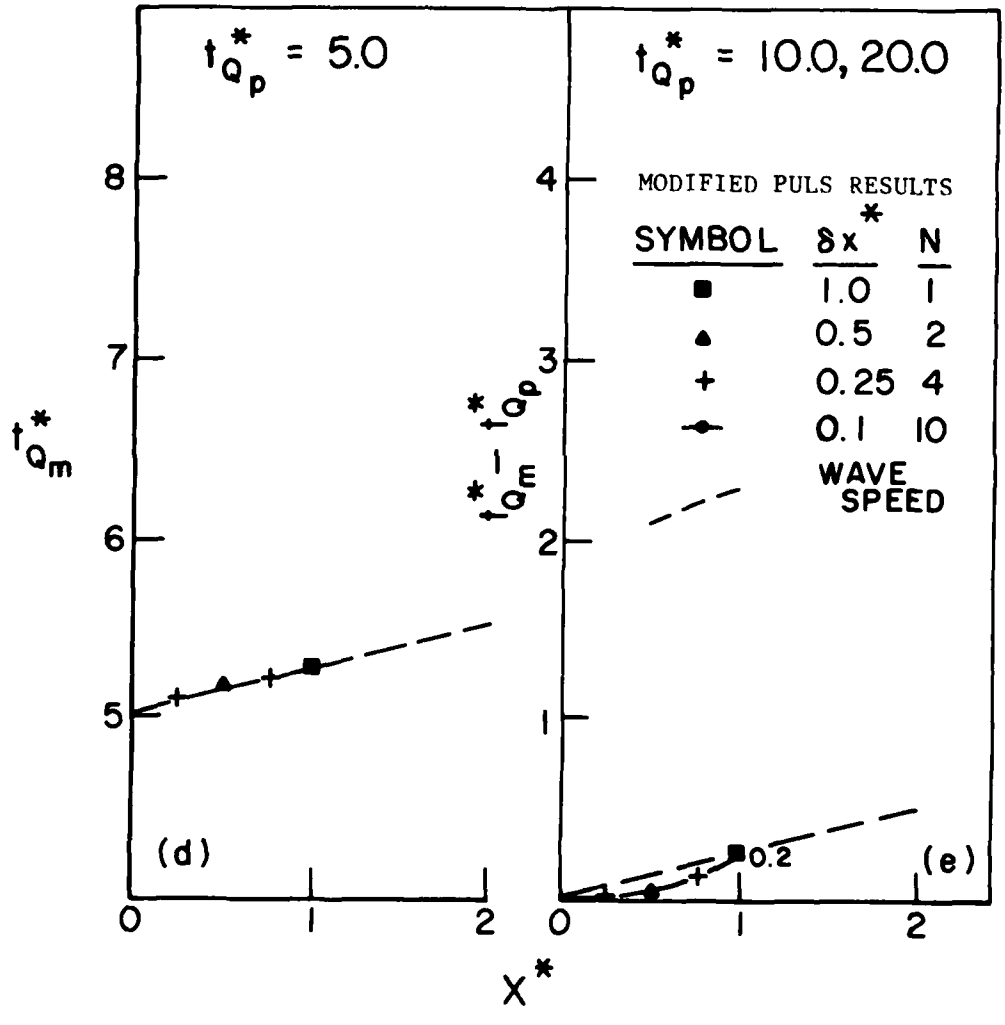

Fig. 23 d-e Time of arrival of peak discharge, rectangular channel, weir downstream boundary condition.

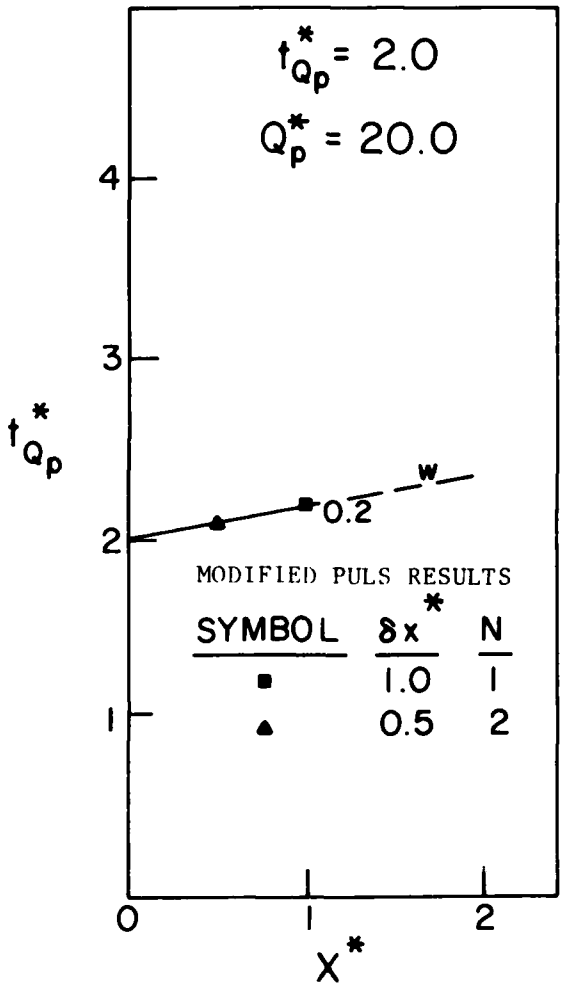

Fig. 23f Time of arrival of peak discharge, rectangular channel, weir downstream boundary condition.

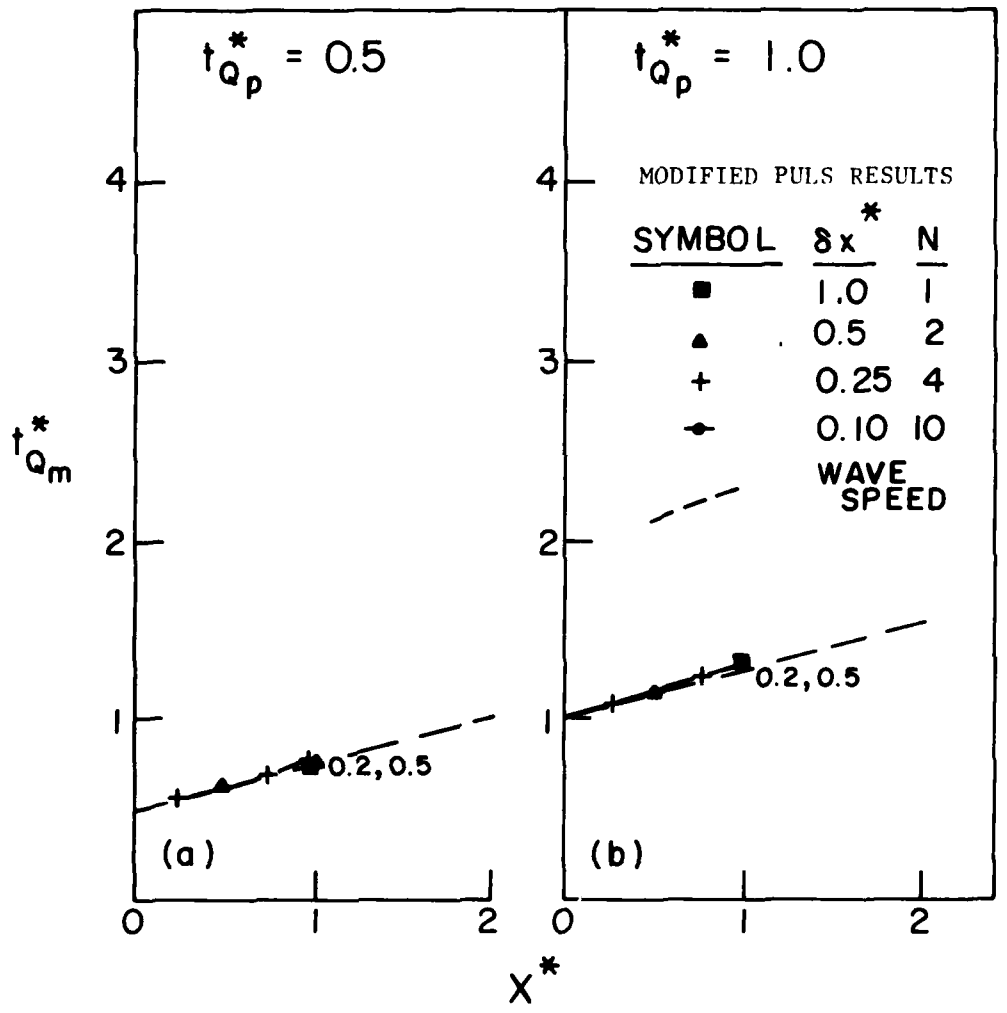

Fig. 24 a-b Time of arrival of peak discharge, rectangular channel, overfall donwstream boundary condition.

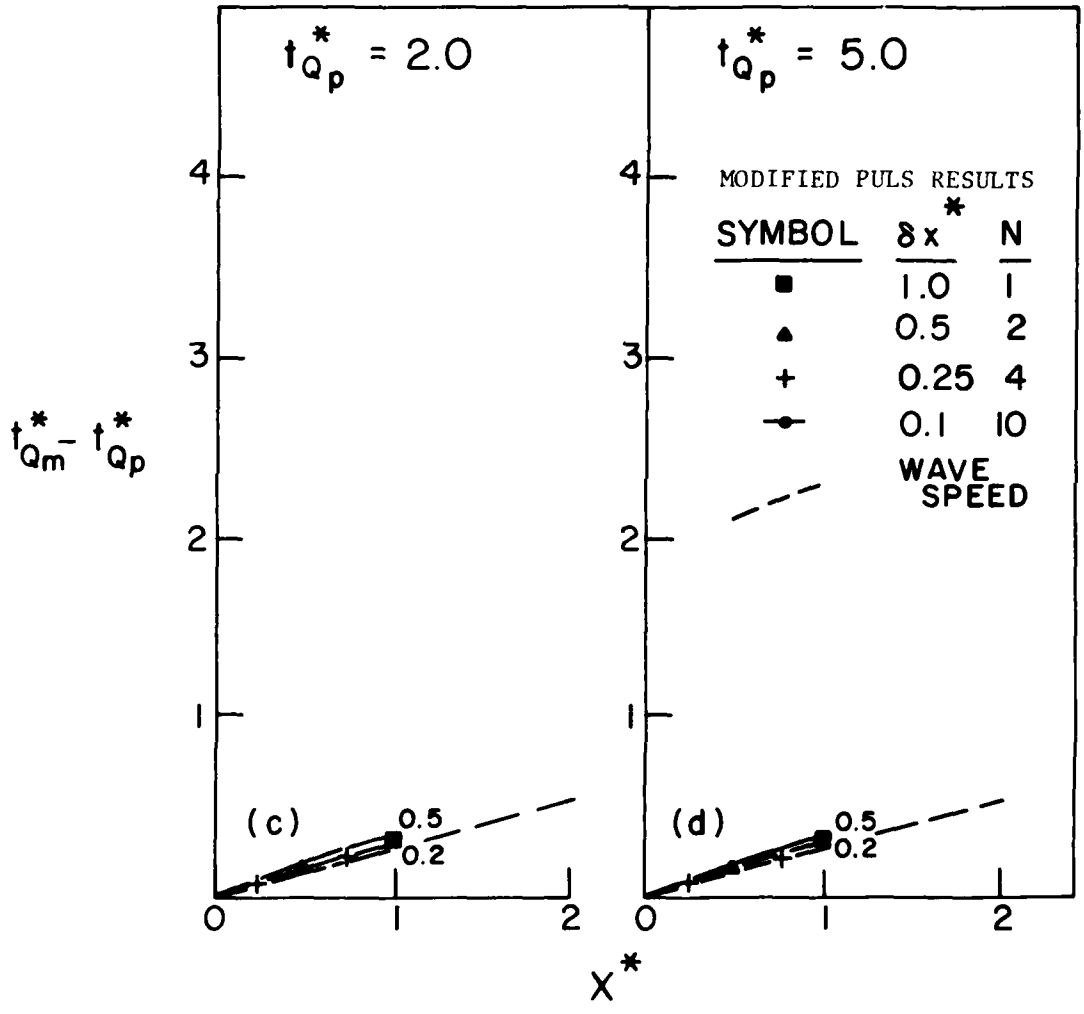

Fig. 24 c-d Time of arrival of peak discharge, rectangular channel, overfall downstream boundary condition.

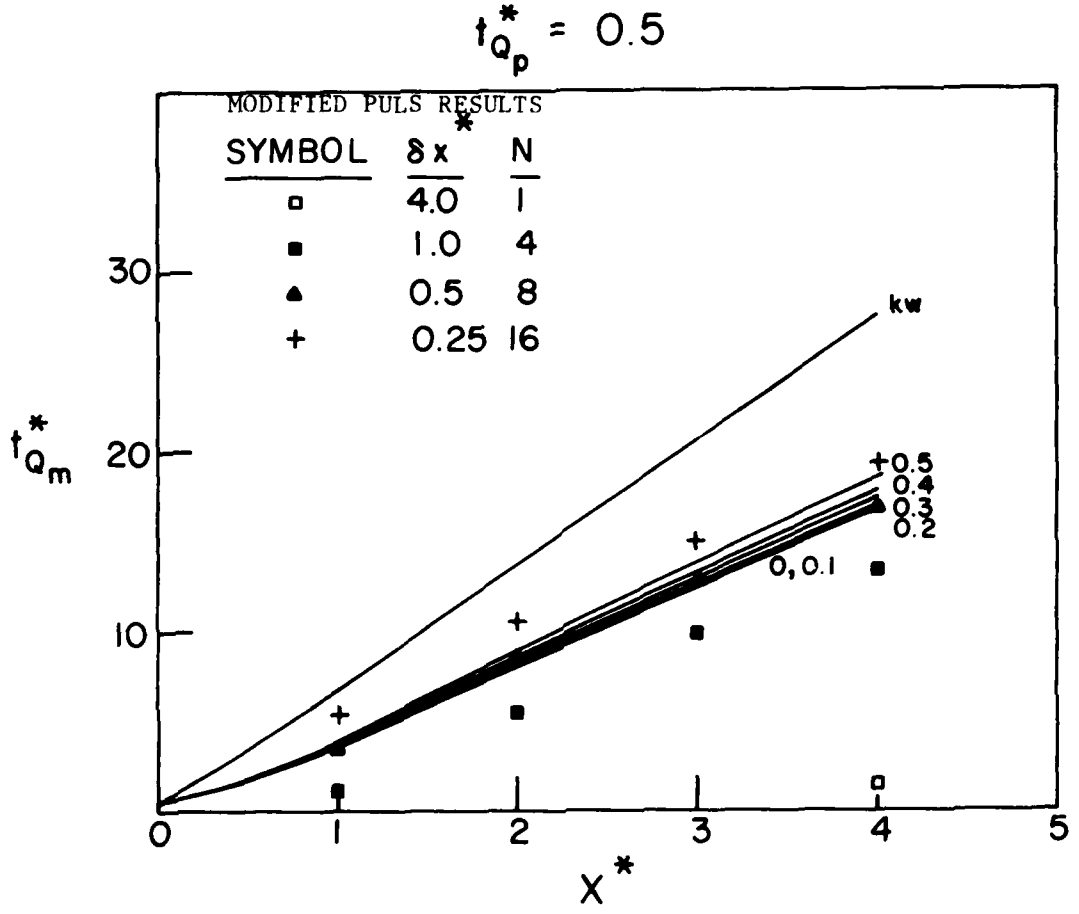

Fig. 25a Time of arrival of peak discharge, channel with floodplain, normal depth downstream boundary condition.

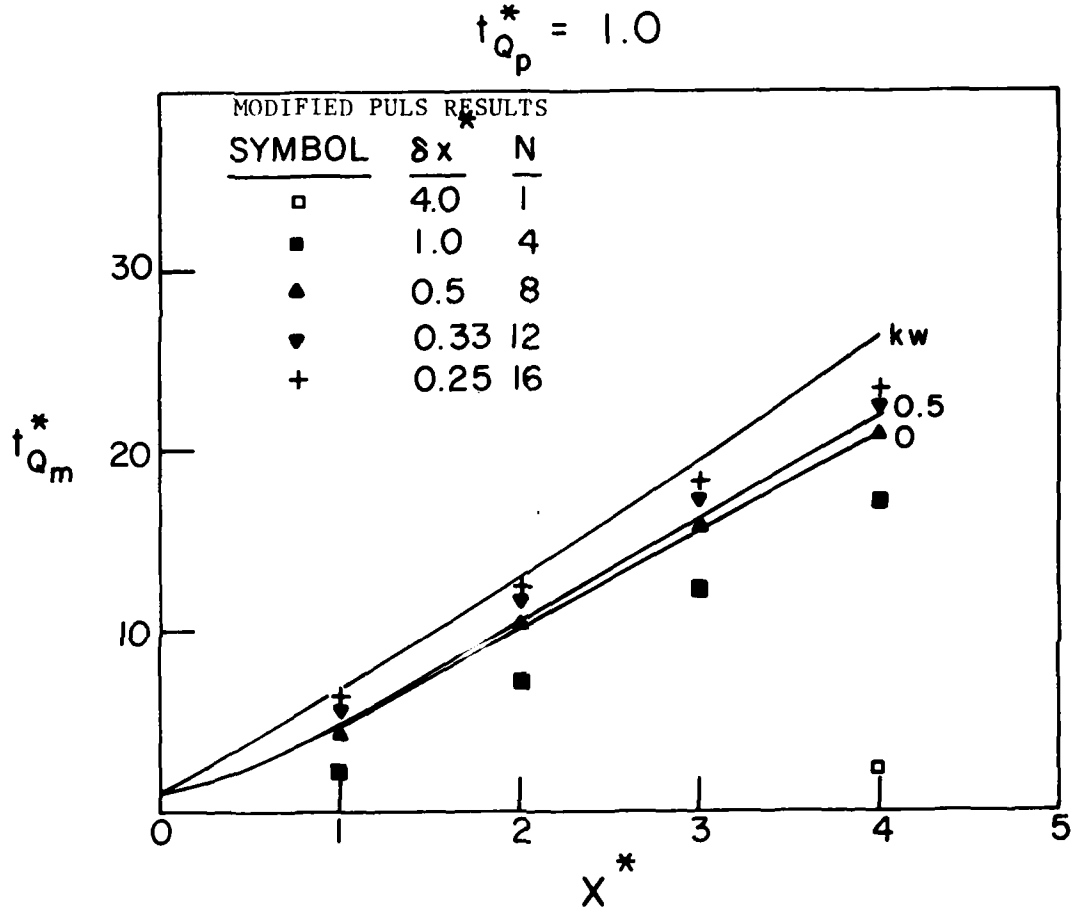

Fig. 25b Time of arrival of peak discharge, channel with floodplain, normal depth downstream boundary condition.

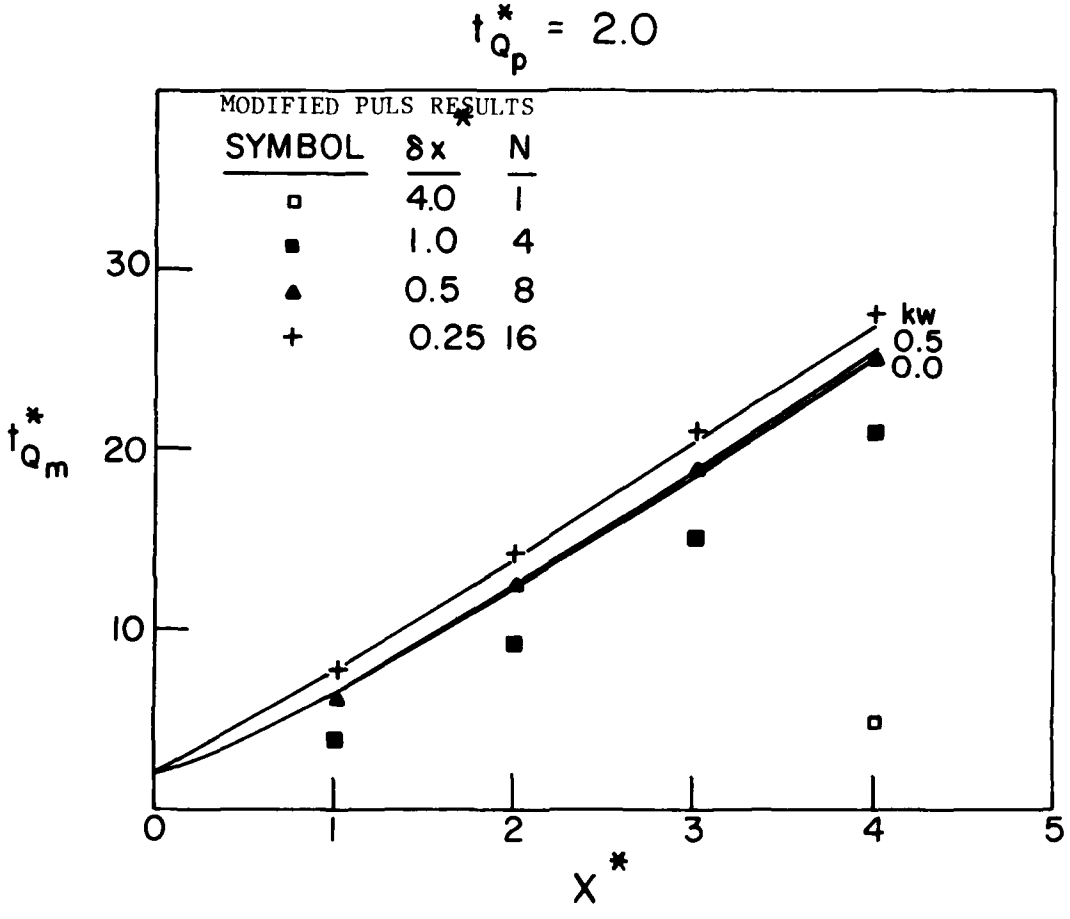

Fig. 25c Time of arrival of peak discharge, channel with floodplain, normal depth downstream boundary condition.

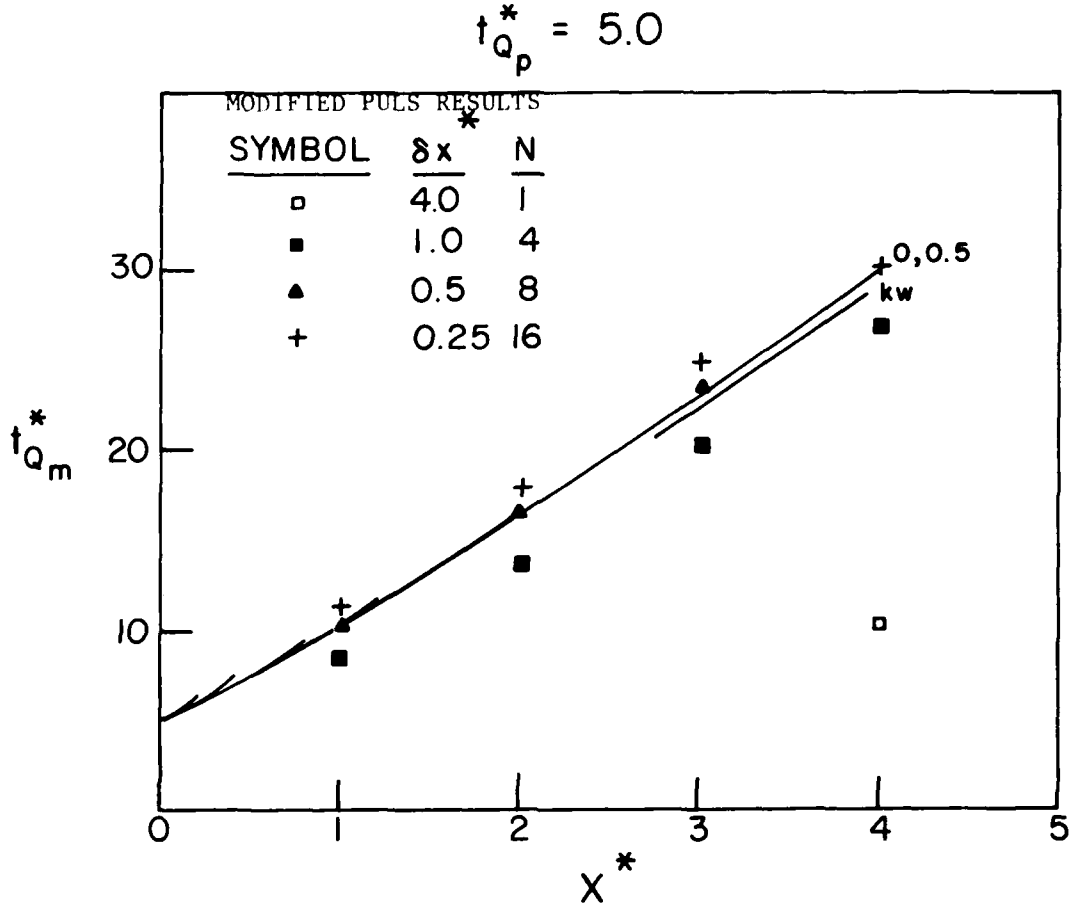

Fig. 25d Time of arrival of peak discharge, channel with floodplain, normal depth downstream boundary condition.

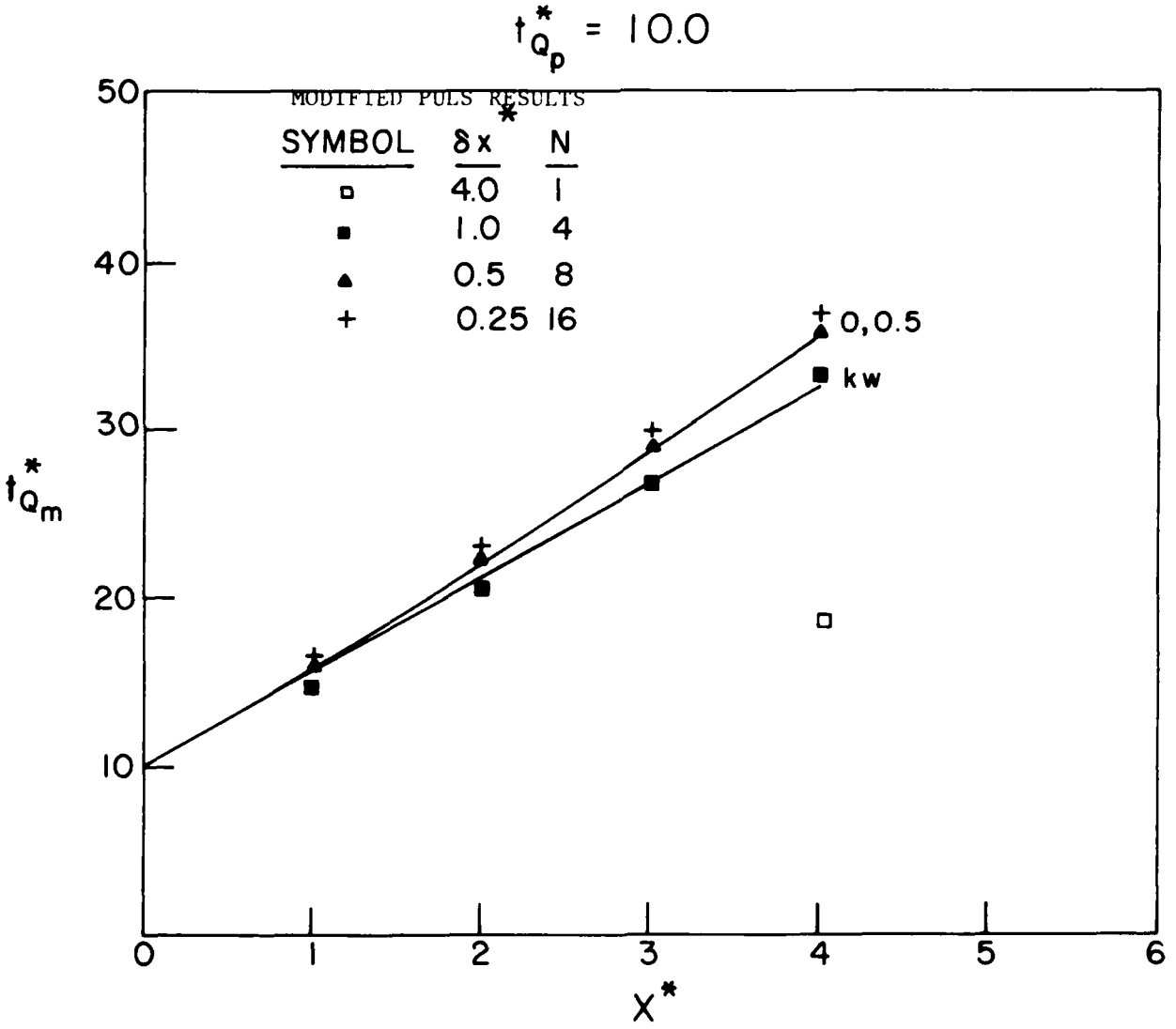

Fig. 25e Time of arrival of peak discharge, channel with floodplain, normal depth downstream boundary condition.

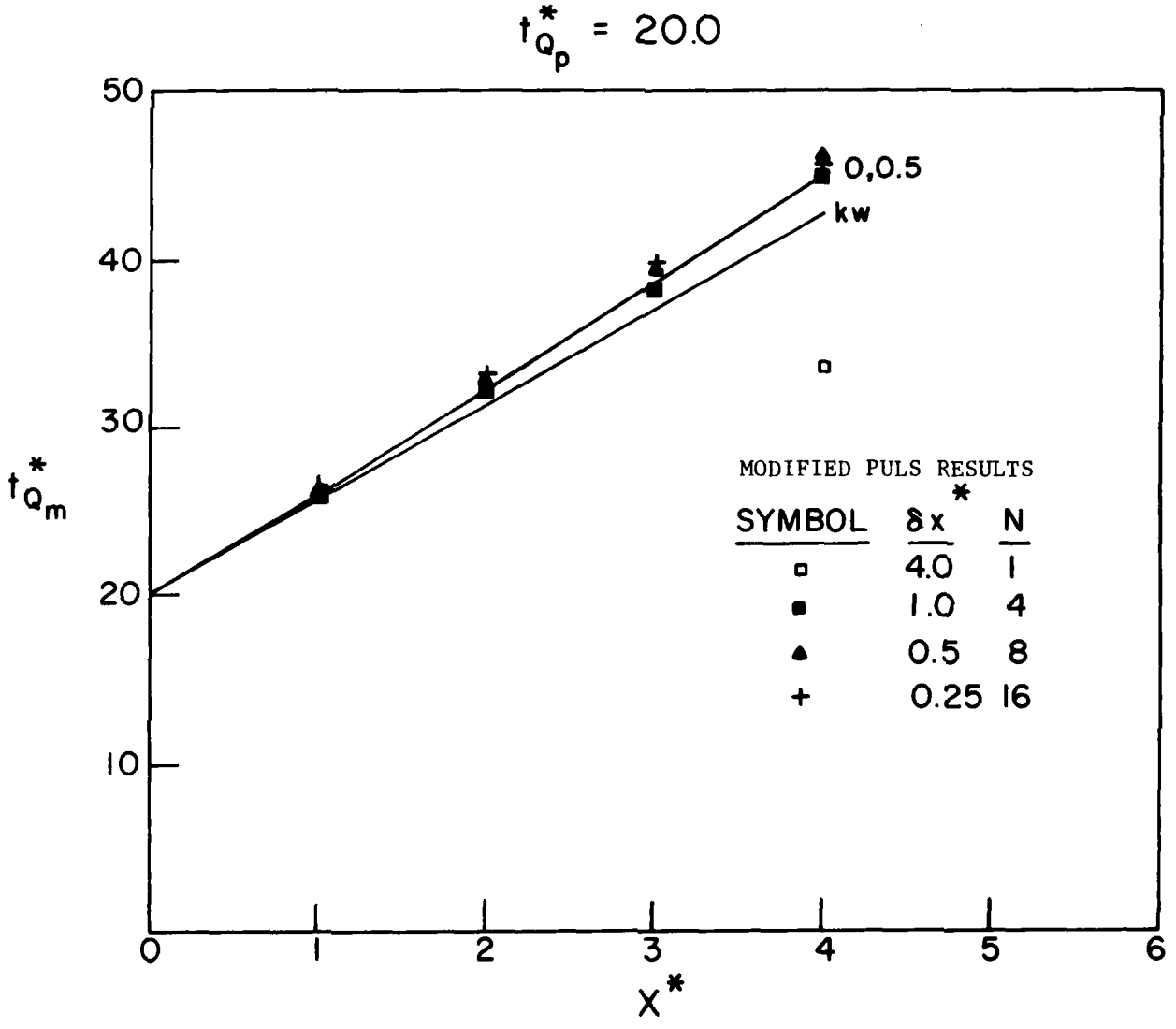

Fig. 25f Time of arrival of peak discharge, channel with floodplain, normal depth downstream boundary condition.

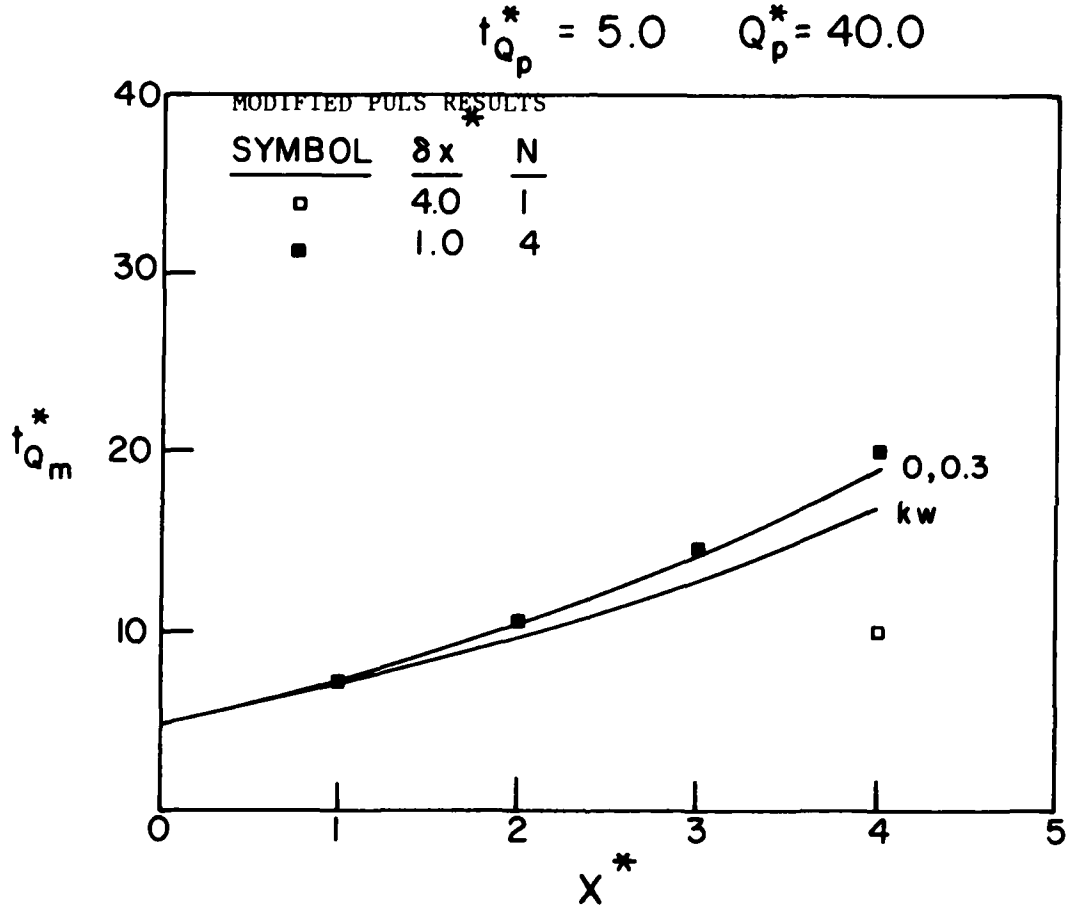

Fig. 25g Time of arrival of peak discharge, channel with floodplain, normal depth downstream boundary condition.

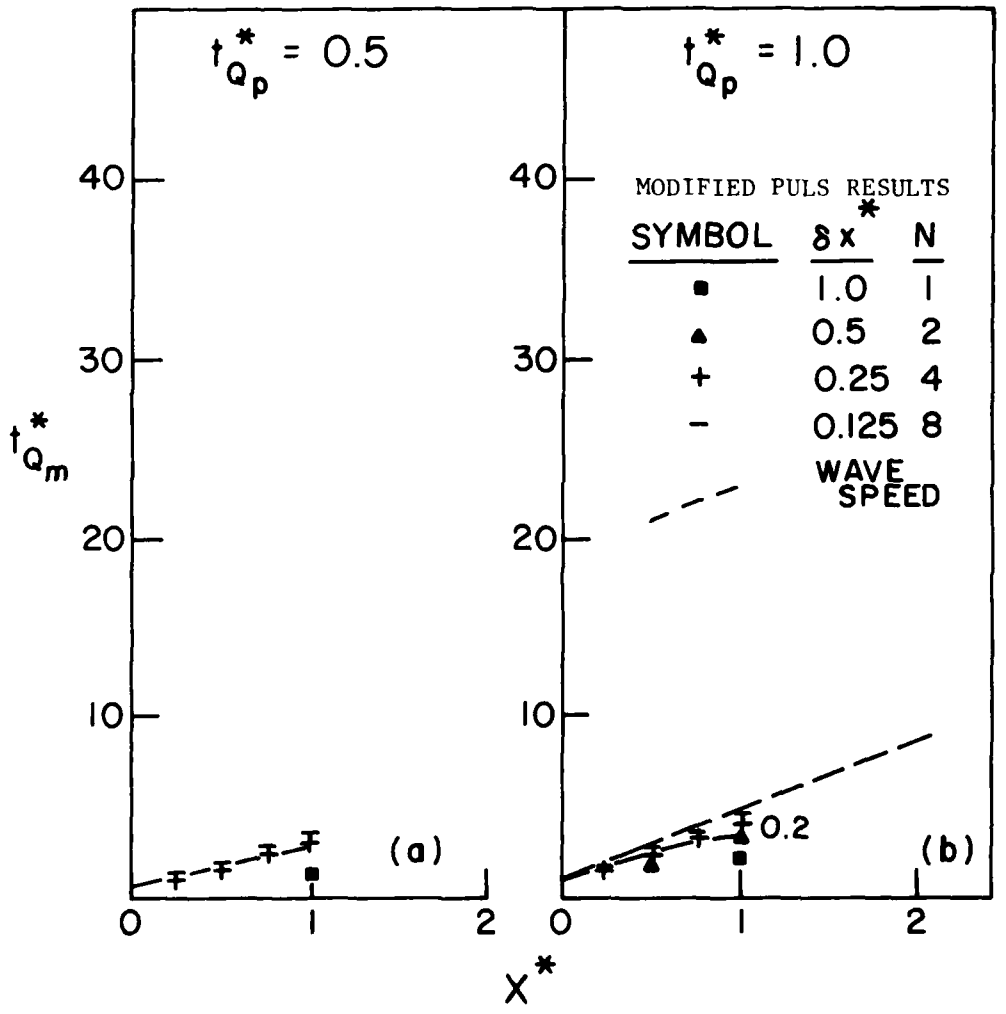

Fig. 26 a-b Time of arrival of peak discharge, channel with floodplain, weir downstream boundary condition.

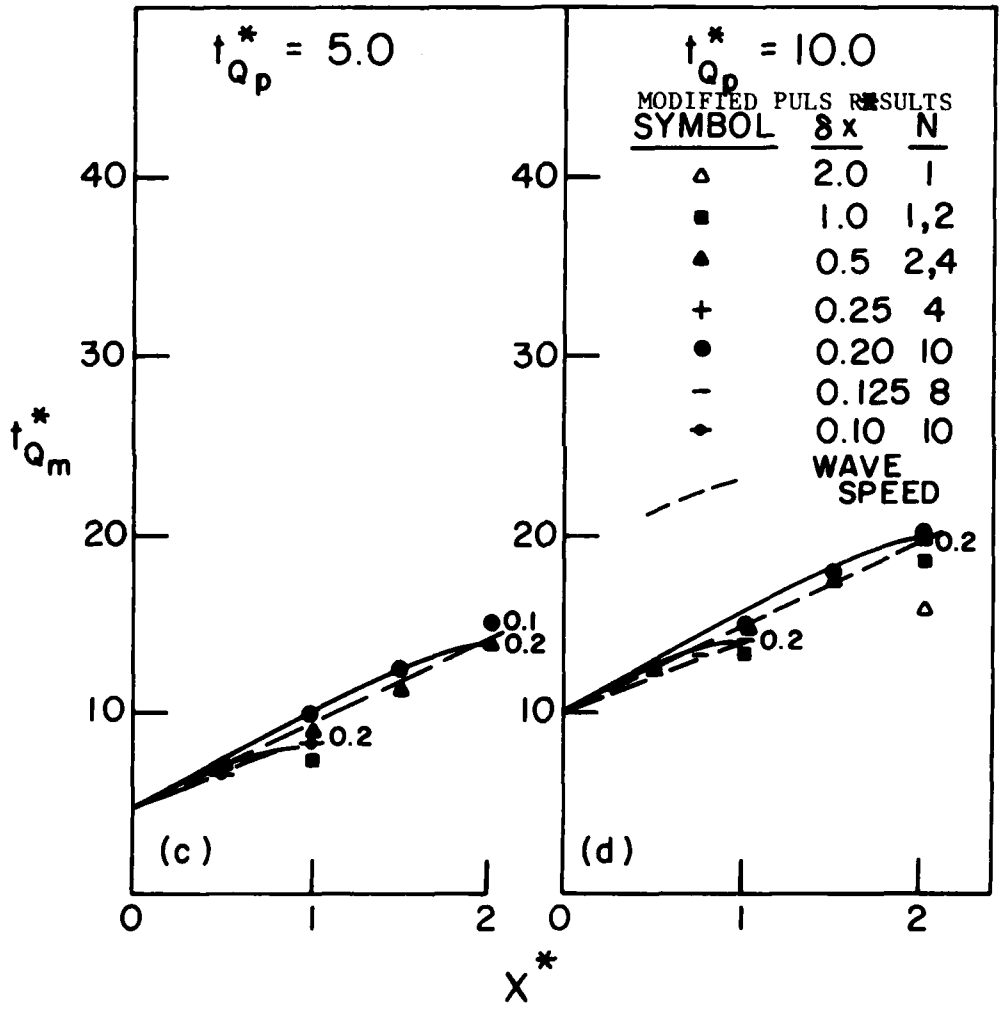

Fig. 26 c-d Time of arrival of peak discharge, channel with floodplain, weir downstream boundary condition.

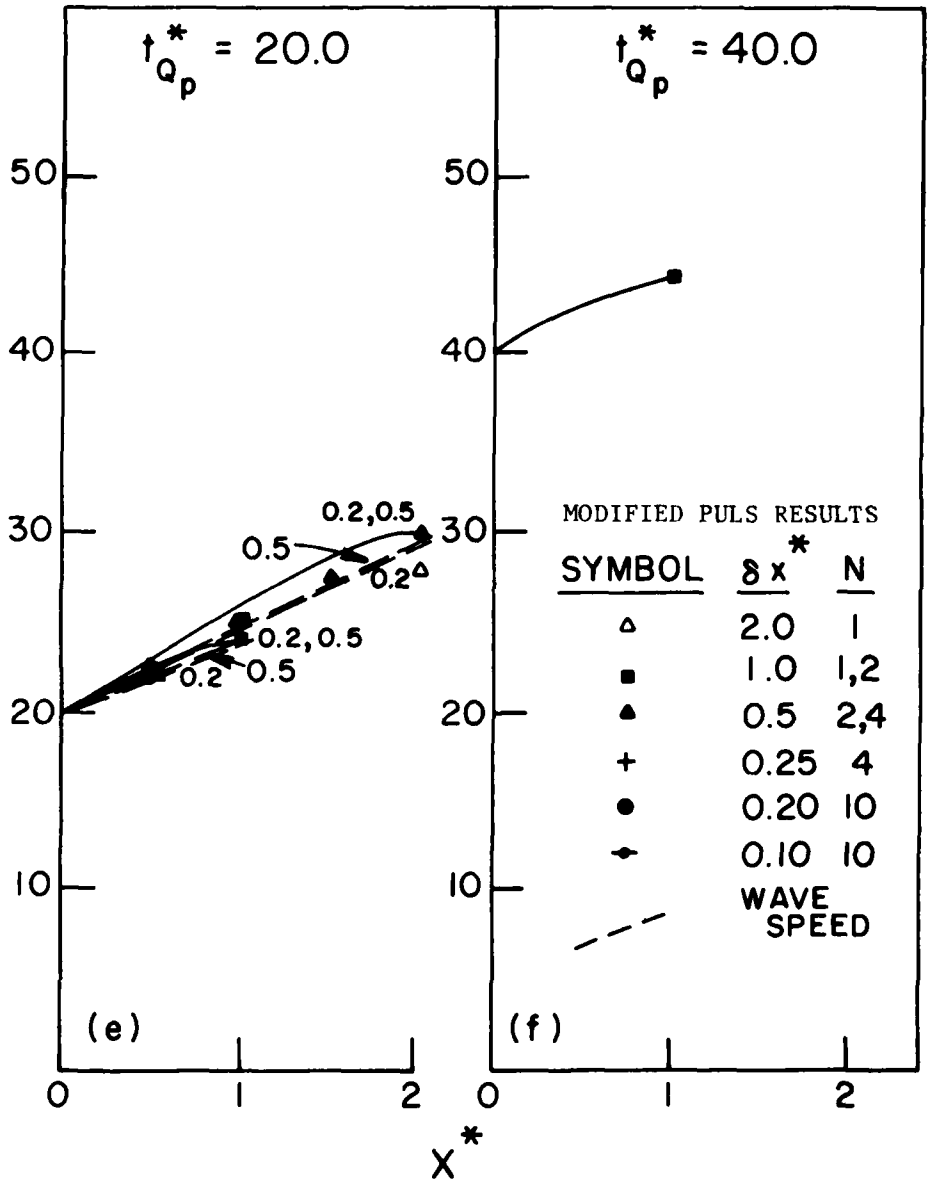

Fig. 26 e-f Time of arrival of peak discharge, channel with floodplain, weir downstream boundary condition.

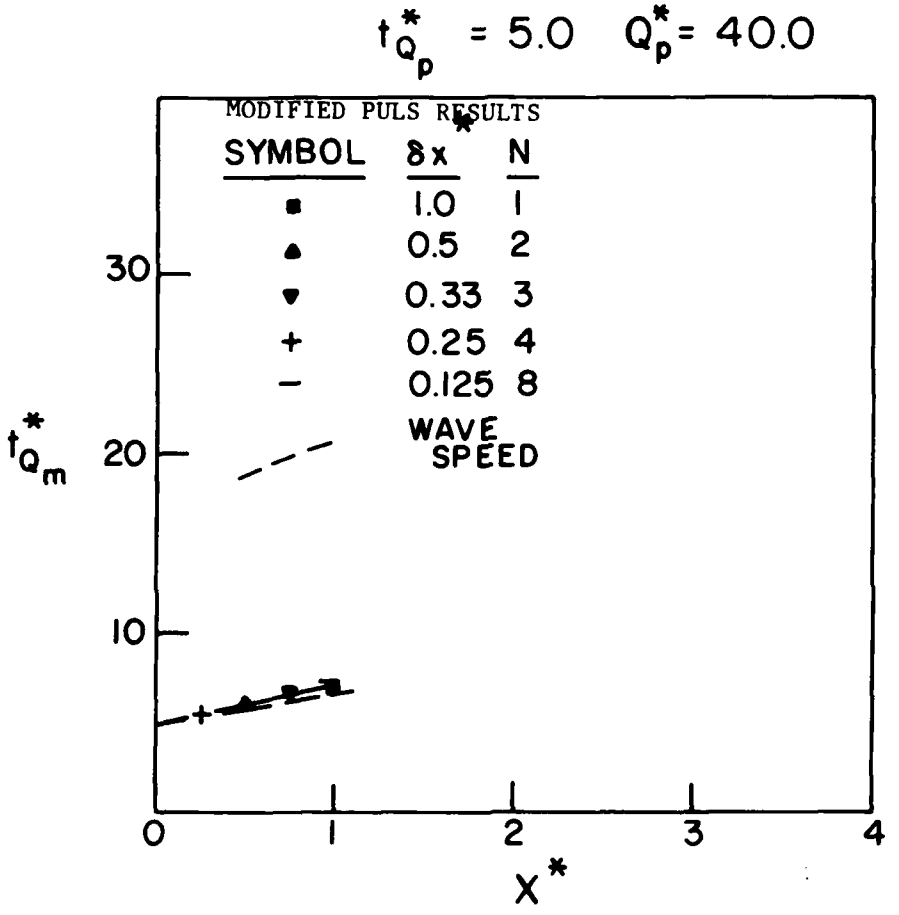

Fig. 26g Time of arrival of peak discharge, channel with floodplain, weir downstream boundary condition.

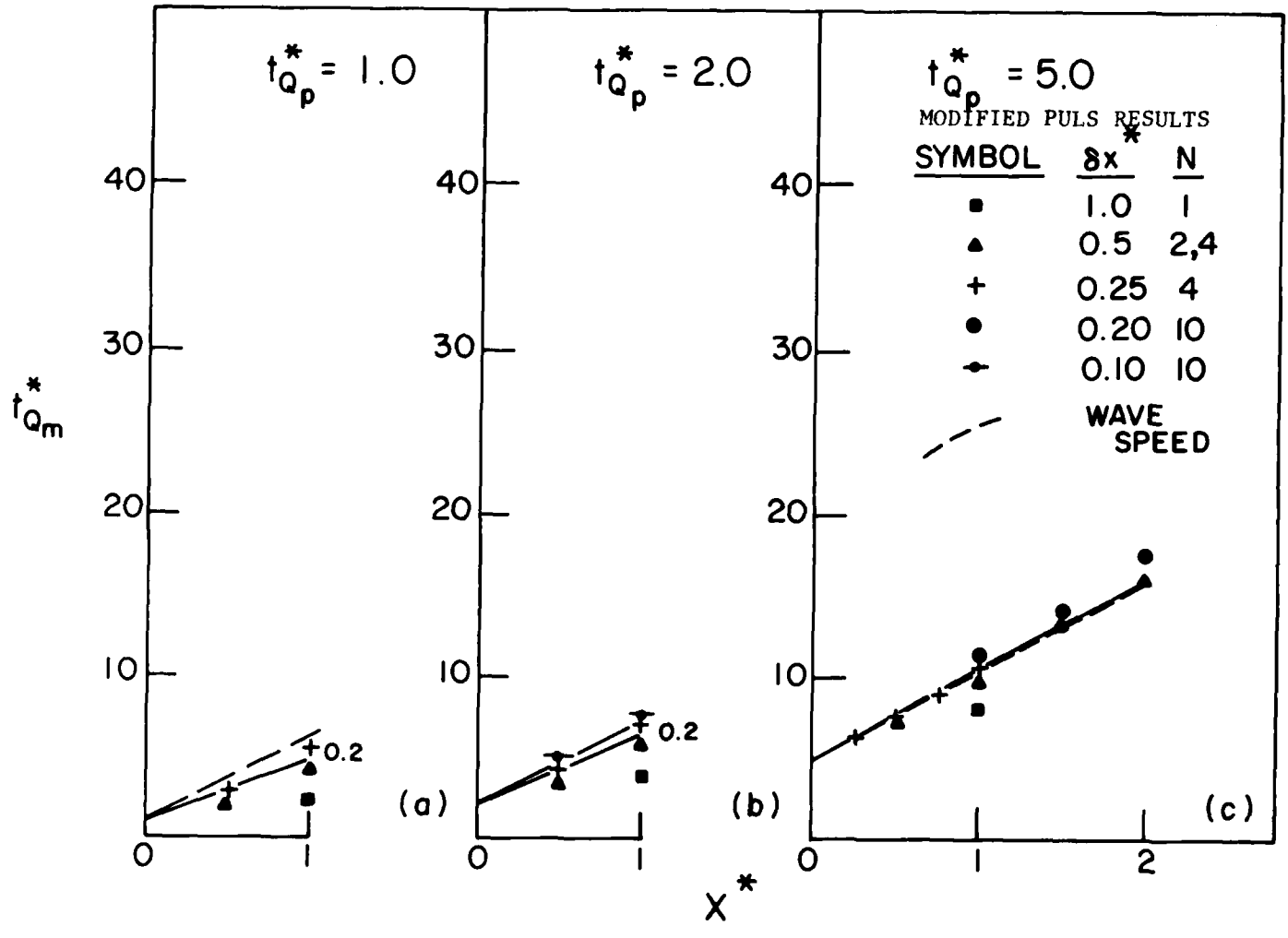

Fig. 27 a-c Time of arrival of peak discharge, channel with floodplain, overfall downstream boundary condition.

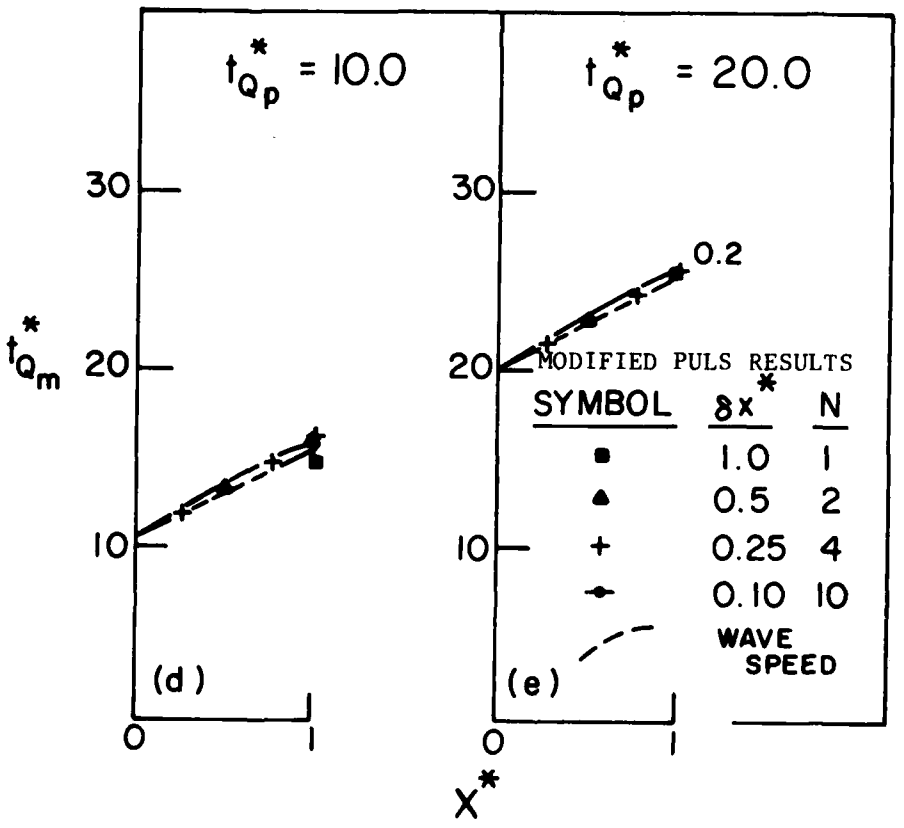

Fig.27$_{d-e}$ Time of arrival of peak discharge, channel with floodplain, overfall downstream boundary condition.

SECURITY CLASSIFICATION OF THIS PAGE *(When Data Entered)*

REPORT DOCUMENTATION PAGE		READ INSTRUCTIONS BEFORE COMPLETING FORM
1. REPORT NUMBER Research Document No. 24	2. GOVT ACCESSION NO.	3. RECIPIENT'S CATALOG NUMBER
4. TITLE *(and Subtitle)* Comparative Analysis of Flood Routing Methods		5. TYPE OF REPORT & PERIOD COVERED 6. PERFORMING ORG. REPORT NUMBER
7. AUTHOR*(s)* Theodor Strelkoff		8. CONTRACT OR GRANT NUMBER*(s)*
9. PERFORMING ORGANIZATION NAME AND ADDRESS U.S. Army Corps of Engineers Hydrologic Engineering Center 609 Second Street, Davis, California 95616		10. PROGRAM ELEMENT, PROJECT, TASK AREA & WORK UNIT NUMBERS
11. CONTROLLING OFFICE NAME AND ADDRESS		12. REPORT DATE April 1985 13. NUMBER OF PAGES 122
14. MONITORING AGENCY NAME & ADDRESS*(if different from Controlling Office)*		15. SECURITY CLASS. *(of this report)* Unclassified 15a. DECLASSIFICATION/DOWNGRADING SCHEDULE

16. DISTRIBUTION STATEMENT *(of this Report)*

Distribution of this document is unlimited.

17. DISTRIBUTION STATEMENT *(of the abstract entered in Block 20, if different from Report)*

18. SUPPLEMENTARY NOTES

This work was performed under contract (DACW0-80-P-0323) to the Hydrologic Engineering Center.

19. KEY WORDS *(Continue on reverse side if necessary and identify by block number)*

Flood routing, unsteady flow, hydrologic vs. hydraulic routing, Modified-Puls, kinematic wave, zero inertia, St. Venant

20. ABSTRACT *(Continue on reverse side if necessary and identify by block number)*

Given inflow hydrographs were routed downstream using several different techniques. The resulting outflow and stage hydrographs were then compared. The standard for comparison was chosen to be the solution of the one-dimensional Saint-Venant equations. The approximate techniques considered were the zero-intertia equations, kinematic-wave model, and Modified-Puls with optional subdivision of the reach lengths. The effect of floodplains was considered in contrast to channels of simple cross section. Downstream

DD FORM 1 JAN 73 1473 EDITION OF 1 NOV 65 IS OBSOLETE

SECURITY CLASSIFICATION OF THIS PAGE *(When Data Entered)*

boundary conditions consisted of one of the following: normal-depth stage-discharge relation, broad-crested overflow weir, or free overfall.

Dimensionless graphs of hydrograph-peak attenuation and arrival time as computed by the various techniquea are presented. The accuracy of the approximate techniques is found to depend on the values of certain dimensionless parameters. This suggests numerical limits on those parameters for application of a particular method. Application of the results to prototype conditions is demonstrated in a companion report titled "Modified-Puls Routing in Chuquatonchee Creek."

END

FILMED

10-85

DTIC